# Energy & Environmental Science

Accepted Manuscript




This is an *Accepted Manuscript*, which has been through the Royal Society of Chemistry peer review process and has been accepted for publication.

*Accepted Manuscripts* are published online shortly after acceptance, before technical editing, formatting and proof reading. Using this free service, authors can make their results available to the community, in citable form, before we publish the edited article. We will replace this *Accepted Manuscript* with the edited and formatted *Advance Article* as soon as it is available.

You can find more information about *Accepted Manuscripts* in the Information for Authors.

Please note that technical editing may introduce minor changes to the text and/or graphics, which may alter content. The journal's standard Terms & Conditions and the Ethical guidelines still apply. In no event shall the Royal Society of Chemistry be held responsible for any errors or omissions in this *Accepted Manuscript* or any consequences arising from the use of any information it contains.



ROYAL SOCIETY OF CHEMISTRY

www.rsc.org/ees

# Organometal Halide Perovskite Solar Cells: Degradation and Stability

**Taame Abraha Berhe[1], Wei-Nien Su[1,*], Ching-Hsiang Chen[1], Chun-Jern Pan[2], Ju-Hsiang Cheng[2], Hung-Ming Chen[2], Meng-Che Tsai[2], Liang-Yih Chen[2], Amare Aregahegn Dubale[2], Bing-Joe Hwang[2, 3 *]**

[1]NanoElectrochemistry Laboratory, Graduate Institute of Applied Science and Technology, National Taiwan University of Science and Technology, Taipei 106, Taiwan

[2]NanoElectrochemistry Laboratory, Department of Chemical Engineering, National Taiwan University of Science and Technology, Taipei 106, Taiwan

[3]National Synchrotron Radiation Research Center, Hsin-Chu, 30076, Taiwan

Corresponding Authors: E-mail: bjh@mail.ntust.edu.tw (B.J. Hwang) and wsu@mail.ntust.edu.tw (W.N. Su)

## Abstract

Organometal halide perovskite solar cells have evolved in an exponential manner in the two key areas of efficiency and stability. The power conversion efficiency (PCE) reached 20.1% late last year. The key disquiet was stability, which has been limiting practical applications, but now is in a promising state of the art, measured in thousands of hours. These improvements have been achieved with the application of different materials, interfaces and device architecture optimizations, especially after the investigation of hole conductor free mesoporous device, incorporating carbon electrodes, which promise stable, low cost and easy device fabrication methods. However, this work is still far from complete. There are various issues associated with the degradation of Omh-perovskite, interface and device instability which must be addressed to achieve good reproducibility and long lifetimes for Omh-PSCs with high conversion efficiencies. A comprehensive understanding of these issues is required to achieve stability breakthroughs and practical outdoor applications for Omh-PSCs. For successful small and large scale applications, next to the improvement of the PCE, the stability of Omh-PSCs has to be improved. The causes of failure and associated mechanisms of device degradation followed by the origins of degradation, approaches to improve stability, and methods and protocols are discussed in detail and form the main focus of this review article.

**Keywords:** perovskite solar cell, degradation mechanism, origin of degradation, stability



Energy & Environmental Science Accepted Manuscript

Energy & Environmental Science Accepted Manuscript

## 1. Background

To become economically feasible, organomietal halide perovskite solar cells (Omh-PSCs) should remain free from degradation under normal operating conditions over several years, preferably tens of years. Stability is vital for practical application, but evaluation and the prediction of device lifetime are not easy as stability related to individual solar cells fading process.[1] Because varieties of solar devices have various degradation mechanisms, the accelerated stress tests appropriate for one type of solar cell may not be useful in studying the degradation of other types. Organomietal halide (Omh) perovskites are a class of materials in the perovskite family with alternating layered structures of organic and inorganic constituents. Omh-perovskites are noted for cheap production and methylammonium lead iodide ($CH_3NH_3PbI_3$) is one of the most representative materials. Solar cells made of this kind of materials have grown so fast within a few years and reached a certified efficiency over 20%. Its theoretical maximum is greater than 30% and this could beat the efficiency of silicon, its theoretical maximum is limited to 27%, and economically and practically limited to ~25%.[2]

However, long term stability of this kind of solar cells is far from practical. *Ex-situ* long-term stability tests for $CH_3NH_3PbI_3$ solid-state solar cells stored in air at room temperature without encapsulation were carried out for over 500 hrs under one sun illumination[3] and 1000 hrs under full sun light[4]. This revealed that light soaking alone is not a major reason for this poor stability. Furthermore, long-term stability of Omh-PSCs for 500 hrs at 45 ˚C, under constant illumination[5] at approximately 100 mW



Energy & Environmental Science Accepted Manuscript

$cm^{-2}$ and 1000 hrs at 40 ˚C, with continuous exposure and operation under full spectrum simulated sunlight[6] has also been achieved. The light-soaking tests become more challenging as the temperature increased; in fact, a light soaking test Omh-PSCs has not yet reported at 80 ˚C for 1000 hrs. The device stability of mesoporous $TiO_2/CH_3NH_3PbI_3/C$ heterojunction (HJ) solar cells without encapsulation is 2000 hrs at room temperature, in air and in the dark[7]. The high temperature (80 ˚C) dark test may be too demanding for these solar cells as it has not yet been demonstrated. It is obvious that at high temperatures, i.e. above 60 °C, either certain fading mechanisms are accelerated or new degradation reactions occur, causing rapid absorber material and/or device degradation. The major causes responsible for this kind of degradation may be related to various possible external factors, such as moisture, oxygen, temperature, UV light, etc., as well as internal intrinsic factors such as ion migration, electro-migrations and interfacial reactions. Thus, setting standard stability testing protocols needs an understanding of how and why the device degrades. Such an understanding should facilitate future production of better materials for the cells.

In order to set up typical stability testing protocols for Omh-PSCs, stability purposes should be well understood. For example, to what range of drop or raise in performance of Omh-PSCs can be accepted for the device to be taken as a stable device? Second, is efficiency the only criterion to assess the performance? As a final point, the ultimate application should also be taken into account. Even though standard protocols are not well-outlined, various frequently utilized protocols such as temperature (60 ˚C and 80 ˚C dark tests), light soaking tests at 1 Sun at 60 ˚C or 80 ˚C, heat-cycle durability test, ultraviolet (UV) test, and humidity test can be used to assess the stability, which commonly run for 1000 hrs. Hence, the aim of this article is to comprehensively review the causes of failure and associated possible mechanisms of degradation, origins of degradations followed by the approaches to improve stability as well as methods and protocols to study degradation. Its objectives are also to shed light on possible approaches directed towards a more systematic study of degradation phenomena in Omh-PSCs. Therefore, the scope of this article is to critically assess stability and degradation information to aid the commercial enterprises and research institutes that work with these technologies.

The organization of this review originates from its background followed by the overview information focusing on the need for Omh-PSCs and its associated mechanistic processes as well as major



Energy & Environmental Science Accepted Manuscript

contributions to the current status of performance improvement in order to provide an overview of basic principles and progressive improvements in efficiency and stability. Only promising steps have been achieved mainly in the area of device stability from minutes to thousands of hours. Thus, various causes of failure and associated mechanisms of degradation has been comprehensively reviewed. Furthermore, the origins of device degradation in different device components that are capable of prohibiting the devices out of the inert atmosphere are discussed in-depth. These components have been subdivided into Omh-perovskite, mixed Omh-perovskite, a hole transport layer, counter electrode and each contributing their own degradation mechanisms. The device architecture is also another important issue which has an impact on the device stability. The main device architectures: planar (regular $TiO_2$), inverted and mesoporous $TiO_2$ are reviewed in line with their stability issues. The sequence of the different layers in the three architectures results in different interfacial reactions which can further affect the stability. The discussion of this interface is subdivided into ion migration into the interface and reactivity in the interface. Finally, we wrap up our discussion with possible ways for stability improvements as a function of material, device architecture, and interface aspects as well as protective means during operation. Test, evaluation methods and protocols for stability studies are also suggested for future material and device development. This review manuscript is finalized with a comprehensive conclusion and prospects.

## 2. Overview of Omh-PSCs Devices

### 2.1 The need for Omh-PSCs

Studies focusing on Omh-PSCs are growing in number and attracting scientists from other subject areas: 1) Physicists, constructing devices from new materials, typifying and optimizing performance, and realizing the basic photo-physical mechanisms; 2) Chemists, developing and manufacturing suitable Omh-perovskite absorber and dealing with structure–property relationships and 3) Engineers, building novel device design. The interplay among all the subjects would have a great contribution for potential improvements of Omh-PSCs in the future.

Solar cells with effective PCEs require materials to absorb in a wide spectral range, from visible to near infrared, to harvest most of the solar photons, and to efficiently convert the photon into free charges. In order to reduce the energy costs related to electron/hole separation and charge extraction



Energy & Environmental Science Accepted Manuscript

highly crystalline materials having good carrier mobility are required. However, these are hampered by unreasonable costs; due to production procedures that use vacuum based, or high-temperature processing, thereby limiting commercial application. On the other hand, third generation photovoltaic devices, e.g. amorphous silicon (a-Si), dye sensitized solar cells (DSCs) and organic photovoltaic (OPVs) can be made using simple low cost manufacturing processes.[8, 9] These technologies utilize a combination of amorphous and disordered materials. Hence, the energy costs associated with the extraction of free charges impose a fundamental limitation upon high efficiency systems. As shown in Fig.1**,** the new Omh-perovskite structure based materials are revolutionizing the photovoltaic field, with the efficiencies of Omh-PSCs, a-Si, DSC and OPVs being 20.1%[10], 13.44%[11], 13%[12]and 12%[13] respectively. Recent research shows there is a tradeoff between a wide spectral absorption range, highly crystalline structures that induce effective charge extraction, and low-cost fabrication techniques.


**Fig. 1** Power conversion efficiency comparison of third generation solar cells: a-Si, DSSC, OPV and Omh-PSCs

The material's organic-inorganic hybrid nature is what makes Omh-PSCs so efficient. Firstly, the organic constituent offers good solubility to the Omh-perovskite and facilitates self-assembly together with its precipitation and/or deposition from solution. Secondly, the inorganic part provides a comprehensive network by covalent and/or ionic interactions, instead of the weaker forces such as Van der Waals or π-π interactions. Such strong interactions account for the accurate crystalline structure in the deposited films. Thirdly, powerful optical absorption is a means to attain an excellent performance and literature reports confirmed that Omh-perovskites of interest are direct-bandgap semiconductors. [9]

### 2.2 Mechanistic processes in Omh-PSCs

The basic energy diagram and elements of the mechanistic process of Omh-PSCs are represented in Fig. 2. The key idea behind efficient solar energy conversion is the combination of 'carrier generation' by light absorption and 'charge separation'. In the absorber perovskite, see Fig. 2 (a) electrons become undergo excitation. Fig. 2 (b) shows the electron transport layer (ETL) and hole transport layer (HTL),



Energy & Environmental Science Accepted Manuscript

both in contact with the Omh-perovskite. These electrons and holes are separated by an ETL that is conductive to electrons and rejects holes, and by a HTL that allows transport of the holes with no impedance, while blocking electrons, respectively. Such arrangements permit the Fermi level in the metal contacts to equilibrate with the separate Fermi levels of electrons and holes, generating an external voltage, and to extract the carriers giving a photocurrent in the external circuit.

The mechanistic processes in the device using mesoporous $TiO_2$ are still under debate[14], as Omh-perovskite materials combine both the functions of light absorption and n-type or p-type conduction. The present mechanistic representation is explained as follows: The Omh-perovskite absorbs light and an excited state (electron-hole pair) is produced. Charge separation can take place at the interface through two processes: injection of a photogenerated electron into a $TiO_2$ nanoparticle (Equation (1)), or hole injection into a HTL (Equation (2)).

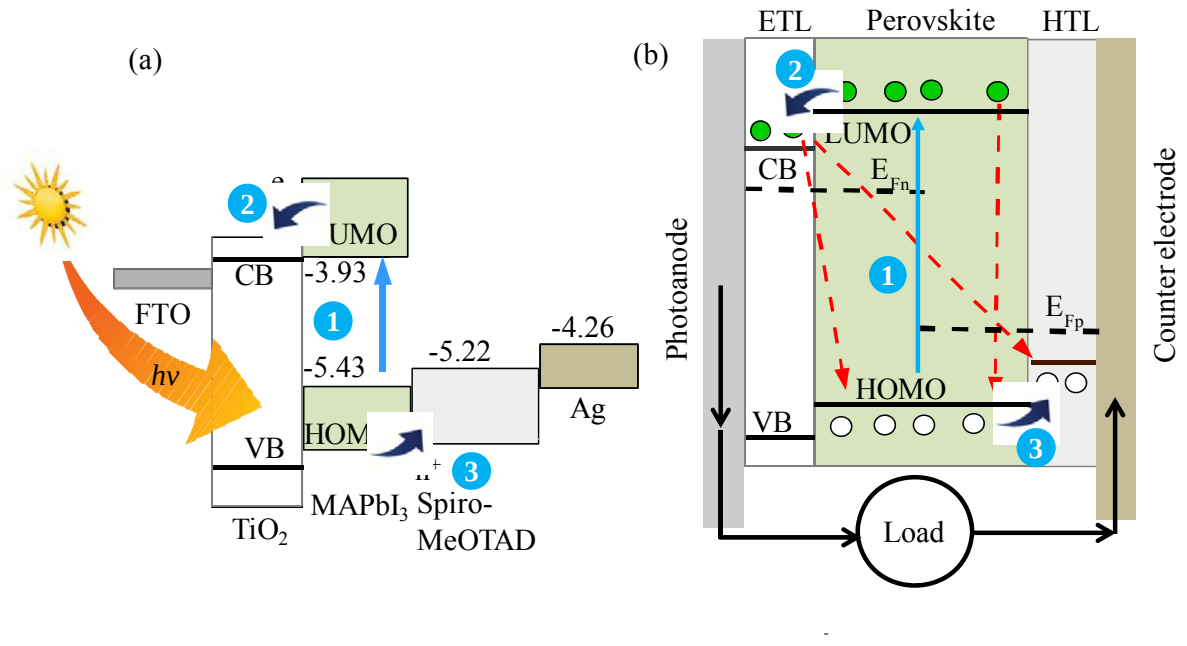


**Fig. 2** (a) Schematic representation of energy diagram in an oh-perovskite (1) generating electrons and hole carriers that rapidly relax (2) to the conduction band (EC) of ETL ($TiO_2$) and (3) to HOMO of HTL, respectively. (b) The scheme of main process in Omh-PSCs, formed by the Omh-perovskite absorber material, supplemented by two selective contacts, ETL and HTL.



Energy & Environmental Science Accepted Manuscript

Charge separation reactions are in kinetic competition with other reactions, such as exciton annihilation, and lead to photoluminescence (Equation (3)), recombination in perovskite (Equation (4)), as well as recombination of the charge carriers at the different interfaces (Equations (5), (6)). [14]

Electron injection:

$$e^-_{perovskite} + TiO_2 \rightarrow e^-_{TiO_2} \quad (1)$$

Hole injection:

$$h^+_{perovskite} + HTM \rightarrow HTM^+ \quad (2)$$

Luminescence:

$$e^-_{perovskite} + h^+_{perovskite} \rightarrow hv \quad (3)$$

Recombination in perovskite:

$$e^-_{perovskite} + h^+_{perovskite} \rightarrow \nabla \quad (4)$$

Recombination at interface:

$$e^-_{TiO_2} + h^+_{perovskite} \rightarrow \nabla \quad (5)$$

$$e^-_{perovskite} + HTM^+ \rightarrow \nabla \quad (6)$$

In Omh-PSCs solar cell, the incoming light is absorbed by the Omh-perovskite, which is anchored to the surface of $TiO_2$ nanocrystals. Theoretically, for efficient Omh-PSCs the Omh-perovskite absorber regeneration by HTM must happen more rapidly than electron recombination.

### 2.3. Current status of performance in Omh-PSCs

As an area of focus in Omh-PSCs devices, PCE is an important consideration when making comparisons with the more mature silicon technology. Besides the PCE and fabrication processes, there are at least two other factors that have an impact on the success of Omh-PSCs. These factors, which have been given relatively little consideration, are stability and cost.[8, 9, 15,16] Inorganic silicon-based solar cells may last approximately 25 years; so in this respect, Omh-PSCs devices must be improved to become technologically attractive, economically feasible and commercially practicable.

#### 2.3.1 Efficiency



Energy & Environmental Science Accepted Manuscript

Omh-perovskite materials were pioneered and studied, at first by Mitzi and co-workers[16-20], as active layers in light-emitting diodes and field-effect transistors. Different structures, i.e. 2D and 3D spatial distributions, of the Omh-perovskite materials were fabricated and their optoelectronic proprieties exploited in the fabrication of transistor and light emitting diodes.[20] Omh-PSC evolution efficiency is shown in Fig. 3. In 2009, Miyasaka and coworkers[21] demonstrated the potential of $CH_3NH_3PbI_3$ absorber in solar cell devices based on $TiO_2$ mesostructure photoanodes with a power conversion efficiency of 3.81%. The authors were attracted by its self-organizing potential in the nanoporous $TiO_2$ layer of the solar cell. Later, Etgar and coworkers[22] demonstrated that $CH_3NH_3PbI_3$ can act both as light harvester and HTM in a $CH_3NH_3PbI_3/TiO_2$ heterojunction device. A HTM-free solid state mesoscopic $CH_3NH_3PbI_3/TiO_2$ heterojunction solar cell was demonstrated with a PCE of 5.5% under standard AM 1.5 solar light of 1000 $W/m^2$ intensity and a PCE of 7.3% at a lower light intensity of 100 $W/m^2$.[22] The advent of such straightforward solution-processed mesoscopic heterojunction solar cell shows the way to low-cost, high-efficiency solar cells.

Among the Omh-perovskite-structure based semiconductors, $CH_3NH_3PbI_3$ is the most common one, and these perovskites have a tendency to possess high charge carrier mobility.[18, 20, 21, 23, 24] For an Omh-PSCs device, adequate mobility and high charge carrier lifetimes are important. Both Xing[25] and Stranks[26] confirmed that $CH_3NH_3PbI_3$ have relatively large diffusion lengths i.e. about 100 -130 nm for both electrons and holes which is higher value compared to other solution based processed semiconductors at low temperature.

Omh-perovskites absorbers have been used as light absorbers in liquid electrolyte–based photoelectrochemical cells with PCEs from 3.81[21] to 6.5%.[27] However, it will dissolve in the electrolyte, resulting in a fast performance decline. This degradation leads to the replacement of liquid electrolyte with solid hole transporter material(HTM) in 2012.[15,28] The HTM, spiro-MeOTAD originally produced for organic light emitting diodes (LEDs)[29] but was also found to be useful for solid state dye sensitized solar cells (ssDSSCs)[30] and boosted the reported efficiency (9.7%) for Omh-PSCs.[15] In the middle of 2012, other successes were reported using [28]. Firstly, mixed-halide $CH_3NH_3PbI_{3-x}Cl_x$, which displayed better stability and carrier transport than its pure iodide equivalent, was successfully used.[28,31] Secondly, coating nanoporous $TiO_2$ surfaces with a thin Omh-perovskite layer thereby forming extremely thin absorber solar cells. Thirdly, conducting nanoporous $TiO_2$ was



Energy & Environmental Science Accepted Manuscript

replaced by a similar but non-conducting $Al_2O_3$ insulator. This increased $V_{oc}$, raising the cell efficiency to 10.9%. Omh-perovskites have a broader potential due to their ambipolar properties. The fourth one is its ability to form simple planar device with the scaffolding totally removed.[31]

The cooperative work of Seok, Grätzel and colleagues led to a reported efficiency of 12.0%, using both optional layers, including a solid Omh-perovskite capping layer overlying the scaffolding (nanoporous $TiO_2$ infiltrated by Omh-perovskite).[32] Different HTMs were investigated including spiro-MeOTAD, with poly-triarylamine proving to be the best. Seok and coworkers further report another efficiency improvements of 12.3% with same structures and $CH_3NH_3PbI_{3-x}Br_x$.[33] Less than 10% of Bromine gave the best initial efficiency, because of its smaller band gap, but higher Br greater than 20% offered moisture stability. This is caused by structural transition from tetragonal to pseudo-cubic due to the smaller ionic radius of Br.[18] A PCE of 15.0% was reported from the Grätzel research group using a nanoporous $TiO_2/CH_3NH_3PbI_3$/spiro-MeOTAD/Au device architecture.[5] They used $TiO_2$ as scaffolding and a two-step method for perovskite absorber deposition, which improved the morphology.

Snaith and coworkers[34] illustrated a high PCE of 15.4% with an open-circuit voltage ($V_{oc}$) of 1.07 V and a short-circuit current density ($J_{sc}$) of 21.5 $mAcm^{-2}$ using mixed halide, $CH_3NH_3PbI_{3-x}Cl_x$ deposited as light absorber thin layer material with spiro-MeOTAD as the hole transporter. Furthermore, Seok and coworkers realized cell efficiency of 16.2% using the $CH_3NH_3PbI_{3-x}Br_x$ (10–15% Br) and a poly-triarylamine HTM.[35] Thickness ratio of perovskite-infiltrated $TiO_2$ scaffolding relative to the continuous perovskite layer was the key to the improved efficiency. This was increased to PCE of 17.9% in early 2014.[35] The efficiency of 19.3% in a planar geometry without antireflective coating was demonstrated by Yang and coworkers.[36] To improve the electron transport property, Y-doped $TiO_2$ has been successfully used as the mesoporous scaffold in perovskite solar cells. Recently, Seok and colleagues have developed a solar cell with an efficiency of 20.1%[10, 37] by combining the MA and FA (Formamidinium), as confirmed in November 2014, by the U.S. National Renewable Energy Laboratory. Similar to MA, FA is a small, positively charged molecule made of carbon, hydrogen, and nitrogen. But $FAPbI_3$ absorbs light further into the near infra-red, thereby potentially boosting the cells efficiency.[38] Despite accommodating a wide variety of cell designs and producing excellent PCEs, Omh-PSCs must first overcome a number of technical issues before widespread



Energy & Environmental Science Accepted Manuscript

commercialization is possible. These include scale-up of the cell area, the elimination of lead toxicity and lack of long-term device stability.[39] Efforts to address these shortcomings have begun to show promise, with ca. 1 $cm^2$ Omh-perovskite device producing efficiency as high as 8.3%[40] and lead-free Omh-PSCs being now reported.[41, 42]

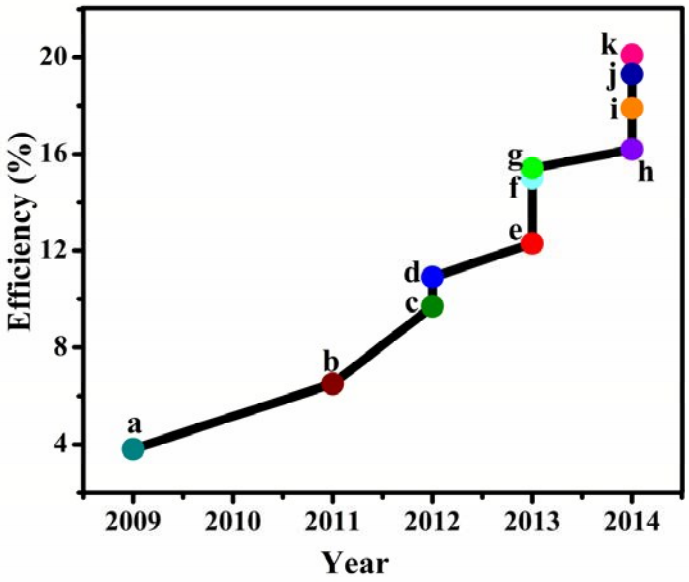


**Fig. 3** Efficiency Roadmap for Omh-PSC Devices: Efficiency values taken from publications and NREL's latest chart on record cell efficiencies.

Table 1 Summary of device structure and corresponding efficiencies for Omh-PSCs roadmap in Fig. 3

| Symbol | Device structure | Efficiency (%) | Ref. |
|---|---|---|---|
| **a** | Liquid Electrolyte/$CH_3NH_3PbI_3/TiO_2$ | 3.81 | [21] |
| **b** | Liquid Electrolyte/ $CH_3NH_3PbI_3$ QD/$TiO_2$ | 6.5 | [27] |
| **c** | Spiro-MeOTAD /$CH_3NH_3PbI_3$/ mesoporous$TiO_2$ | 9.7 | [15] |
| **d** | Spiro-MeOTAD /$CH_3NH_3PbI_2Cl$/mesoporous $Al_2O_3$ | 10.9 | [28] |



Energy & Environmental Science Accepted Manuscript

| | | | |
|---|---|---|---|
| **e** | PTAA/$CH_3NH_3PbI_{3-x}Br_x$ /mp-$TiO_2$ | 12.3 | [33] |
| **f** | Spiro-MeOTAD/$CH_3NH_3PbI_{3-x}Cl_x$/$TiO_2$, 2-step solution deposition | 15.0 | [5] |
| **g** | Spiro-MeOTAD /$CH_3NH_3PbI_{3-x}Cl_x$/$TiO_2$, evaporated thin film p-i-n architecture | 15.4 | [34] |
| **h** | PTAA/$CH_3NH_3PbI_{3-x}Br_x$ /mesoporous$TiO_2$ | 16.2 | [35] |
| **i** | PTAA/$CH_3NH_3PbI_{3-x}Br_x$ /mesoporous$TiO_2$ | 17.9 | [35] |
| **j** | Spiro-MeOTAD /perovskite/Yttrium-doped $TiO_2$ | 19.3 | [36] |
| **k** | PTAA/$(FAPbI_3)_{1-x}(MAPbBr_3)_x$/mesoporous-$TiO_2$ | 20.1 | [10, 37] |

### 2.3.2 Stability

The current highest PCE reached by Omh-PSCs is 20.1% and, while low stability, it is by no means a barrier to application in many situations. The major obstacle is the relatively short lifetime achieved with current technology. To bring Omh-PSCs onto the market, in addition to higher efficiencies and cost-effective processing, long device lifetime will be necessary. In 2011, the devices were only stable for 10 minutes before degradation (about 80% degradation)[27] because $CH_3NH_3PbI_3$ QDs tend to dissolve gradually into the redox electrolyte (unstable in iodide-containing liquid electrolyte, due to rapid dissolution). In 2012, stability was remarkably improved from minutes to over 500 hrs by using spiro-MeOTAD based solid-state Omh-PSCs device.[15] This improvement is attributed to the discovery of solid hole conductor.[33] Fig. 4 shows effect of moisture on stability of heterojunction like Omh-PSCs solar cells made of $MAPb(I_{1-x}Br_x)_3$. The device was maintained at 35% humidity, stored in air at room temperature and intentionally exposed to a humidity of 55% for one day on the fourth day. This device showed enhanced stability at low humidity (<50%). On the other hand, device stability began to reduce at relatively high humidity (≥55%). This might be due to degradation of $MAPb(I_{1-x}Br_x)_3$ material.[33] The performance of this device is more stable after 20 days at values of x=0.2 and x=0.29 compared to the values of x=0 and x= 0.06. Thus, an appropriate atomic ratio of the



Energy & Environmental Science Accepted Manuscript

halide anions is an important implication for improving the stability.[33]

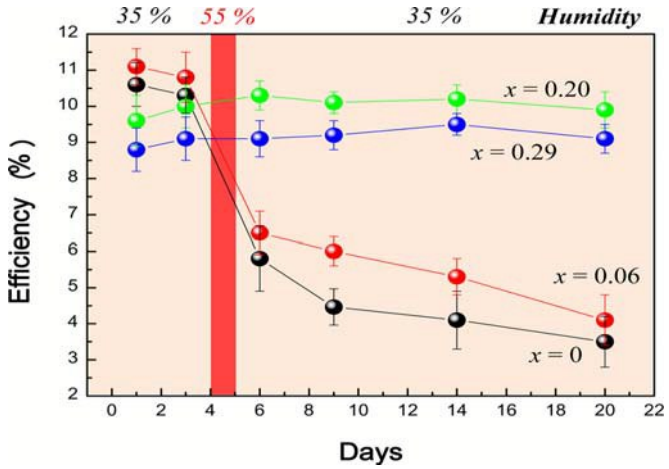


**Fig. 4** Moisture effect on stability of heterojunction solar cells based on $MAPb(I_{1-x}Br_x)_3$. Reprinted with permission.[33]Copyright 2013 American Chemical Society.

Since $CH_3NH_3PbI_3$ films is not stable in humid atmosphere, controlling environmental conditions and moisture level less than 1% are recommended for device preparation.[5] Moreover, a sealed device subjected to long-term light soaking at a light intensity (100 $mWcm^{-2}$) and a temperature of 45 ˚C showed a promising stability and maintained more than 80% of its initial PCE after a period of 500 hrs.[5] The device was prepared under argon filled glovebox and maintained at the optimal electric power output during the ageing using maximum power-point tracking.

It is obvious that meso-porous $TiO_2$ free solar cells are significantly much flexible to UV irradiation compared to $TiO_2$ based solar cells. The performance of $TiO_2$ based devices is limited to only 5 hrs stability due to its fast decay in photocurrent and a small decay in photovoltage when tested in ambient conditions.[6] Opposing to the behaviors of $TiO_2$-based solar cells, the photocurrent become stable nearly at 15 $mAcm^{-2}$ for over 1,000 hrs in $Al_2O_3$-based Omh-perovskite solar cell.[6] Fig. 5 shows the stability test of meso-super structured $Al_2O_3$-based Omh-perovskite solar cell (MSSC) exposed to continuous simulated AM 1.5 76.5 $mWcm^{-2}$ illumination at 40 $^0$C. The FF and $V_{oc}$ started to drop in the first 200 hrs experience and this initial decline may be because of different factors such as: oxygen desorption at vacancy sites on the compact $TiO_2$ layer, partial de-doping of the spiro-MeOTAD,[43] modifications at the spiro-MeOTAD/Au interface, or slight modifications within the Omh-perovskite.



Energy & Environmental Science Accepted Manuscript

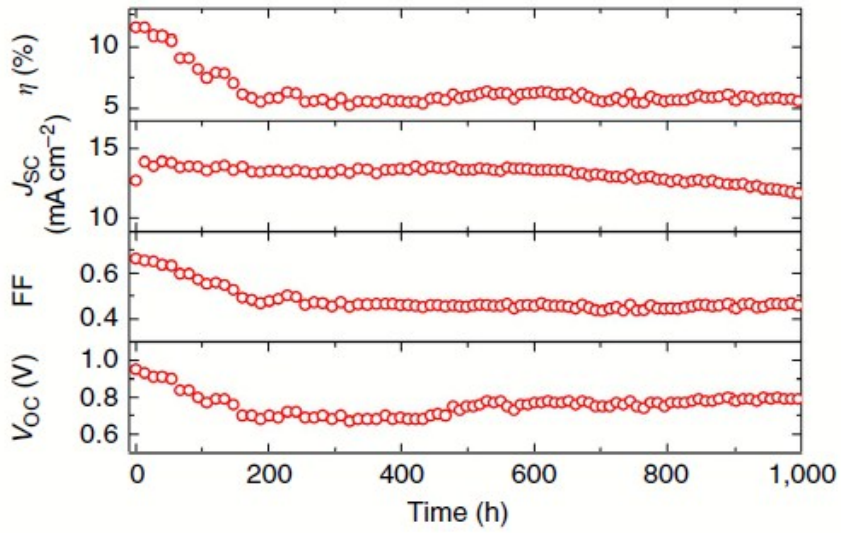


**Fig. 5** Stability test of mesoporous $TiO_2$-free solar cell device. Reprinted with permission.[6]

Kwon and co-workers[44] reported the *ex-situ* long-term stability of Omh-PSCs using three HTMs, spiro-MeOTAD, P3HT and Poly[2,5-bis(2-decyl dodecyl) pyrrolo [3,4-c]pyrrole-1,4(2H,5H)-dione-(E)-1,2-di(2,20-bithiophen 5-yl)ethene](PDPPDBTE) under a 20% humidity atmosphere for over 1000 hrs. The PCE of the spiro-MeOTAD based device slowly reduced when the ageing period was extended. The device showed a 28% decrease of PCE in relation to the early PCE. Furthermore, the stability of the PDPPDBTE cells improved remarkably, and the initial performance was retained at an 8.4% PCE after 1000 hrs. The improved stability may be because of its hydrophobic behaviours, which avoided water flow into the Omh-perovskites. Moreover, the solar cell stability of mixed halide perovskites, $MAPb(Br_xI_{1-x})_{3-y}Cl_y$, grown on nanostructured-$TiO_2$ and in thin film configuration, was monitored to study cell stability as a function of the halide composition.[45] Hence, the stability of Omh-PSCs devices has been limited, mainly due to ambient moisture because alkylammonium salts are, in general, highly hygroscopic. Interestingly, the insertion of bromine into the Omh-PSC structure benefits cell stability.[34] Those cells without bromine show an efficiency drop of 20%, 30 days after preparation, ascribed mainly to a decrease in the FF. However, the equimolar Br/I devices showed a significant enhancement with 37% PCE.[45]

This improvement could be a consequence of the rearrangement of the Omh-PSCs 3D configuration



Energy & Environmental Science Accepted Manuscript

over time. In particular, the efficiency improvement may be attributed to the insertion of the smaller bromine anions, leading to a more compact Omh-PSCs structure in which the degradation of the MA cation is prevented.[45] Therefore, a deeper analysis including microstructural and crystallographic studies must be performed to elucidate the origin of this observation. Recently, it has been pointed out that the presence of nano-structured $TiO_2$ changes the crystalline properties of synthesized Omh-PSCs, affecting the photoluminescence behavior.[46-48] In addition, recombination effects should be also expected, but further research is needed to correlate the observed changes in recombination with the crystalline properties of Omh-perovskite samples.

Han and co-workers[4] applied solution drop-casting method to fabricate novel device where its scaffolding made of double layer of $TiO_2$ and $ZrO_2$ enclosed in a porous carbon film. The resulting mixed cation Omh-perovskite showed higher electrical charge efficiency than conventional (planar) Omh-perovskite cells. The triple layer also resulted in better surface contact, leading to a considerably higher stability of 1008 hrs in direct sun exposure. It was also shown that devices with mesoporous $TiO_2/CH_3NH_3PbI_3/C$ architectures, without encapsulation, had stabilities of over 2000 hrs in air in the dark.[7] The stability evolution for Omh-PSCs is shown in Fig. 6.

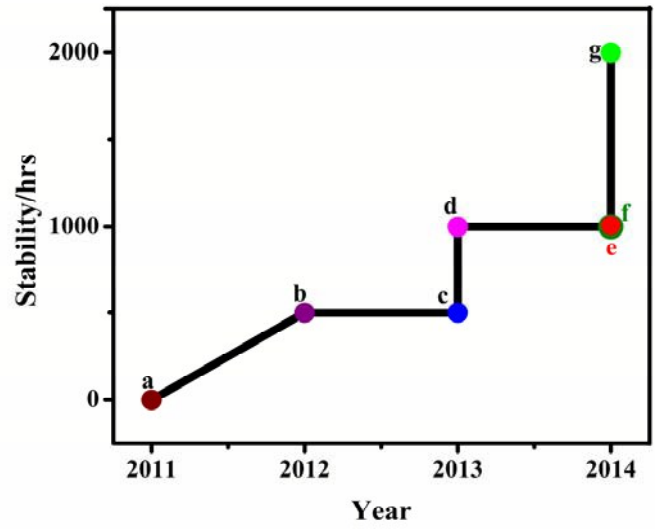


**Fig. 6** Roadmap in stability for Omh-PSCs made from Omh-perovskite absorbers

The ability to process carbon electrodes at low temperatures on top of the $CH_3NH_3PbI_3$ layer without destroying its structure not only reduces costs and simplifies the fabrication procedures but also



Energy & Environmental Science Accepted Manuscript

improve device stability.

Table 2 Summary of device architecture and its stability for Omh-PSCs based on the roadmap in Fig. 6

| Symbol | Device structure | Stability /hrs | Conditions | | | Ref |
|---|---|---|---|---|---|---|
| | | | Temp | Atmosphere | H | |
| a | $TiO_2/CH_3NH_3PbI_3QD$/liquid electrolyte/Pt[k] | 0.17 | RT | Air | - | 27 |
| b | $TiO_2/CH_3NH_3PbI_3$/ spiro-MeOTAD/Au[k] | 500 | RT | Air | - | 15 |
| c | $TiO_2/CH_3NH_3PbI_3$/ spiro-MeOTAD/Au[m] | 500 | 45 ˚C | Ar gas | <1% | 5 |
| d | $Al_2O_3/CH_3NH_3PbI_{3-x}Cl_x$/spiro-MeOTAD/Au[m] | 1000 | 40 ˚C | $N_2$ atmosphere | - | 6 |
| e | $TiO_2/CH_3NH_3PbI_3$/PDPPBTE/Au[k] | 1000 | RT | Air | 20% | 44 |
| f | $TiO_2/ZrO_2/(5\text{-AVA})_x(MA)_{1-x}PbI_3$/ C [k] | 1008 | RT | Air | - | 4 |
| g | M-$TiO_2$/ $CH_3NH_3PbI_3$/C[k] | 2000 | RT | Air | - | 7 |

[m]encapsulated, [k]not encapsulated device, Temp = temperature, H= Humidity, RT = room temperature

Although some improvements have been made in the stability of Omh-PSCs, stability issues are not yet well-addressed. The major issue pertaining to the commercialization of an Omih-PSCs solar device is mainly its stability. Not only issues of ambient stabilities with respect to moisture, temperature, light and oxygen, but also issues concerning intrinsic stabilities at the interface, together with questions related to the device's architecture remain as major obstacles to practical applications. All these stability issues or obstacles are the main focus of this review article and will be discussed separately in the following sections.

## 3. Causes of failure and associated mechanisms of degradation



Energy & Environmental Science Accepted Manuscript

The formation of Omh-perovskite materials depends on the chemical composition of the precursor; reaction controlling parameters, such as temperature and pressure of the system. Dualeh and co-workers proposed that at lower temperature, the conversion to the Omh-perovskite dominates following Equations (7-9)[49] however, at higher annealing temperature, there is additional formation of $PbI_2$ (Equation (8)).[50]

$$PbCl_2 + 3CH_3NH_3I \rightarrow CH_3NH_3PbI_3 + 2CH_3NH_3Cl \quad (7)$$

$$PbCl_2 + 3CH_3NH_3I \rightarrow PbI_2 + CH_3NH_3I + 2CH_3NH_3Cl \quad (8)$$

$$CH_3NH_3PbI_3 \rightarrow PbI_2 + CH_3NH_2 + HI \quad (9)$$

It has been confirmed that $CH_3NH_3PbI_3$ crystal lattice do not decompose up to 300 °C, after which the organic constituent rot, governed by Equation (9).[24, 32] However, recent studies show that $CH_3NH_3PbI_3$ begins to transform to $PbI_2$ at lower temperature upto 140 °C.[50] The excess organic $CH_3NH_3Cl$, formed in this reaction, is believed to sublime, leaving only the $CH_3NH_3PbI_3$ on the mesoporous $TiO_2$ film as observed from XRD measurements.[51] The rate of sublimation of the organic species $CH_3NH_3Cl$ increases with temperature, as does the precursor $CH_3NH_3I$, thus driving Equations (7) and (8). From these measurements it is evident that the formation of the Omh-perovskite films is a multistage process, comprising solvent vaporization, perovskite crystallization and the sublimation of excess organic $CH_3NH_3Cl$. These processes occur simultaneously and their relative rates determine the composition and morphology of the final film.

The release of chlorine-containing compound(s) clearly suggests the formation of crystalline $MAPbX_3$ films. Thus, it is vital to realize the potential chemical reaction mechanisms for the formation process of $MAPbX_3$. Dualeh and co-workers anticipated that Equation (10) dominates the annealing process.[51] However, Zhao noted that the initial $CH_3NH_3I$ and $PbCl_2$ behaves white and solution mixture appears to be light yellow color, indicating that a chemical reaction should take place forming a new phase.[49] Hence, Equation (10) possibly will engage numerous intermediate steps.



Energy & Environmental Science Accepted Manuscript

$$PbCl_2 + 3CH_3NH_3I \rightarrow CH_3NH_3PbI_3 + 2CH_3NH_3Cl\,(g) \quad (10)$$

$$PbCl_2 + 3CH_3NH_3I \rightarrow PbI_2 + CH_3NH_3I + 2CH_3NH_3Cl \quad (11)$$

$$PbI_2 + 3CH_3NH_3I + 2CH_3NH_3Cl \rightarrow CH_3NH_3PbI_3 + 2CH_3NH_3Cl\,(g) \quad (12)$$

$$PbI_2 + xCH_3NH_3I + yCH_3NH_3Cl \rightarrow (CH_3NH_3)_{x+y}PbI_{2+x}Cl_y \ \text{(intermediate phase)}$$

$$\rightarrow CH_3NH_3PbI_3 + 2CH_3NH_3Cl\,(g) \quad (13)$$

Firstly, since the molar amount of $CH_3NH_3I$ is 3 times that of $PbCl_2$, Equation (11) is proposed, where part of $CH_3NH_3I$ reacts with $PbCl_2$ to form $PbI_2$. As a result of Equation (11), the spun film contains mixed phases of $PbI_2$ (appears in light yellow), $CH_3NH_3I$, $CH_3NH_3Cl$, and possibly some unreacted $PbCl_2$. During annealing two reaction processes may occur: 1) For Equation (12), $CH_3NH_3I$ reacts with $PbI_2$ to form the dark brown $CH_3NH_3PbI_3$; meanwhile, the excess $CH_3NH_3Cl$ break away from the film. The question how excess $CH_3NH_3Cl$ escape from the film remains unclear, but different literatures reported as either sublimation or decomposition.[52] 2) During the early stage of annealing or during spin coating, an intermediate phase may appear as indicated in Equation (13). In this case, during the decomposition of this intermediate phase the $CH_3NH_3PbI_3$ crystal network can grow, during which the driving force can be the release of gaseous $CH_3NH_3Cl$ (or other organic chlorides).[49]

Despite the understanding of formation of Omh-perovskite materials for solar cell use, full advantage, of these materials and their device are still not realized due to the presence of unsolved problems. One typical example is lack of clear understanding on the mechanism of active material and device degradations which controls the essential processes; like device life time and mechanical stability of Omh-PSCs panels. For successful development of Omh-PSCs, it is essential to understand the degradation behaviour of Omh-perovskite and device in general. Study of Omh-perovskite degradation behaviour is pre-requisite for Omh-PSCs applications. Such degradations can be linked to extrinsic (oxygen, light, moisture and temperature) induced and intrinsic (thermal and electric field) induced degradations. Fig. 7 shows a general scheme representing recombination process at mesoporous $TiO_2$, moisture dissolution of Omh-perovskite and photooxidation processes take place at the interface between HTM and the counter electrode. Diffusion of $O_2$ is gradually sped up by UV light in the presence of $TiO_2$. The produced oxygen free radicals can then react with HTM and/or active Omh-perovskite materials. $H_2O$ is also readily activated by oxygen and light in the presence of organic molecules. Moreover, molecular oxygen and moisture may flow through the tiny pinholes



Energy & Environmental Science Accepted Manuscript

present in the counter electrodes as represented in Fig. 7. Omh-perovskite materials such as $CH_3NH_3PbI_3$ and $CH_3NH_3PbBr_3$ are prone to chemical attack, thus devices typically degrade in a matter of minutes to hours under 1000 $Wm^{-2}$ illumination in the ambient atmosphere. However, the impacts of these parameters that decrease or increase the degradation rate are not exactly clear. The objective of this section is to draw the extrinsic and intrinsic degradation phenomena and associated degradation mechanisms of Omh-perovskite materials and Omh-PSCs devices when built-in in photovoltaic systems and to review the various factors influencing the Omh-perovskite materials and Omh-PSCs stability.

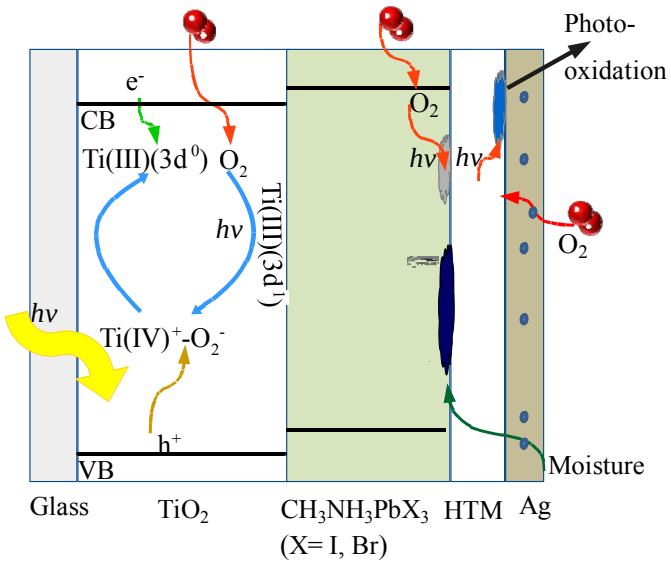


**Fig. 7** General schematic representation of hole-electron pair recombination, moisture dissolution of Omh-perovskite and photooxidation processes at the interface between HTM and counter electrode.

### 3.1. Oxygen induced degradation

An important for the operation of any device is being stable in air without the use of any type of encapsulation. The rationale behind is that every group of materials in a device that realizes ambient stability will address an input to future improvement. Yang and co-workers compared devices stored in dry air and under nitrogen atmospheres and showed that degradation of the Omh-perovskite materials occurred in ambient air – thereby, highlighting the need for protection.[36] The diffusion of molecular oxygen can be activated by UV illumination in the presence of organic molecules,[53-55] which promote the formation of peroxide or superoxide compounds that attack and degrade the active



Energy & Environmental Science Accepted Manuscript

layers.[56]

The defect chemistry of the n-type semiconducting oxide gives rise to the curious behavior of fast device decline, which is primarily introduced by oxygen vacancies and interstitial defects, resulting in a non-stoichiometric composition ($TiO_{2-x}$). Two under-coordinated Ti (III) and one oxygen vacancy is generated when bridging oxygen atoms become eliminated. The elimination of bridging oxygen atoms from the lattice frequently results from thermal annealing. Because of their unsaturated co-ordination the generated under-coordinated Ti (III) and oxygen vacancy are reactive and adsorb $O_2$ molecules to form Ti $(IV)^+$ - $O_2^-$ complex.[57] Among various types of adsorbed oxygen ($O^+$, $O_2^-$, $O^-$), superoxide radical, ($O_2^-$) is thermodynamically stable and electron is transported to the adsorbed oxygen from the $TiO_{2-x}$ surface.[58] Likewise, formation of $O_2^-$ can take place through a different reaction if electrons are available in excess in sub-bandgap states or CB,[57] i.e. Ti(IV) + e*CB* + $O_2 \rightarrow$ $Ti(IV)^+$ $O_2^-(\alpha)$. Fig. 8 represents formation of deep trap states and depletion area as a result of oxygen adsorption and desorption processes at the mesoporous $TiO_2$. In Omh-PSCs, formation of Ti(III) ($3d^1$) trap state is due to transfer of one electron to the Ti (IV) ($3d^\circ$) of $TiO_2$ from the perovskite. Thus, the electron easily transfers in to Ti (IV) from Ti (III) because of smaller bandgap between Ti(III) and Ti(IV). Those under-coordinated Ti (III) generated due to oxygen vacancy reside in sub-band gap states and work as deep trap sites. Furthermore, it attracts molecular oxygen in an ambient conditions, resulting in formation of $\alpha(Ti(IV)^+O_2^-(ads))$.[57, 59, 60] Likewise, electrons in sub-band gap states may create $\beta(Ti(IV)^+O_2^-(ads))$. These modified states do not interfere with the device's performance when illuminated. The formation of depletion layer can be as a result of the positive potential at the $TiO_2$ surface, caused by the presence of $O_2^-$. [6, 61] Devices continuously illuminated at high temperatures deteriorate. Changing the α superoxide complex to a Ti(III) and liberating $O_2$ may take place when photo-excitation of the mesoporous $TiO_2$ results in the formation of electron-hole pairs through which holes in the VB trapped with $O_2^-$ in the $Ti(IV)^+O_2^-$ as shown in Fig. 8(b). The corresponding free electron in the conduction band (CB) is then trapped at the regenerating deep trap site and will ultimately recombine with an excess hole in the spiro-MeOTAD as shown in Fig. 8(c). An adsorbed negative charge may result in increasing the depletion area, thereby creating an upward bend in the CB that diminishes interfacial charge carrier recombination. In addition, $O_2$ desorption upon illumination diminishes this upward band bending and hence results in the disappearance of the Schottky barrier, a flattening of the CB-edge and a lowering of the Fermi level[62, 63] as shown in Fig.



Energy & Environmental Science Accepted Manuscript

8(d). Oxygen-induced defects in $TiO_2$ are the major reasons to cause device degradation during operations. [64,65]

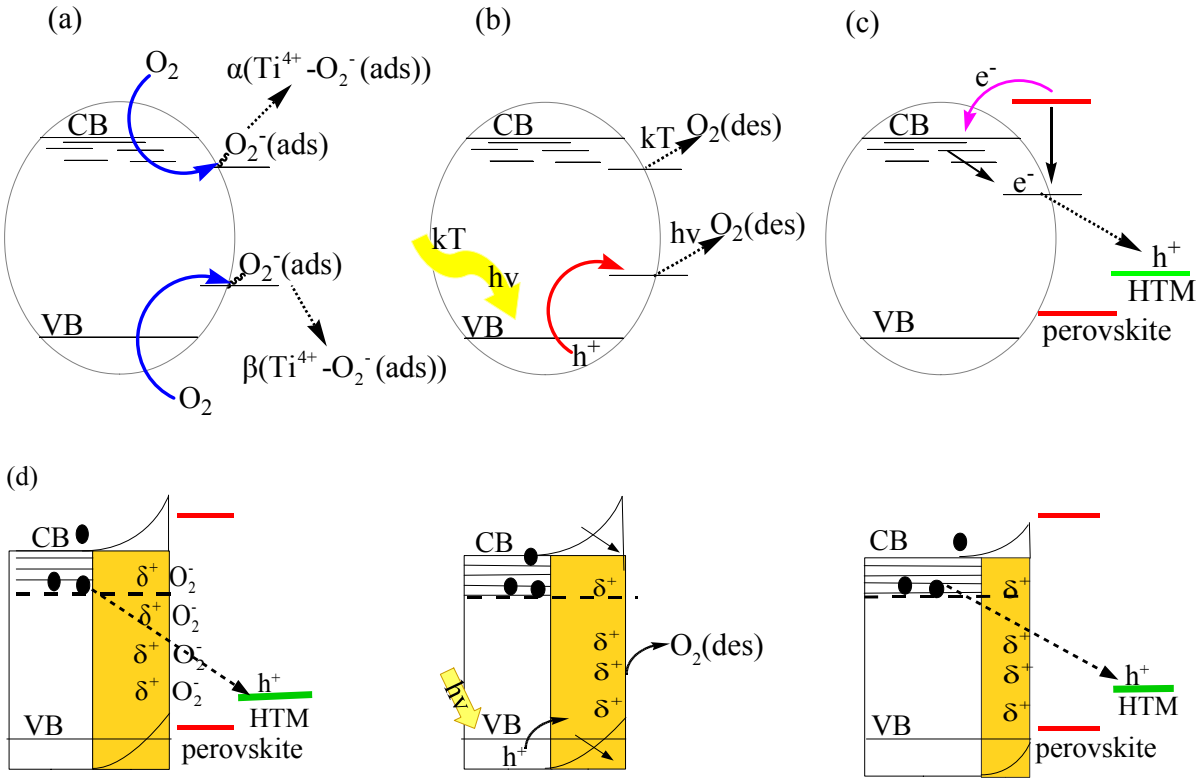


**Fig. 8** Oxygen induced formation of deep trap states and depletion area at mesoporous $TiO_2$ surface and interface: (a), (b), and (c) The patterning of superoxide, α and β $(Ti(IV)^{+}\text{-}O_2^{-})$. (d) Desorption of negatively charged superoxide molecules and their impact on the depth of depletion zone (orange shaded area).

### 3.2 Light induced degradation

UV illumination can diminish the performance of Omh-PSCs upon exposure during long-term operation due to the generation of many possible fading processes. Electron recombination thereby creating localized trapping sites and, diminishing the depletion layer and $TiO_2$ band excitation. This may lead to oxidation of halogen in the Omh-perovskite or HTM occurring due to UV illumination. Of course, it should be recognized that there are other sources of degradation besides UV light, e.g. oxidation, heat and ordinary visible light. UV illumination is in many cases the major cause of degradation and is of great concern, making it necessary to use stable and broadly absorbing UV



Energy & Environmental Science Accepted Manuscript

materials in order to protect both the light absorber and the substrate-by either initiating a decomposition that proceeds by another mechanism such as oxidation, or by directly absorbing UV energy.

UV-induced degradation mechanisms can be explained by considering the surface chemistry of $TiO_2$. Mesoporous $TiO_2$ incorporates surface trapping states or defects ($Ti^{3+}$), functioning as efficient deep electron-releasing states,[66, 67] the electrons in these localized trapping states,[68] bind with $O_2$ molecule from the environment, adsorbing the trapping states,[69-72] generating a complex of $O_2^-$–$Ti^{4+}$.[71-73] Hence, the adsorption process is responsible for the photocurrent degradation caused by adsorption of oxygen on $TiO_2$ surfaces,[66, 67, 69-73] Upon bandgap excitation of $TiO_2$, the hole in the VB recombine with the electron at the oxygen adsorption site. This creates an electron-hole pair and desorbs oxygen.[61, 72] The excess holes in the HTM will gradually rebound with the unbound electron remain from the $E_g$ excitation of the Titania.[53,74, 75] The holes in spiro-MeOTAD recombine the trapped electrons.[76-78] At steady-state, the partial pressure of oxygen within deep trap sites governs the quantity of unfilled oxygen vacancy states. This is because of sluggish and reversible desorption rate of oxygen.[72, 73]

In the Omh-PSCs, the inorganic $Pb^{2+}$-$X^-$ creates a well ordered inorganic matrix which successfully absorbs and re-emits light. Thus, UV illumination of the local environment of Pb-X bond could generate halogen free radicals and break down the perovskite into dihalogens ($I_2$, $Br_2$, and $Cl_2$). Therefore, oxidation induced halogen elimination may be one possible reason for degradation of the Omh-PSCs. Likewise, light exposed $MAPbI_3$ leads to an irreversible breakdown into $PbI_2$.[51, 79, 80]

### 3.3 Moisture induced degradation

Moisture is one of the mainly vital degradation reasons that diminish PCE of unencapsulated Omh-PSCs solar devices. Seok and co-workers[33] suggested that moisture degrades the PCE of unencapsulated Omh-PSCs solar devices causing device fading and recommended that the fabrication of Omh-PSCs to be in a controlled atmosphere with humidity of <1%.[5] Besides, a proper humidity level (30 ±5% relative humidity) is essential for high quality films, enhanced optoelectronic properties, and improved mass transport processes.[36] For instance, the $CH_3NH_3PbI_{3-x}Cl_x$ film grown at 30% relative humidity in air had improved optoelectronic properties compared with a film grown in dry conditions. Moreover, You and coworkers[81] reported significant improvement in film morphology



Energy & Environmental Science Accepted Manuscript

when Omh-perovskite precursor films were annealed in ambient air (humidity of 35% ±5%) compared to films annealed in a nitrogen filled glovebox with $O_2$ and $H_2O$ level lower than 5 ppm. The latter annealing process results in a pristine film with a grain size of 100–300 nm, and apparent pin holes and grain boundaries. [81]

These pin holes and grain boundaries introduce 'energetic disorder' that impedes charge transport, induces recombination, and lowers photovoltaic performance.[82] Omh-perovskite films annealed in ambient air, however, give larger individual crystal and grain sizes (beyond 500 nm), as well as reduced pin-holes and grain boundaries.[81,82] This indicates that moisture-assisted crystal growth induces grain boundary creep as a result of the absorption of moisture within the grain boundaries and then merging adjacent grains together. Consequently, this effectively increases grain size, avoids pinhole formation and finally improves the carrier lifetime.[81,82] Additionally, the adsorbed water molecule could undergo auto-ionization at the surface into hydroxyl and proton ions. As a result surface $OH^-$ sites may be formed between which protons may migrate and act as charge carrier. Thus, it would be interesting to investigate the contribution of these ions into the mass transport processes and optoelectronic properties. Furthermore, You and co-workers[81] systematically studied the effect of the moisture level (20%–80% humidity) on Omh-perovskite film formation. Omh-perovskite films annealed above 80% humidity showed a small amount of $PbI_2$ phase present in the crystals, indicating Omh-perovskite film decomposition to $PbI_2$ at higher humidity levels. While moisture is beneficial for high quality Omh-perovskite film growth, the relative amount should be carefully controlled.[81]

Moisture degradation of the Omh-perovskites may be correlated with the transformation of $MAPbI_3$ to its MAI salt and metal halides, hence metal halide removal may also cause Omh-PSCs device degradation. Wang and co-workers[83] reported that during the process of assembling and testing, moisture in the atmosphere can directly degrade these materials as indicated by the XRD pattern for films of $TiO_2/CH_3NH_3PbI_3$ and $TiO_2/CH_3NH_3PbI_3/Al_2O_3$ in Fig. 9. They proposed that first step in Omh-perovskite decomposition is the reversible deprotonation of the MA cation by water, forming methylamine, hydrated HI, and $PbI_2$. If this hypothesis is correct, one would expect that the volatile $CH_3NH_2$ would be rapidly flushed from the headspace of the *in-situ* sample holder, meaning the process would be unlikely to be reversible. Given the apparent reversibility in the bulk powder, thin films would also display a similar reversible conversion to the hydrate phase. Furthermore, the



Energy & Environmental Science Accepted Manuscript

exposure of $CH_3NH_3PbI_3$ to moisture produce a hydrate product rather than simply resulting $PbI_2$.[84]

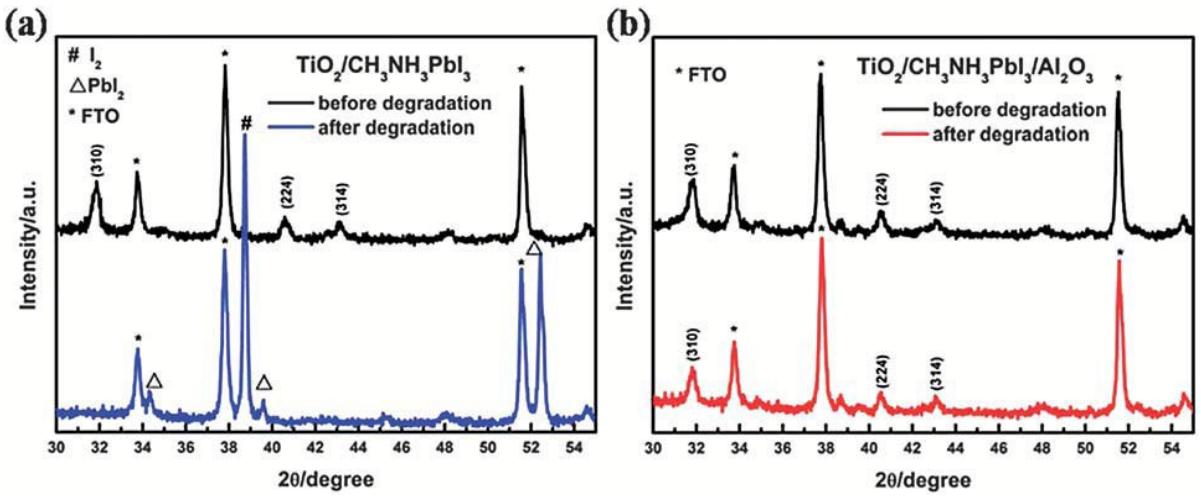


**Fig. 9** XRD patterns of film of (a) $TiO_2/CH_3NH_3PbI_3$ before and after degradation. (b) $TiO_2/CH_3NH_3PbI_3/Al_2O_3$ before and after degradation. Reproduced from Ref. 83 with permission from The Royal Society of Chemistry.

In the past, Vincent and coworkers were able to study $(CH_3NH_3)_4PbI_6{\cdot}2H_2O$, which forms readily by the addition of aqueous $Pb(NO_3)_2$ to an aqueous solution of $CH_3NH_3I$.[85] In contrast to the perovskite crystal structure of $CH_3NH_3PbI_3$, the crystal structure of $(CH_3NH_3)_4PbI_6{\cdot}2H_2O$ consists of an assembly of $PbI_6^{4-}$ octahedral and $(CH_3NH_3{\cdots}H_2O{\cdots}H_3NH_3C)_2^{4+}$ dimmers arranged on a distorted NaCl-type lattice.[85] This unique structure creates a zero-dimensional network of isolated $PbI_6$ octahedra, as opposed to the extended three-dimensional network observed in $CH_3NH_3PbI_3$. Similarly, $(CH_3NH_3)_4PbI_6{\cdot}2H_2O$ is a pale yellow crystalline solid, and it has been suggested that the conversion from $CH_3NH_3PbI_3$ to $(CH_3NH_3)_4PbI_6{\cdot}2H_2O$ can occur in humid air.[79] Similarly, Kelly and co-workers reported further evidence for this intermediate product using a more systematic investigation of Omh-perovskite degradation processes except where they found $PbI_2$ as ultimate product.[86] The formation of a hydrated intermediate containing isolated $PbI_6^{4-}$ octahedra as the first step of the degradation mechanism strongly suggests that the initial step of the Omh-perovskite decomposition process is not an acid-base reaction of the MA cation, but rather hydration of the Omh-perovskite film (as illustrated in Equation (14) with $(CH_3NH_3)_4PbI_6.2H_2O$, although other hydrate compositions may be possible):[86]

$$4CH_3NH_3PbI_3 + 2H_2O \rightleftharpoons (CH_3NH_3)_4PbI_6.2H_2O + 3PbI_2 \quad (14)$$



Energy & Environmental Science Accepted Manuscript

Since Equation (14) does not produce any volatile byproducts, it would be expected to be at least partially reversible; however, given the propensity of $PbI_2$ to crystallize and phase separation, the process is unlikely to be fully reversible. The formation of hydrated intermediates containing isolated $PbI_6^{4-}$ octahedral as the first step in the decomposition process at 98 ± 2% RH and further decomposition of $CH_3NH_3I$ to $CH_3NH_2$ and HI would ultimately leave $PbI_2$ as the only byproduct of the reaction.[86] Similarly, density functional theory analysis confirms that moisture degrades the Omh-perovskite structure because it weakens hydrogen bonding between the $PbI_6$ octahedra and methyl ammonium cation.[87] While previous studies proposed $(MA)_4PbI_6.2H_2O$ as the first moisture degradation product,[84,86] Leguy and co-workers, recently, confirmed that the first hydrate produced is monohydrate, $MAPbI_3{\cdot}H_2O$ rather than the dihydrate ($(MA)_4PbI_6 .2H_2O$). $(MA)_4PbI_6.2H_2O$ can be produced upon additional hydration of $MAPbI_3{\cdot}H_2O$, as revealed in (Equation (15)). [88]

$$4\left(CH_3NH_3\right)PbI_3 + 4H_2O \rightleftarrows \left[4\left(CH_3NH_3\right)PbI_3.H_2O\right] \rightleftarrows \left(CH_3NH_3\right)_4 PbI_6.2H_2O + 3PbI_2 + 2H_2O \quad (15)$$

The formation of $MAPbI_3{\cdot}H_2O$ can be a reversible process and form crystalline $MAPbI_3$ when it is dehydrated. Primary confirmation recommends that even photovoltaic performance could be restored using dehydration.[88] In contrast, exposure to excess water consequences in an irreversible change into $PbI_2$ and leads to the complete dissolution of the $MAPbI_3$ layer ultimately.[89] These results help elucidate fundamental decomposition pathways in Omh-perovskite films, which should lead to more stable materials and more commercially viable devices. It is, therefore, important to figure out the thermodynamic and kinetic merits of these degradation mechanisms. Moreover, the chemistry of moisture degradation still requires further more detail computational and experimental evidences in order to rationalize and establish clear moisture degradation mechanisms.

### 3. 4 Temperature induced degradation

Increasing the annealing temperature, from 40 ˚C to 100 ˚C for 30 min, improved the performance of perovskite QD-sensitized $TiO_2$ film.[21] However, further increasing the annealing temperature from 100 ˚C to 160 ˚C diminished the efficiency from 4.73% to 3.71%, due mainly to the decay in photocurrent density. External quantum efficiency (EQE) spectra showed that the decreased



Energy & Environmental Science Accepted Manuscript

photocurrent density with high temperature treatment (160 ˚C) is attributed to a significant loss in EQE in the long wavelength region (above 500 nm). Both the annealing temperatures and the storage temperature are important parameters that may cause Omh-PSCs device degradation as shown from Table 2. Though there is no literature report, it is clear that Omh-PSCs devices need to pass tests such as thermal stress tests at 80 ˚C, run for 1000 hrs, for practical applications purpose. It is obvious that the operating temperature will increase to even higher than 80 ˚C and heat the sample film during operation due to continuous illumination with solar simulator (e.g., 0.1 $Wcm^{-2}$ sun light).[90] In addition to light, moisture and oxygen induced degradations; Omh-perovskites undergo thermal degradations. This fact will, therefore, lead to additional primary problems in the course of Omh-perovskite degradation processes. This degradation may produce $PbI_2$ and organic salt forms. The thermal stability of $CH_3NH_3PbI_3$ was confirmed to be even higher than 300 ˚C.[24, 32, 91] However, latest literatures confirmed that the organic decomposition temperatures could be lowered upto 140 ˚C.[51, 52, 83] The temperature induced decomposition of methylammonium iodide may lead to the formation of HI and $CH_3NH_2$. $CH_3NH_2$ could stay within the network of the perovskite, and then disturbing photovoltaic processes.[52] Furthermore, the presence of metal halides, for example, $PbI_2$ as degradation product of Omh-perovskite, is another issue. Due to its poor optical behaviour and poor light absorption ability as well as its higher bandgap, lead halide causes device deterioration. Additionally, mechanism of expansion and compression in the dimensional changes of the perovskite structure at low and high temperature is not yet clear. Moreover, high temperature can cause diffusion of interlayer, diffusion of metal counter electrode, ohmic contact degradation and device architecture degradation and thus the mechanisms for these phenomena should be reported carefully. For this reason, new Omh-perovskites which posses enhanced intrinsic resistance towards temperature are better candidates for future development in areas of Omh-PSCs based photovoltaic technologies. [79, 92] For instance, $FAPbI_3$ is temperature more resistant than $MAPbI_3$. [92]

### 3.5 Thermal and electric field induced intrinsic degradation

The interface is the main origin of degradation in Omh-PSCs. The question of how interface can cause degradation is related to intrinsic deprivation of Omh-PSCs. The origin of this degradation is: (1) temperature induced flow of components due to thermal evaporation during deposition and light illumination during operations. This thermal induced migration of component materials at the interface resulting inter-diffusion, phase segregation and separation, where an inherent strain presents.



Energy & Environmental Science Accepted Manuscript

(2) Electric field induced ion migration which leads to electro-migration and hysteretic effects. In electro-migration process, an electric current flowing in a conductor may move metal ions, referred to as electromigration. Electro-migration pushes anions to the anode and builds up a compressive stress there. The vacancy concentration in the anode becomes less than the equilibrium vacancy concentration according to the Nabarro Herring model of point-defect formation in a stressed solid.[93] In hysteresis process, ion migration is particularly sensitive to the concentration of mobile vacancies (or interstitials) depending on the mechanism. Thus, size of crystalline domains, degree of crystallinity and stoichiometry can affect the transient behavior of Omh-PSCs devices.[94] This transient behavior is different from device to device. For instance the larger transient difference between mesoporous and planar devices is most probably due to variation in composition stoichiometry or morphology. Therefore, minimizing ion migration is an essential mechanism to extend stability.

Moreover, $TiO_2$ has a strong ability to extract electrons from organic materials as photocatalysts and from iodide ($I^-$) as electrodes in DSSCs. Hence, the driving force of the decomposition mechanism may be due to the effect of electron extraction by $TiO_2$ from an iodide anion accelerated with light illumination during operations. The possible decomposition pathway at the $TiO_2$ surface may be as shown in Equations (16 −18): [95]

$$2I^- \leftrightarrow I_2 + 2e^- \quad (16)$$

$$3CH_3NH_3^+ \leftrightarrow 3CH_3NH_2(g) + 3H^+ \quad (17)$$

$$I^- + I_2 + 3H^+ + 2e^- \leftrightarrow 3HI(g) \quad (18)$$

Decomposition of $CH_3NH_3PbI_3$ crystal under UV light illumination is shown in Fig. 10. Since $CH_3NH_3PbI_3$ is a combination of $CH_3NH_3^+$, $Pb^{2+}$, and $I^-$ ions, $TiO_2$ can extract electrons from $I^-$, giving $I_2$ at the interface between $TiO_2$ and $CH_3NH_3PbI_2$ as shown in Equation (16). This will lead to breakdown the perovskite crystal. Equation (17) is in equilibrium. The electron taken by $TiO_2$ can go back to the $TiO_2$ surface, and Equation (18) can take place while releasing HI (Fig. 10). Consuming $H^+$ by Equation (18), the equilibrium of Equation (17) can favor to the right with the release of $CH_3NH_2$ due to low boiling point of $CH_3NH_2$ (17 °C).[96] It is, therefore, crucial to realize three of the possible major consequences of iodide ion migration that could occur in $MAPbI_3$ based Omh-PSCs: (i)



Energy & Environmental Science Accepted Manuscript

iodide may out-diffuse into the $TiO_2$ layer, (ii) its distribution may be influenced by the electric field in the Omh-perovskite materials or by any modification of it. This is because iodide moves as a negative ion, (iii) iodide migration may appear to be involved in some of the observed electrical metastability of the device, which all are pertinent to the interface stability. The stability of the Omh-perovskite layer under light exposure drastically vanished, and shorten the lifetime of the Omh-perovskite. The origin of degradation for $CH_3NH_3PbI_3$ layer is the interface between $TiO_2$ and $CH_3NH_3PbI_3$. This degradation is as a result of the variable positioning of the $CH_3NH_3^+$ cation in the $CH_3NH_3PbI_3$ crystal. [97-99]

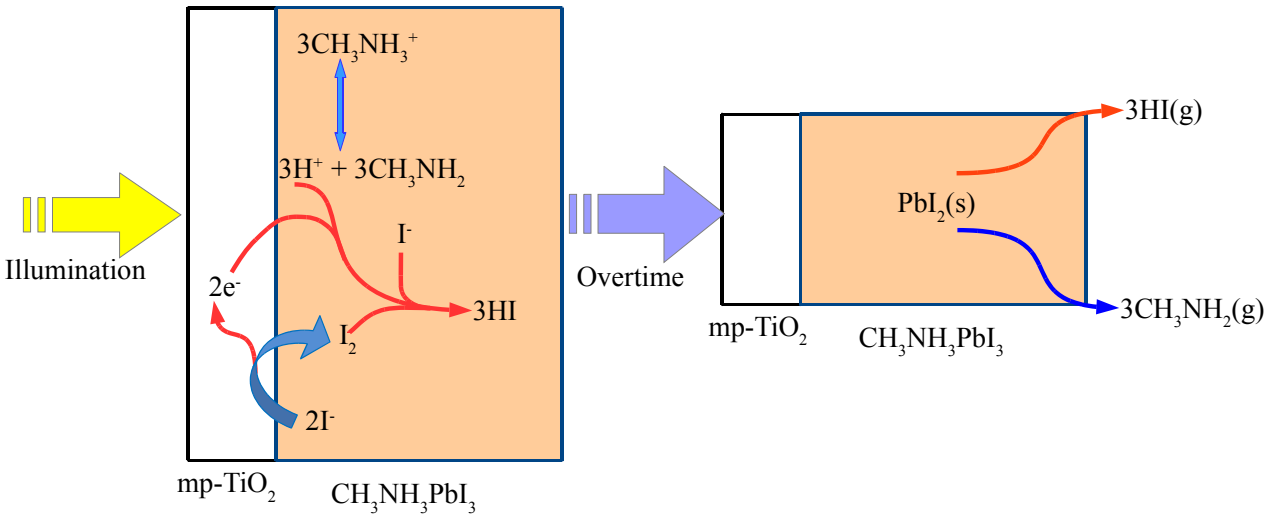


**Fig. 10** Degradation scheme of $CH_3NH_3PbI_3$ on mesoporous $TiO_2$ (mp-$TiO_2$) during UV light exposure tests. Redrawn based on reference [95].

Moreover, recent computational reports[100-104] overviews the defect formation energy for various defects together with the cations ($MA_{Pb}$ and $Pb_{MA}$) and antisites ($MA_I$, $Pb_I$, $I_{MA}$, and $I_{Pb}$) exchange, interstitials ($MA_i$, $Pb_i$, and $I_i$) and vacancies ($V_{MA}$, $V_{Pb}$, and $V_I$). The kinetically and energetically unstable antisites impulsively break up into the respective vacancies and interstitials.[104] Because of their low formation energy interstitials and vacancies are the most possible defects. Interestingly, Angelis and coworkers[105] developed diffusion path to model vacancies and defect migration along the perovskite crystal for all the four explored defects as shown in Fig.11. Vacancies and interstitial defects are referred with dashed circles and red atoms, respectively. While dashed lines show the trajectory of the vacancies, solid lines represent migration of the ions. Fig. 11a shows the formation



Energy & Environmental Science Accepted Manuscript

of vacancy, $V_I$, in an equatorial position and migration towards an axial site. $V_I$ in equatorial or axial sites is basically almost the same energy (< 0.01 EV). However, the axial site is preferred by 0.07 EV over the equatorial site for $V_{Br}$ as shown in the supplementary information of ref. 105. The inorganic scaffold is responsible for the hopping of $V_{MA}$ between its nearby cavities that lie in the ab plane as shown in Fig. 11b. Moreover, $V_{MA}$ diffuses across the framework of $Pb_4I_4$ structure. Similarly, Fig. 11c indicates an in-plane migration of $V_{Pb}$ where $V_{Pb}$ travel beside the square created by four I and four Pb atoms. Similar to $V_I$, the pathway in the direction of the c axis from Fig 11d refers to me. In the initial and /or last configurations, the interstitial iodine atom places in between a couple of equatorial and/or axial I atoms, with almost the same lengths (3.96 and 3.87 Å), respectively. [105, 106]

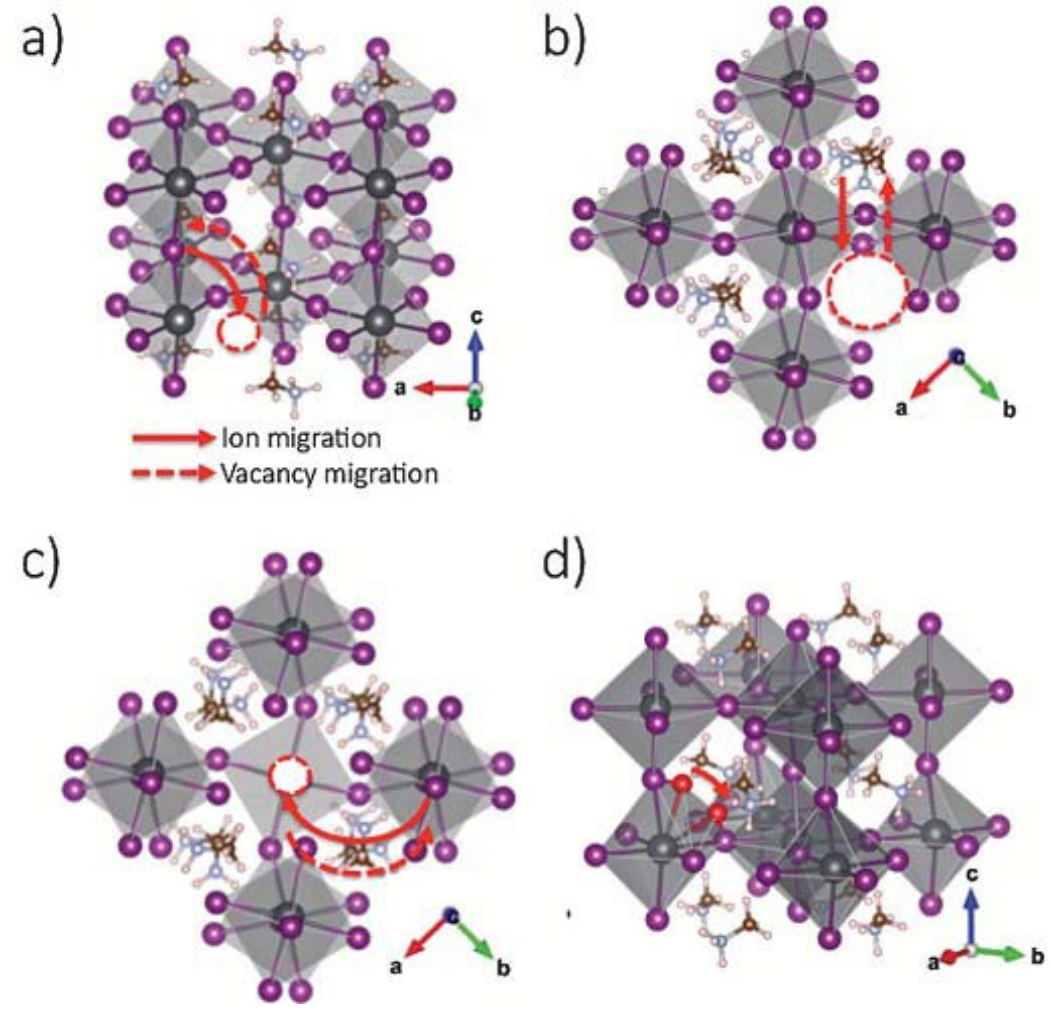


Fig. 11 Pathway for migration of vacancies and defects: iodine (a), methylammonium (b), lead (c) and iodine defects (d). The colours of black, purple, white, blue and brown represent Pb, I, H, N and



Energy & Environmental Science Accepted Manuscript

C atoms, respectively. Reproduced from Ref. 105 with permission from The Royal Society of Chemistry.

This migration of defects/ion such as iodine vacancies across the interface can induce interface degradation, affect device operational mechanisms and finally cause device failure during operations.[105] Formation of metal oxides, metal halides and molecular halogens can take place due to oxidation and reduction processes in the presence of oxygen and light. The chemistry of such ion/defect migration induced interfacial reactions as well as its impact on the device stability needs further detail computational and experimental study. Above all, in order to investigate the ion-migration mechanisms of $MAPbI_3$, studies on ion occupations are of very important.

## 4. Origins of Omh-PSCs degradation

In addition to identifying the main causes of degradation, it is critical to isolate the key origin of degradation. Thus, more detail discussion on device components and architecture, and interface, including the buffer is essential, all of which are the focus of this section.

### 4.1. Effects of device components

Omh-PSCs are multilayered devices which are a combination of active Omh-perovskite material, n-type and p-type electron and hole selective layers, as well as the counter electrode. In addition, different interlayers for different functions can be inserted. These multilayered devices are prone to component degradation. The origin of this degradation can be from the components such as light harvesting active materials, electron and hole selective layers, anode and cathode materials, as well as of the interlayer or buffer layer materials, which are of the main focus of this subsection.

#### 4.1.1 Omh-Perovskites

Omh-perovskite semiconductor materials include $CH_3NH_3PbI_3$, $CH_3NH_3PbBr_3$, mixed Omh-perovskites such as mixed metal cation, organic cation and mixed halide anions. Omh-perovskite structures have become innovative alternatives for next-generation of high performance solar cells, because they combine the advantages of both systems (organic and inorganic cages).

##### 4.1.1.1 Triiodide anions



Energy & Environmental Science Accepted Manuscript

A critical issue for Omh-perovskite materials is their stability. The highest reported stability of Omh-PSCs with light absorbing $MAPbI_3$ is 2000 hrs.[7] Compared to the Si solar cells this stability is quite poor due to ambient sensitivity of $CH_3NH_3PbI_3$ semiconductor. The instability has been a major obstacle since Omh-perovskite-type materials contain hygroscopic amine salts. In the presence of moisture, $CH_3NH_3PbI_3$ undergoes rapid change to hydrated $CH_3NH_3PbI_3$ and then to $PbI_2$ in the presence of moisture at room temperature,[84, 86] resulting in a significant decline in device performance.[107] Furthermore, formation of stress and microstrain, and the origin of degradation in $CH_3NH_3PbI_3$ perovskite structure at severe conditions are still open questions. $CH_3NH_3PbI_3$ structural changes during operation are also other challenges. For instance, it can cause poor thermal and photoconductivity, and hysteresis in device during operation.[108, 109] Furthermore, when operating temperature increases to higher temperature (~58 °C) the structure of $MAPbI_3$ changes from ordering tetragonal into the disordered cubic structure. Conversely, when the operation/processing temperature decreases to room temperature its structure returns back to its ordered tetragonal shape.[110, 111] Thus, how this order-disorder structure of $MAPbI_3$ material could affect both performance and long term stability is also another issue.

Moreover, the poor resistance of $CH_3NH_3PbI_3$ and a device based on this material towards the combined effect of all these operating conditions can be even more problematic. This may restrict the use of these compounds for many practical applications and commercialization. Interestingly, the beneficial or detrimental behavior of grain boundaries in $CH_3NH_3PbI_3$ film remains still in debate. Previous reports in perovskites have demonstrated that grain boundaries are less harmful than in other semiconductors,[112, 113] it is rather beneficial for collecting perovskite carrier efficiency.[114] On the other hand, it is reported that single-crystal perovskites demonstrated rather higher performance[115-117] and illustrating a progress in carrier lifetime.[118, 119] Conversely, current reports suggested that grain boundaries are connected with PL quenching, demonstrating that they are not as kind as have been recommended in the past. Instead of this, it destructs the carrier lifetime.[120] These interesting debates on the role of grain boundaries for carrier lifetime and performance in perovskite materials would be future interesting topics of study. Despite its impact on carrier lifetime and performance, the contributions of these grain boundaries towards operational and long term stabilities of Omih-PSCs are not yet revealed.



Energy & Environmental Science Accepted Manuscript

#### 4.1.1.2 Tribromide anions

$MAPbI_3$ reverts to its precursors, due to its hydroscopic nature.[33] However, the bromide-based perovskites have been proved to be less moisture-sensitive.[121] Higher stability or resistance to photobleaching and decomposition was reported after exposing $MAPbBr_3$ films to stress conditions (i.e. light intensity, and temperature).[122] The better stability of $MAPbBr_3$ films, compared with their iodide counterpart, may be related to differences in bond strengths and the crystalline forms of the two Omh-perovskites. Thus, further investigation is still required on how bromine inclusion provides better stability in both material and device aspects. Despite the better photochemical stability of $MAPbBr_3$ films, its larger optical band gap (Eg ≈ 2.3 vs 1.58 eV for $MAPbI_3$) would reduce the PV performance of $MAPbBr_3$ single junction devices.22 Katz proposed that $MAPbBr_3$ can be efficiently used as top sub cell in future tandem Omih-perovskite-based PV architectures.[122] A mixed halide Omh-perovskite, $MAPbI_{3-x}Br_x$, with a larger band gap than $MAPbBr_3$, may therefore have applications in Omh-perovskite based solar cells that combine high efficiency and stability.

### 4.1.2 Mixed Omh-perovskites

As discussed in the sub-section 5.1.1.1, $CH_3NH_3PbI_3$ suffers from long-term ambient stability due to its sensitivity towards moisture.[84, 86] In addition, Weber and co-workers reported the temperature-dependent structure of $CH_3NH_3PbX_3$ (X = Cl, Br, I).[99] The structure of $CH_3NH_3PbX_3$ ranges from orthorhombic to cubic structures as a function of temperature. The order of the methylammonium cation is also different in different crystal structures. It is also worth noting that at room temperature, $CH_3NH_3PbI_3$ forms a tetragonal structure under 327.4K, whereas $CH_3NH_3PbBr_3$ and $CH_3NH_3PbCl_3$ form cubic structures at 236.9K or above. This order–disorder behavior of the perovskite structure caused by thermal cycles could give a variance in microstructures and stability. Moreover, Swainson and co-workers found a phase transition of $CH_3NH_3PbBr_3$ just below 1 GPa and amorphorized around 2.8 GPa, without the process undergoing long-range orientation ordering of cations.[123] The volume reduction under compression was attributed to the tilting of the $PbBr_6$ octahedral. Suga and co-workers also gave the pressure–temperature phase relations of $CH_3NH_3PbX_3$ crystals in the range between 0.1 Pa and 200 MPa in detail.[124] The crystalline phase of Omh-perovskite can change, due to environmental conditions, such as temperature, pressure, which directly affect the stability of Omh-PSCs. In order to improve the stability of Omh-PSCs, emphasis should be given to gaining a comprehensive understanding of the crystal structure of Omh-perovskite under conditions, such as



Energy & Environmental Science Accepted Manuscript

moisture, temperature, as well as the relationship of the crystal structure to pressure. In general, such a poor structural stability of Omh-perovskites could be improved by modifying the Goldschmidt tolerance factor ($t_f$) using appropriate substitutions, which can be defined by the following mathematical expression in Equation (20), [125, 126]

$$t_f = \frac{r_A + r_x}{\sqrt{2}(r_B + r_x)} \quad (19)$$

Where $r_A$, $r_B$, and $r_x$ are the radii of cation A, cation B, and halogen, respectively in $ABX_3$ structure. That is applied at room temperature to the empirical ionic radii. In order to stabilize the cubic structure, the $t_f$ of Omh-perovskites should be closer to unity.[127] To form a stable Omh-perovskite structure, the size of the ionic radius is restrained by the tolerance factor. The ionic radius is the most important ionic parameter that dominates the crystal structure of ionic compounds. The ideal cubic structure may be seen as a network of $BX_6$ octahedra, where all the octahedra are corner sharing. The 'A' ions occupy the cubo-octahedral holes in between the octahedral. Many derivatives of the ideal structure are found and the distortion of the structure from cubic is often considered to be determined by the relative sizes of the different ions of the compound.

#### 4.1.2.1 Metal (B) cation

The organic cation $CH_3NH_3^+$ in $ABX_3$ is responsible for the structural stability of the Omh-perovskite materials, while the electronic properties are largely determined by the inorganic matrix (metal-halide hybridized orbital).[102, 128, 129] The main problem of $MAPbI_3$ is poor ambient stability under different environmental conditions.[24, 33] In order to avoid this limitation for indoor and outdoor applications, any modifications that can strengthen the material stability would be beneficial. One successful technique is to combine $PbI_2$ with $SnI_2$ to form $CH_3NH_3Sn_xPb_{1-x}I_3$, with $E_g$ of 1.1eV. The edge of the incident-photon-to-current efficiency (IPCE) curve extended to 1060 nm.[25, 82, 130] Nevertheless, $Sn^{2+}$ easily changes to $Sn^{4+}$ in the atmosphere. Consequently, this leads to device deterioration. Other Omh-perovskites incorporating divalent metal cations such as $Be^{2+}$, $Mg^{2+}$, $Ca^{2+}$, $Sr^{2+}$, $Ba^{2+}$, $Zn^{2+}$, $Ge^{2+}$, $Fe^{2+}$, $Co^{2+}$ and $Ni^{2+}$ do not yet report on this application. Another tactic is to replace the organic cations, as it has been established that enlargement of the octahedral network significantly influences the bandgap of the Omh-perovskite.

#### 4.1.2.2 Organic 'A' cation



Energy & Environmental Science Accepted Manuscript

The organic cation in $ABX_3$ is a key part of the Omh-perovskite that determines its structure and dimensionality, and has a direct influence on the stability and opto-electronic properties of the material. The cubo-octahedral cavity, defined by the four edge-sharing $BX_6$ octahedra, permits the incorporation of only small cations into the 3D perovskite structure. The phenomenological derivation of $t_f$ allows an estimation of the stability based on the size of its constituents. [131] To obtain cubic phase $t_f$ should be unity; however, for most of the cubic structures the $t_f$ ranges from 0.78-1.05, due to a slight expansion in distorted structures.[132] In fact, by changing $r_A$, the $t_f$ can be varied but only in a restrict range of values around the unity ($t_f$ =1 corresponds to a perfectly packed Omh-perovskite structure) to have a stable, even distorted, 3D Omh-perovskite structure.[133] The dynamic position conduction band of $CH_3NH_3PbI_3$ film due to the disordered organic cation has great role in extending the lifetime.[134]

So far, the most investigated organic cation counterpart for substituting MA ($CH_3NH_3^+$) has been FA ($HC(NH_2)_2^+$), with a $t_f$ of 0.99, higher than $t_f$=0.91 for $CH_3NH_3PbI_3$ (ion size: FA -2.53 Å, MA -2.17 Å, $Pb^{2+}$ -1.19 Å and $I^-$ - 2.20 Å). In a recent report, the FA cation, which is slightly larger than methylammonium, was confirmed to form 3D Omh-perovskite with a lower bandgap of about 1.47 eV. Omh-perovskites are described as any compound which crystallizes in the $ABX_3$ structure, containing corner-sharing of $BX_6$ octahedra with the cationic component neutralizing total charge. $MAPbI_3$, behaves as tetragonal shape at room temperature as a result of distortion of the cubic crystal.[135] The organic cation was considered as it does not take part in determining the band structure, and works to fulfill charge neutrality within the lattice.[136] However, its size is quite vital. The size of organic cation can cause the entire network to enlarge or compress.

$FAPbI_3$ are not sensitive even at high temperature compared to $MAPbI_3$. While $MAPbI_3$ discolors in 30 minutes, $FAPbI_3$ does not discolor even at 150 °C under ambient. Subjecting to a moist atmosphere resulted in fading of the $FAPbI_3$, same as $MAPbI_3$.[137] However, recent work on long-term stability of Omh-PSCs suggests that with sufficient encapsulation, $FAPbI_3$ functions continuously under illumination for thousands of hours, and this is not likely to act as serious limitation to commercialization.[5, 6] Furthermore, superior temperature stability is an exceptionally hopeful long term thermal durability, and this would be additional topic that needs to be studied. Stable Omh-PSCs with cationic alloy structure has recently been fabricated in the laboratory.[4] A 5-aminovaleric acid (5-



Energy & Environmental Science Accepted Manuscript

AVA) cation replaced some of the MA cation in the cuboctahedral site of $MAPbI_3$, forming the new mixed cation Omh-perovskite, $(5\text{-}AVA)_x(MA)_{1-x}PbI_3$. A more stable new Omh-perovskites, $(PEA)_2(MA)_2[Pb_3I_{10}]$ ($PEA=C_6H_5(CH_2)_2NH_3^+$, $MA=CH_3NH_3^+$) has also been reported.[138] Films of these materials are more moisture resistant than films of $MAPbI_3$ and devices can be fabricated under ambient humidity levels. This moisture resistance ability may be due to the more hydrophobic tail 'R' group, which may mask the hydrophilic nature of the materials. However, the fundamental reason for alloy stabilization of the structures requires further study.

#### 4.1.2.3 Mixed anion halides

**$MAPb(I_{1-x}Br_x)_3$:** The stability of $MAPbI_3$ can be significantly improved with a small fraction of Br or Cl substitution.[33, 139] Although the $MAPbI_3$ hybrid solar cell does not show significant PCE degradation at low humidity (<50%), the $MAPbI_3$ began to decompose at relatively high humidity (≥55%), displaying a color change from dark brown to yellow.[33] Hence, it was intentionally exposed the solar cells to a relatively high humidity (55%) for one day while keeping the humidity to 35% on the other days. Interestingly, the $MAPb(I_{1-x}Br_x)_3$ (x = 0, 0.06) hybrid solar cells exhibited serious PCE degradation after exposure to 55% humidity, whereas the other $MAPb(I_{1-x}Br_x)_3$ (x = 0.2, 0.29) cells maintained the PCE. A low sensitivity to humidity of cells based on $MAPb(I_{1-x}Br_x)_3$ ($x \geq 0.2$) might be associated with its compact and stable structure, because the substitution of larger I atoms with smaller Br atoms in $MAPb(I_{1-x}Br_x)_3$ leads to the reduction of the lattice constant and a transition to a cubic phase. As a result of introducing $Br^-$ ions in the perovskite structure, the lattice parameter changes from 5.921 for the $CH_3NH_3PbBr_3$, 6.144 for the MABr/MAI 2:1, and 6.223 for the MABr/MAI 1:2. The change in the lattice parameter is due to the difference in the ionic radius of $Br^-$ (1.96 Å) and $I^-$(2.2 Å).[140] The smaller ionic radius of the $Br^-$ is the main reason for the formation of the cubic structure when Br is introduced into the perovskite structure.[141] Thus, the role of bromine inclusion in thermal, light and ambient stabilities should be identified. Such comparative study could help for better stability improvements.

**$MAPbI_{3-x}Cl_x$:** In contrast to $CH_3NH_3PbI_3$, this iodide-chloride mixed-halide Omh-perovskite was remarkably stable to processing in air. The absorption spectra demonstrated good light-harvesting capabilities over the visible to near-IR spectrum and were also stable to prolonged light exposure, as demonstrated by 1000 hrs of constant illumination under simulated full sunlight.[6, 139] The improved



Energy & Environmental Science Accepted Manuscript

stability can be associated with its compact and stable structure, due to the substitution of larger I atoms with smaller Cl atoms in $MAPbI_{3-x}Cl_x$ leads to the reduction of the lattice constant and a transition to a cubic phase, similar to iodide substitutions using bromide.[122] This compact structure would decrease the sensitivity of the $MAPbI_{3-x}Cl_x$ material to moisture, light and temperatures due to its higher binding constant compared to the $MAPbI_3$ materials. But, these need to be investigated. Overall, there is no clear evidence of the role of chlorine insertion to enhance stability. Both $MAPbI_3$ and $MAPbI_{3-x}Cl_x$ have similar light absorption ranges, while $MAPbI_{3-x}Cl_x$ has a longer recombination lifetime than $MAPbI_3$, followed by a longer electron diffusion length. In this regard, $MAPbI_{3-x}Cl_x$ does not require a mesoporous electron transport layer (e.g. $TiO_2$) unlike $MAPbI_3$.[26, 112] The long electron diffusion length enables $MAPbI_{3-x}Cl_x$ to work perfectly on insulating scaffolds and in bulk films.[34, 142]

**$MAPbBr_{3-x}Cl_x$:** Among the family of Omh-perovskites, $MAPbBr_{3-x}Cl_x$ has a larger band gap than iodine based Omh-perovskite such as $MAPbBr_{3-x}Cl_x$ and $MAPbBr_{3-x}Cl_x$. $MAPbBr_{3-x}Cl_x$ has enormous capability for high energy photons in photovoltaic applications such as tandem cells or other devices which possess photon spectral splitting.[143, 144] But, the Omh-perovskite materials suffered from a moisture-related decomposition because of the hygroscopic amine salts.[33, 145] In the stability test, $MAPbBr_{3-x}Cl_x$ is less moisture-sensitive.[121] The as prepared $MAPbBr_{3-x}Cl_x$ films were left in the dark at room temperature with exposure to ambient air for 30 days. The materials are not showing any apparent changes in the XRD patterns observed after this time, indicating a good stability of $MAPbBr_{3-x}Cl_x$. This significantly improved stability may be due to a small fraction of Br or Cl substitution.[33, 139] it is not clear which atom contributes more to the structural stability. Similarly, thermal and radiation stability of $MAPbBr_{3-x}Cl_x$ is not yet resolved. Hence, detail evidences for the contributions of bromine and chlorine to thermal and radiation stability of perovskite structure and to the thermal and photoconductivity are required.

#### 4.1.2.4 Chloride inclusion

The issue of chloride loss has recently been raised.[49, 51, 146] Currently considered loss pathways center around MACl[49, 51, 147] sublimation, or the degradation of MACl into volatile hydrochloric acid (HCl) and methylamine species facilitated by residual water.[83] The loss mechanism suggests that chloride must diffuse into the film's surface to ultimately escape the system, meaning that bulk sensitive



Energy & Environmental Science Accepted Manuscript

composition measurements, e.g. XRD, EDS may miss residual chloride remaining at the Omh-perovskite's surface.[148]

$$Cl^- + CH_3NH_3^+ \rightleftharpoons CH_3NH_3Cl(s) \quad (20)$$

$$CH_3NH_3Cl(s) \rightleftharpoons CH_3NH_3Cl(g) \quad (21a)$$

$$CH_3NH_3Cl(s) \rightleftharpoons HCl + CH_3NH_3 \quad (21b)$$

Sublimation of $CH_3NH_3Cl$ (Equation 21a), or decomposition into HCl and $CH_3NH_2$ (Equation 21b), may be responsible for the loss of chloride during film growth. Thus, the inclusion of $Cl^-$, from either metal chloride (e.g., $PbCl_2$) or organochloride such as $CH_3NH_3$-Cl, has become the most commonly applied strategy.

How the Cl additives such as $CH_3NH_3Cl$ contributes to improve stability and/or reduce degradation, several reasons are considered. (1) Cl inclusion could increase the binding constant which may reduce the rapid dissolution or degradation of $CH_3NH_3PbI_3$ in moisture. This fact might be related with the stable structure of $CH_3NH_3Cl$, owing to a more compact Omh-perovskite cubic structure in which the degradation of the methylammonium cation is prohibited.[122, 149] (2) It facilitates the removal of excess $CH_3NH_3^+$ ions.[49] Excess $CH_3NH_3^+$ ions may act as defect or impurities at surface or interface sites which may lead to block interfacial processes. (3) Cl-rich nucleation sites lead to better crystal coalescence[146] or high quality film crystallinity,[49] and also provides stable morphology as well as better coverage in Omh-PSCs fabricated by one-step solution processes (because poor morphology stability and poor coverage could lead to device deteriorations). (4) it enhances the lifetime of the photoexcited species (the presence of chlorine may creep grain boundaries[120] and ultimately controls perovskites grain structures[150]). All of these factors contribute to higher stability. Despite this helpful information, there is no clear evidence on chlorine inclusion /stability relationship. In general, mixing halides in Omh-perovskites has shown beneficial effects in enhancing stability. $CH_3NH_3PbI_{(1-x}Cl_x)_3$ is remarkably stable during processing in air, compared to $CH_3NH_3PbI_3$. The atomic ratio of Cl in $CH_3NH_3Pb(I_{1-x}Cl_x)_3$ was proposed to be up to one third, as it is in precursors.[97, 139] However, recent experiments[142, 151] showed that its atomic ratio is less than 4% and that most of the precursor Cl may be lost. Therefore, the ratio of Cl into iodine should be seriously controlled. For real practical



Energy & Environmental Science Accepted Manuscript

applications, the miscibility between Cl and iodine mixed halide, and fundamental contributions of Cl to stability need to be addressed. Similarly, different devices incorporating $CH_3NH_3Pb(I_{1-x}Cl_x)_3$ material showed performance - one has inferior performance but the other improved performance.[150] Thus, how chlorine inclusion mechanisms during fabrication processes affect device stability is not yet well understood. Could bromide sources act similar to chloride sources as additives in Omh-PSCs fabrications is also another important open question for the community.

### 4.1.3 Hole transport layer

Hole transporting layers such as spiro-MeOTAD, PEDOT:PSS and other polymers, and inorganic materials are significantly more stable than liquid electrolytes, but devices based on these materials are also susceptible to chemical degradations during which photooxidation processes and hole-electron pair recombination may occur. In this section we mainly focus on the most commonly used HTMs, spiro-MeOTAD and PEDOT:PSS.

#### 4.1.3.1 Spiro-MeOTAD

Spiro-MeOTAD is a material widely used Omh-PSCs for hole transporting purposes. Spiro-MeOTAD coated beneath the counter electrode and can easily be exposed to the atmosphere. As a result, degradation can take place due to air exposure, continuous light irradiation, elevated temperature and dust. Qi and colleagues investigated the causes of degradation of Omh-PSCs which use spiro-MeOTAD as hole selective material. [152, 153] Due to its amorphous properties, spiro-MeOTAD is very crucial HTM; on the other hand, small molecular species from the air could simply spread, and pass freely through miniscule pinholes in the amorphous material. Unfortunately, these pinholes are too small to be seen with an optical microscope.[152, 153] Moreover, the decline in $j_{sc}$ and FF is possibly caused by Omh-perovskite layer degradation, which can be caused by (1) air molecules ($O_2$, $H_2O$, etc.) migration and interaction with Omh-perovskite via the pinholes and/or (2) out-diffusion of mobile ions in the Omh-perovskite film via the pinholes in the spin coated spiro-MeOTAD.[154] The pinholes may create pathways for foreign molecules such as water and other gas molecules in air to diffuse through the thin film as shown in Fig. 12. These air molecules would then become impurities in the solar cells, leading to degradation and resulting in a drop in solar cell efficiency.



Energy & Environmental Science Accepted Manuscript

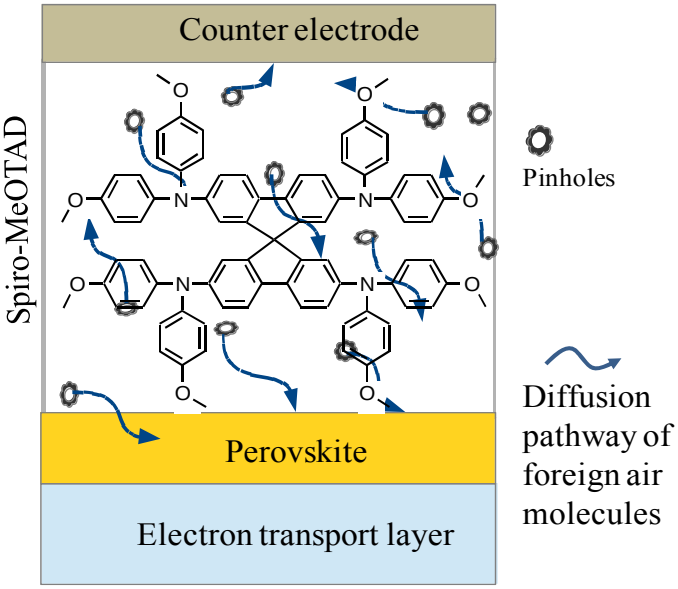


**Fig. 12** Diffusion of foreign air molecules into the device through the spiro-MeOTAD

It is now clear that the presence of the oxidized spiro-MeOTAD is required for Omh-PSCs. However, oxygen reduction reactions might also occur. The generation of $O_2^-$ would change the oxidized spiro-MeOTAD concentration and device characteristics during the operation. For future development of devices with long-term stability it will be important to exclude oxygen reduction. Further work is needed to determine if this can be achieved by sealing the devices after preparation under ambient atmosphere, or whether the devices should be fabricated and sealed to exclude oxygen and moisture.

#### 4.1.3.2 PEDOT:PSS

Poly(ethylenedioxythiophene) poly(styrene sulfonic acid) (PEDOT:PSS) is generally used in the form of water solution/suspension for solar cells as the HTM,[155] which recently has been used in inverted Omh-PSCs as a hole selective material.[156, 157, 158] This hygroscopic property of PEDOT:PSS destabilize the interface and will result in device deterioration. Moreover, as compared to PEDOT, the amount of PSS is usually dominating in the polymer mixture and the diffusion of PSS into other layers can occur and possibly results in degradation. For instance, the PSS may undergo a oxido-de-sulfonato-substitution forming the phenolate which can then react with PSS forming two PSS chains linked together via a sulfonic ester group as shown in Scheme 1.[159] An asterisk in the Scheme 1 indicates oxidation of the carbon. Additionally, corrosion will be enhanced not only in connection



Energy & Environmental Science Accepted Manuscript

with low work function metals such as Al or Ca used as counter electrode, but also in connection with ITO electrode.[56, 160]

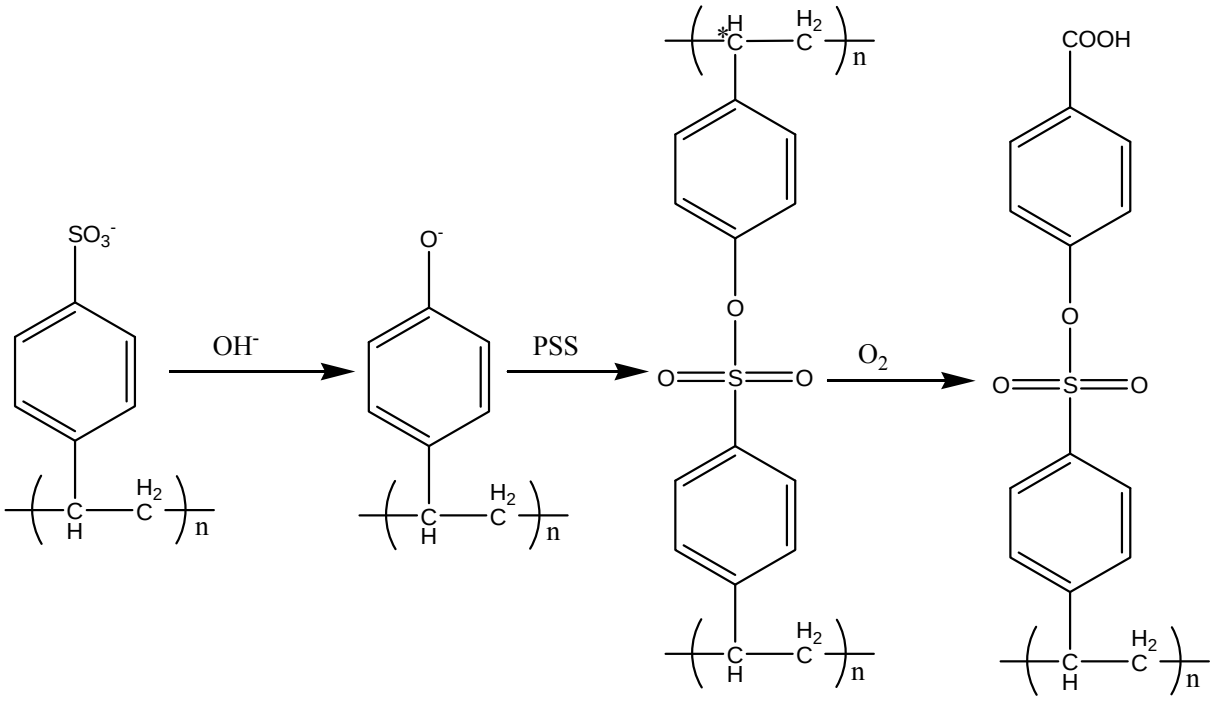


**Scheme 1** Proposed oxido-de-sulfonato substitution of PSS in PEDOT:PSS layers. Reprinted from 159. Copyright 2008, with permission from Elsevier.

Dauskardt and coworkers[161] verified how the hygroscopic properties and poor adhesion of PEDOT:PSS onto the active layer causes a general loss of device performance in a roll-to-roll processed normal geometry organic photovoltaic devices. The objective was to show the thermomechanical stress in a real life device would suffer.

### 4.1.4 Metal counter electrode

Gold, silver and aluminum metals are commonly used as counter electrode materials in mesoporous, planar and inverted Omh-PSCs.[157] The drawbacks of silver may be its corrosion in contact with the halide ions from Omh-perovskite light absorber by forming silver halides such as formation of AgCl in humid environments, and short circuits or shunting paths with the mesoporous $TiO_2$, leading to device degradation.[6] The high cost of the Au electrode also requires a high-vacuum evaporation technique, thereby limiting its future application. Low-cost carbon may be an ideal material to



Energy & Environmental Science Accepted Manuscript

substitute Au as a back contact with Omh-perovskite heterojunction (HJ) solar cells at low temperature because its function is similar to that of Au.[7]

### 4.2 Effect of device architecture

Both device stability and efficiency of Omh-PSCs depend on their architecture which will in turn influence the choice of materials and deposition methods. Three main device architecture present in Omh-PSCs: the planar (regular $TiO_2$ based), inverted (PEDOT:PSS based) and mesoporous structures schematically represented in Fig. 13. Since the initial evolution of Omh-PSCs, many research groups have been focusing on efficiency and fabrication processes; hence, several review papers are available.[96, 162-165] In this section we will only focus our discussion on device architecture stability. Device architecture, which remains unclear in terms of its effects on the device stability, should also be included in long-term stability tests.

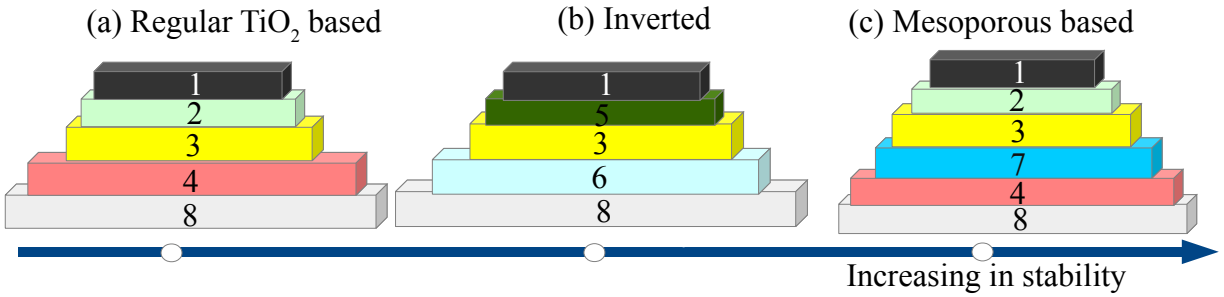


**Fig.13** Stability comparison of three Omh-PSCs device architectures

#### 4.2.1 Planar (Regular) TiO2

Planar (or alternatively regular) architecture inherits features of the most commonly utilized mesoscopic Omh-PSCs device architecture (FTO/cl-$TiO_2$/perovskite/spiro-MeOTAD/Au). Primarily any excellent electron transporting layer can be deposited on the fluorine doped tin oxide or other substrate, and then after Omh-perovskite layer, HTM and finally the counter electrode are coated in chronological order. The application of a single compact n-type metal oxide layer makes the regular



Energy & Environmental Science Accepted Manuscript

type different from the mesoporous devices which consist of both compact and meso-structured scaffolds. The regular configurations have been observed to boast high efficiencies, similar to their mesoscopic counterparts. Stability, however, is still in minutes[94] compared to their mesoscopic counterparts. This may be due to: 1) faster charge collection at interface, due to ion migration resulting from applied bias or field, creating transport barriers in the planar and 2) strong hysteresis effect in planar devices-undesirable shifts in electrical conductivity that occurs when applying increasing or decreasing amounts of voltage to a cell.[166] Thus, detailed studies on the stability of the compact $TiO_2$-perovskite and Omh-perovskite-HTM interface stability, pore filing properties, sensitivity towards light and moisture, formation of shunting path with the HTMs and or metal electrodes and carrier accumulation due to excess ions, formation of trap states and defects at the Omh-perovskite and compact $TiO_2$ surfaces, the effects of the presence of excess ions in the Omh-perovskite on the device architecture will be critical.

### 4.2.2 Inverted (PEDOT:PSS based)

Chen and coworkers pioneered inverted based device architecture made of PEDOT:PSS coated directly on the transparent conductive substrate and $C_{60}$ derivatives such as [6,6]-phenyl $C_{61}$-butyric acidmethylester (PCBM) and indene-$C_{60}$ bisadduct (ICBA), coated next to Omh-perovskites, as electron selective layers, respectively.[167] The ambipolar property especially superior p-type character of $CH_3NH_3PbI_3$ which is greatly biased by the p–n heterojunction idea in organic solar cells was the motivation for the authors initial material choice.[168] Planar heterojunction architecture with inverted design achieved higher PCE in a very short time, from 3.9% to over 16%.[157] The PEDOT:PSS has high conductivity and is extensively employed as an electrode in organic electronic devices such as organic light-emitting diodes, organic photovoltaics and organic field-effect transistors[169-171] However, PEDOT:PSS is extremely hygroscopic, thus dispersing it in water may limit the long-term stability of inverted Omh-PSCs devices. Direct coating of PEDOT:PSS aqueous solution would degrade the $CH_3NH_3PbI_3$ film.

Therefore, it can be proposed that the inverted based Omh-PSCs devices may face challenges such as: (1) electrochemical reactions at the ITO and aluminum electrodes, (2) the inclusion of moisture and impurities within the organic-metal interface enhancing ionic conduction and hence accelerating corrosion, (3) accelerated degradation due to illumination of the device, (4) a very high electron



Energy & Environmental Science Accepted Manuscript

affinity of PCBM (and other fullerenes), which would seem more prone to reaction with the metal electrode, and finally (5) the $CH_3NH_3PbI_3$ film is destroyed by the hygroscopic PEDOT:PSS aqueous solution. Aluminum is not a passive metal and it may react with organic compounds producing organo-aluminum compounds or alternatively anion radicals. These compounds are highly reactive species that will react with any proton donors present (e.g. trace of water or with oxygen). None of these challenges are confirmed, thus they should be investigated to obtain a detailed understanding of the stability of inverted Omh-PSCs. 10–20 nm ultrathin layer of poly(N,N0-bis(4-butylphenyl)-N,N0-bis (phenyl) benzidine)(polyTPD) was introduced between PEDOT:PSS and $CH_3NH_3PbI_3$ layers using a meniscus-coating process.[40, 172] 10–20 nm ultrathin hybrid interfacial layer of NiO compact layer and an insulating $Al_2O_3$ (meso-$Al_2O_3$) scaffold, which leads to little hysteresis and more stable power output under working conditions has been confirmed for inverted device.[156] Furthermore, in comparison to PEDOT:PSS based inverted Omh-PSCs with the best efficiencies (~15%),[173, 174] meso-$Al_2O_3$ device showed an improved stability. This shows that the potential of the NiO/meso-$Al_2O_3$ interfacial layer should be superior to that of PEDOT:PSS.

### 4.2.3 Mesoporous $TiO_2$

The stability of Omh-PSCs in liquid electrolyte is approximately 10 min because $CH_3NH_3PbI_3$ tends to dissolve gradually in the redox electrolyte ($I^-/I_3^-$). In order to solve this problem, Grätzel, Park and coworkers investigated a new mesoporous solar cell based on $CH_3NH_3PbI_3$ semiconductor and spiro-MeOTAD as a solid HTM, and submicron thick films of mesoporous Titanium dioxide, showing excellent long term stability of 500 hrs under AM 1.5 G illumination. The mesoporous device structure incorporates active and passive scaffolds such as mesoporous $TiO_2$ and mesoporous $Al_2O_3$ scaffolds, respectively. The highest stability reported with mesoporous $TiO_2$ is 1000 hrs with 28% reduction relative to its initial PCE.[44] There may be many factors causing degradation related to mesoporous $TiO_2$. Some of them are:[175-177] (1) sensitivity to UV exposure, and (2) the presence of surface defects (oxygen vacancies) in $TiO_2$. The interaction of these defects or vacancies with both water and oxygen, creating electronic defect states, can result in device degradation. Oxygen binds to the $Ti^{3+}$ sites and modifies these trap sites.[72] Furthermore, lead iodide can be produced upon the breakdown of Omh-perovskites at the interface.[51] Because of its wide bandgap ($E_g$ = 2.3eV) and poor optical properties formation of $PbI_2$ is unnecessary. For reasons that are not yet completely known, the formation of a $PbI_2$ phase is more well-known in mesoporous scaffold than on a planar substrate.[178]



Energy & Environmental Science Accepted Manuscript

Thus, Mesoporous based solar cell devices prepared with $PbI_2$ have confirmed poor performance, attributable to its appreciably inferior transport properties (smaller diffusion coefficient) compared with $CH_3NH_3PbI_3$-based devices.[179]. Moreover, the presence of $PbI_2$ might result in energy misalignment at the $TiO_2$ interface and trap free charges created in the Omh-perovskite phase, resulting in an inferior device performance. It may also give more stringent requirements for processing of these thin films. [180]

The two devices for mesoscopic architecture Omh-PSCs are HTMs based, and HTMs free structured solar devices. In the former, the breakthrough for better stability of mesoporous architecture was 500 hrs using spiro-MeOTAD, which is now widely used as HTM with excellent PCE. However, due to the limited choice of materials the stability progress of inorganic HTMs has been sluggish compared to their organic counterparts. Although CuSCN (PCE = 12.4%),[181] NiO (PCE = 11.6%)[182] and CuI (PCE = 6%),[183] have been listed as excellent, low cost and stable inorganic HTMs, they still have low efficiency when compared to organic HTMs. On the other hand, polymer HTMs, in addition to the most common spiro-MeOTAD, including poly (triarylamine) (PTAA) and poly (3-hexylthiophene-2,5-diyl) (P3HT), have been tested, because of better hole mobility and good film-forming properties. Among all, PTAA confirmed the highest efficiency of up to 12% in contrast to 6.7% for P3HT.[32] This efficiency has been seriously decayed in 55% relative humidity for one day. This was the first most important breakthrough in the development of polymer HTMs, which undergo pore-filling limitations, and this may lead to diminish the performance, inferior the stability and even harm the device. [184]

The majority of the HTMs uses hygroscopic additives such as Li salts, tetrabutylpyridine (TBP) or a cobalt complex to enhance their conductivity. Several groups have reported Omh-PSCs without additives in the HTM, which simplifies the cost and fabrication procedures. Liu and co-workers described the tetrathiafulvalene derivative as a HTM (TTF-1).[185] Moreover, iodine can react with the TBP leading to an iodopyridinate complexes as in dye sensitized solar cells[186] resulting in iodine depletion from the absorber materials. Han and coworkers introduced a TTF-1 derivative into Omh-PSCs without the use of p-type dopants.[185] The improved stability was attributed to the avoidance of the use of deliquescent and hygroscopic additives. This dopant free approach is responsible for improved lifetime of the device compared to the approach incorporating p-type HTM dopant additives. Moreover, these additives may act as a source of moisture that could degrade the organic HTM



Energy & Environmental Science Accepted Manuscript

materials and finally shorten the device lifetime. Similarly, these HTMs are not only expensive, but also can limit the long term device stability. Although various novel HTMs have shown promising results, the HTM-free Omh-PSCs device schematically illustrated in Fig. 14 has many advantages such as no need of air-sensitive HTMs, simplicity, cheap cost of production and excellent stability. Meng and coworkers demonstrated HTM free Omh-PSCs devices with 10.5% PCE.[187] Excellent carrier lifetime and ambipolar nature[25, 26] enabled pioneering of HTM free architecture. Interestingly, HTM-free structured mesoscopic solar cells have now been made with PCEs over 10% and stability over 2000 hrs.[7] Etgar and co-workers showed an initial study using $TiO_2$ nanosheets as the mesoporous layer.[22]

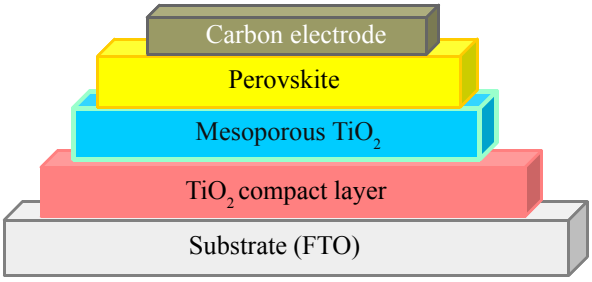


**Fig.14** Typical architecture for Mesoporous $TiO_2$ based HTM free Omh-PSCs

### 4.3 Effect of interface

Although studies have revealed that device degradation is mainly attributable to moisture ingress, high temperatures, and UV light, significant degradation of Omh-PSCs device is still observed even when it is well-encapsulated or characterized in an inert environment.[6] These observations imply that the environmental effects are not the only critical factors determining the device stability, but there are also intrinsic factors within the devices that contribute to degradation. One example is the unstable electronic structure of the organic/cathode interface, due to gradual diffusion of metal into organic films. Similar phenomena are observed in ITO anode/organic interface, where reactive oxygen species generated by UV treatment of the indium-tin oxide (ITO) substrate slowly degrades the organic layer. Other degradations may be related to the organic/electrode interface and time-dependent chemical reactions at the donor/acceptor interface can also cause device deterioration. Other causes may be attributed to the spatial isolation of organic films from electrodes and the reduction of the energetic transport barrier.



Energy & Environmental Science Accepted Manuscript

### 4.3.1 Ion migration

The rate of electromigration increases with temperature, electric field and illumination, and has four prerequisites – mobile ions; a voltage gradient; a continuous flow of moisture; soluble ions. Silver is the metal most susceptible to migration, since it requires low activation energy to initiate the migration process.[188] The severity of electromigration may increase with the applied potential gradient and the time to reach active materials. When Ag is under an applied electric field, or thermal evaporation, it may leave its initial location in ionic form and redeposit at another location. Silver migration causes short circuits and device failure, especially in high humidity environments. Moreover, it is well known that the cations at the A-site and B-site of Pb-based complex $ABX_3$ perovskite minerals such as $PbBO_3$ can be replaced by many other cations. The substitution is mainly determined by the difference of valence and ionic radius.[188] The size of $Ag^+$ is almost the same as for $Pb^{2+}$ (about 0.149 nm), and much larger than for B-site cation, such as $Nb^{5+}$ (0.064 nm) and $Zn^{2+}$ (0.074 nm).[189] Thus, it can be proposed that $Ag^+$ enters into the Pb-site of $MAPbX_3$ Omh-perovskite materials, substituting for $Pb^{2+}$ though this has not yet been reported. The nonequivalent replacement of $Ag^+$ for $Pb^{2+}$ may also be responsible for undesirable $MAPbX_3$ layer structural distortion during device operation. The intrinsic low melting point of silver may account for the structure change and abnormal grain growth of the Omh-perovskites near the interface and this has to be investigated.

The role of ion migration initiated by photo-excitation in slower processes occurring during pre-conditioning of the devices has been proposed as a cause for hysteresis.[94] Hysteresis is commonly takes place in metal halides such as $PbI_2$ in which photo-excitation generates halide vacancies, facilitating halide ion migration.[190] Furthermore, anions such as $I^-$ ions move towards the electron selective layer, i.e. $TiO_2$ and cation such as $MA^+$ and $Li^+$ migrate into the HTM contact when applying a reverse bias during illumination.[94] This causes an injection barrier for both electrons and holes at their respective interfaces, resulting in hysteresis.

### 4.3.2 Reactivity

Chemical reactions and inter diffusion at the interface can greatly affect overall device stability. Indeed, all types of instabilities in the cell, interface instability is the one its chemistry is almost not yet investigated in Omh-PSCs devices. It is, therefore, important considering detrimental interfacial reactions in detail to find out the intrinsic instabilities. The possible origin of degradation that could



Energy & Environmental Science Accepted Manuscript

take place at the interface of Omh-PSCs solar devices forming interface instability are: i) corrosion of silver forming silver halides at the interface; ii) silver connections usually form shunting paths with the mesoporous $TiO_2$ in the absence of oxygen; iii) photo-oxidation of the HTM organic materials will degrade the electron/hole transport properties and thus the photovoltaic stability; iv) Omh-perovskite decomposition at the $TiO_2/CH_3NH_3PbI_3$ interface through light exposure, since $TiO_2$ has a strong ability to extract electrons from iodide ($I^-$); v) formation of metal oxides which finally lead to device deterioration. Docampo and Snaith[6, 191] demonstrated that silver contacts often form shunting paths with the mesoporous $TiO_2$ in the absence of oxygen. As a result, Schottky barrier can be formed. Similarly, Snaith and coworkers[192] confirmed that metal migrating through the HTM layer is partially responsible for the quick device degradation. They showed that depositing the HTM within an insulating mesoporous "buffer layer" comprised of $Al_2O_3$ prevents the migration, while also facilitating control of the HTM thickness. This prevents the device from degradation even after 350 hrs of operation.

## 5. Suggested approaches to improve stability of Omh-PSCs

Not only efficiency but also stability is a critical requirement for the practical application of Omh-PSCs. It is, therefore, necessary to improve stability to an extent that will make Omh-PSCs technology attractive from a commercial standpoint. Based on current information, device instability is the sum of all the device component materials, device architecture and interfaces. Stability improvement therefore can be expected to result mainly from Omh-Perovskite materials, device architectures and interfaces. Researchers must focus on two major issues regarding the stability and longevity of Omh-PSCs. Firstly, strategies to provide extrinsic stability through the use of proper encapsulation to prevent degradation caused by ambient oxygen and water. Secondly, research to improve the understanding of the intrinsic stability of different thin film perovskite materials, array of the device, and interfaces. The most suitable approaches that should be considered include: chemical engineering modifications to active materials, design and optimization of device architecture, systematic interface engineering. These approaches should provide a means to improve both operation and long term stabilities for Omh-PSCs devices.

### 5.1 Omh-perovskite material aspects



Energy & Environmental Science Accepted Manuscript

The stability of Omh-perovskite materials is an issue in Omh-PSCs. Both chemical composition and structure engineering techniques could be considered for issues related to material stability. Appropriate chemical composition engineering is an essential approach to stabilize Omh-perovskite materials by chemical modification of the X site anions and of the organic 'A' site cation.[193] The size of cation A is critical for the formation of stable close-packed Omh-perovskite structures. As aforementioned, the relative ionic radii of A, B and X in the $ABX_3$ Omh-perovskite structures have been widely used as a method of establishing the distortion of the $MX_6$ octahedron; in particular, a relatively smaller ion radius for X favors the formation of cubic structures.[24] In particular, cation A must fit into the space composed of four adjacent corner sharing $MX_6$ octahedra. The structural and opto-electrical differences of $MAPbI_3$ and $FAPbI_3$ are likely to originate from the difference in ionic radius of the MA (1.8 Å) and FA ions (1.9–2.2Å). Such a structural instability of Omh-perovskites can be improved by regulating the Goldschmidt tolerance factor ($t_f$) using appropriate substitutions, which is a useful indicator for the stability and distortion of crystal structures. Another technique is structural engineering of the Omh-perovskite absorbers, to produce moisture resistant 3D structured analogous materials. The recently reported new layered (2D) structure Omh-perovskite absorbers ($(PEA)_2(MA)_2[Pb_3I_{10}]$ (PEA = $C_6H_5(CH_2)_2NH_3^+$, MA =$CH_3NH_3^+$) may offer greater tunability at the molecular level for material optimization and are more moisture resistant than films of commonly used $(MA)[PbI_3]$ materials.[80] Devices containing these layered materials are stable even in moist environment. As a result of the tunability behavior of the layered structure, these materials may be capable of better stability for future development. Understanding the multifaceted and interplay chemistry of Omh-PSCs and developing new materials based on such knowledge will indisputably open up astonishing stability breakthrough and revolution in this solar cell.

### 5.2 Device architecture aspects

While the absorber material and interface stability are essential requirements for long term stability, it is by no means sufficient, because the end user is ultimately interested in the device stability for a given application. Thus, engineering suitable device architectures are required. Among the three Omh-PSCs device architectures-mesoporous, regular and inverted; the mesoporous one incorporating a carbon top electrode without hole conductor is stable, low cost, simple and promising for practical applications.



Energy & Environmental Science Accepted Manuscript

So far, for Omh-perovskite-based solar cells, PCE ranging from 3.81% to more than 20% have been obtained by optimizing the technology and array of device structure, making it competitive for future commercialization. Zhou and coworkers[36] reported an 80% drop in the PCE over a 24 hr period when the device with planar geometry were stored under ambient conditions, and a 95% drop in the PCE after 6 days. While this loss in performance is highly problematic, even more concerning is that the decomposition product ($PbI_2$) is sparingly soluble in water (1.6 mM at 25 °C);[194] this would present an enormous ecotoxicological problem if a module becomes damaged in the field.

With these issues in mind a substantial effort has gone into improving the long-term stability of Omh-PSCs.[79,83, 195] Protective $Al_2O_3$ layers[83] and hydrophobic oligothiophene HTMs[195] have both been employed as a means of protecting the underlying Omh-perovskite film, while alternative Omh-perovskite compositions[33, 80] have also been explored as a way of improving the stability of the Omh-perovskite itself. Moreover, Snaith and coworkers have prepared Omh-perovskite-based MSSCs, within which the mesoporous n-type $TiO_2$ is entirely replaced with an insulating mesoporous $Al_2O_3$ scaffold.[28,142] $Al_2O_3$ scaffold which acts as a scaffold or supporting material showed improved device stability with an almost stable photocurrent of 15 mA/cm$^2$ over 1,000 hrs exposure period.[6] However, some of the most promising results have come from the use of carbon-based electrodes.[4, 79, 196] Wei and co-workers [197] used inkjet printing to produce $CH_3NH_3PbI_3$/C bilayer devices which retained ca. 90% of their initial PCE after storage in 30% relative humidity (RH) for 12 days. Similarly, Zhang and co-workers [196] and Zhou and co-workers[7] replaced the typical Ag or Au back-contact with carbon paste deposited by doctor-blade. Most dramatically, through the use of functionalized carbon nanotubes embedded in an insulating polymer matrix, Habisreutinger and co-workers[79] were able to protect Omh-perovskite devices from a steady stream of running water for a short time. Although these simple Omh-PSCs is a promising photovoltaic device, several HTM and metal counter electrodes related drawbacks hinder its practical application.

Moreover, to accomplish the necessities for commercial applications, two of the most important issues in Omh-PSCs should be addressed.[15, 142, 198] Firstly, devices incorporating HTMs require undesired cost due to the more expensive price of HTMs such as spiro-MeOTAD and the most conserving issue of poor device stability. The second issue is the counter electrode made of Ag or Au, which is related to: (1) silver corrosions and attacks perovskites forming silver halides, (2) noble metals such as Au or



Energy & Environmental Science Accepted Manuscript

Ag are not applicable for large-scale production due to the deposition technique, i.e. thermal evaporation which initiates hot metal to diffuse in to different layers, highly energy consuming and complicated, and (3) The high cost of the Au electrode also requires a high-vacuum evaporation technique, thereby limiting its future commercialization. Therefore, the current goal focuses on removal of the HTMs and substitution of these metal electrodes to improve stability, simplify the cost of device fabrication and recognize large-scale fabrication. Carbon-based electrodes have been extensively investigated, due to its earth abundance, low cost, low-temperature processing (100 °C), large-scale printing processing[34, 113, 199] and appropriate work function of -5.0 eV (-5.1 eV for Au),[7, 200] and promising long-term stability.[4, 7] This remarkable stability can be attributed to the thick carbon cathode layer, which can work as a water-retaining layer to protect the perovskite from being destroyed.[201] This result indicates the underlying potential of commercial carbon paste as promising candidate for stable and highly efficient Omh-perovskite solar cells.[201] Furthermore, many literatures have clearly established that Omh-PSCs can act as a p-i-n device and thus HTMs is not the first priority for operation.[112, 202] Besides, Omh-perovskite has been considered as both light harvester and hole transporting material.[34, 142, 167] The electron-hole diffusion length of $CH_3NH_3PbI_3$ can even exceed 100 nm.[25, 26] All this evidence indicates that complicated HTMs are not necessary in fabricating Omh-perovskite-based photovoltaic devices. HTM free Omh-PSCs device employing impermeable counter electrode have the potential to overcome these drawbacks and extend long term device stability. This new device concept has greatest potential for practical applications and further improvement both in efficiency and stability can be expected.

### 5.3 Interface aspect

The nanoscale interface properties including interface defect structure relaxation, grain boundary phase transformations, grain boundary size present in different layers determine the eventual stability of the device. Thus, understanding these interface properties and, charge separation and transfer across the nanoscale interface is critical. It has been shown that instability of Omh-PSCs is primarily a result of charge accumulation at the interfaces, due to ion migration, resulting in a change in built-in electric field of the devices and hysteretic effects.[102, 112, 128, 145] The long-term stability of Omh-PSCs can be improved by a proper choice of inter layer and appropriate engineering of barrier layers to protect the Omh-perovskite film beneath and avoid unnecessary barrier in different interface layers. The thermal and moisture-sensitive nature of Omh-perovskite interface is an important concern. In



Energy & Environmental Science Accepted Manuscript

order to overcome such challenges, protecting polymer matrix and single-walled carbon nanotubes have been pioneered.[79]

It is obvious that the mesoporous $TiO_2$ is sensitive to UV illumination and acts as a source of interface instability which causes device performance loss. Moreover, this performance loss is not only observed for the unsealed device but also for the sealed devices. And this loss in performance of the sealed device could not be attributed to degradation of Omh-perovskite and/or HTM. Instead of this, it could rather result from mesoporous electrode during device illumination. Therefore, the changes in optical and electrical behavior of the sealed electrode ($TiO_2$) need to be studied in more detail. Fast decay of excited state and appearance of low resistance shunting path could lead to the loss in $J_{sc}$ and $V_{oc}$ for the sealed devices.[59, 203] There are two approaches to overcome the interface destabilization due to mesoporous $TiO_2$: First, mesoporous $TiO_2$ can be replaced by other mesoporous scaffolds such as aluminum-oxide The use of insulating materials $SnO_2$ with a thin MgO[204], $Al_2O_3$[72] and other alternative metal oxides to replace $TiO_2$ showed an improved resistance to UV light. Second, an insulating metal oxide is introduced to passivate the photoinduced trap states in $TiO_2$ formed during illumination. Different techniques have been used to coat the $TiO_2$ by a variety of metal oxides. [205, 206] The purpose of these metal oxides is create energy barriers, change the CB potential, or diminish surface traps, and finally to retard recombination. Semiconductors such as $Al_2O_3$[207-210] have been employed to produce protecting barriers at the $TiO_2$/HTM interface, raising the physical separation of injected electrons from the oxidized Omh-perovskite/HTM. Fig. 15 shows Schematics representation of a device with an ultra-thin layer of coating before and after perovskite coatings. Fig. 15a represents a coating option before the Omh-perovskite coating that is responsible for diminishing localized $TiO_2$ surface traps and recombination from $TiO_2$ conduction band to the HOMO of the perovskite and the HTM. Another problem for Omh-PSCs is that Omh-perovskite cannot totally cover the surface of the $TiO_2$ photoanode completely.[27, 211] Wang and co-workers[83] found a similar phenomenon, i.e. there are uncovered sites on $TiO_2$, forming indirect contact with HTMs. These uncovered sites act as a potential cause of recombination for electrons from CB of $TiO_2$ to HTMs.

The electrode/electrolyte ($TiO_2$/electrolyte) interface is main problem causing recombination of charge in liquid and quasi-solid DSSCs due to its susceptibility to different reactions. Any modification of this interface will have a great role in improving its stability. In the field of liquid



Energy & Environmental Science Accepted Manuscript

DSCs and quasi-solid DSCs,[212,213, 214] post-modification is one of the key techniques. For instance, The use of 4-tert-butylpyridine is an important interface modification means to retard recombination.[212] Insulating metal oxides such as $Al_2O_3$,[215, 216] ZnS[217, 218] and TBAI[219] have also proved to be effective in retarding electron recombination. Post-modification by $Al_2O_3$ has two roles. One is to protect $CH_3NH_3PbI_3$ and the sensitized film degradation due to moisture and sunlight. Another is that $Al_2O_3$ serves as an insulation barrier between $TiO_2$ and HTM to retard the electron recombination process. Though some activity has been directed at investigating the $TiO_2$/HTM interface, little effort has been directed at the Omh-perovskite/HTM interface through post-modification. Recently, post-modification using aluminum oxide[83] and $Y_2O_3$[220] in Omh-perovskite solar cells has been reported. This type of modification protects the active material from moisture degradation shown in Fig. 15b. However, the thickness of the layer has to be controlled. Thicker over-layers between the $TiO_2$ and Omh-perovskite blocks injection efficiency, but enhance recombination or decay of exited state. Therefore, post modification of Omh-perovskite/HTM interface is promising approach for shielding the perovskite, protecting from external factors such as moisture and improving the lifetime of electrons by retarding recombination.

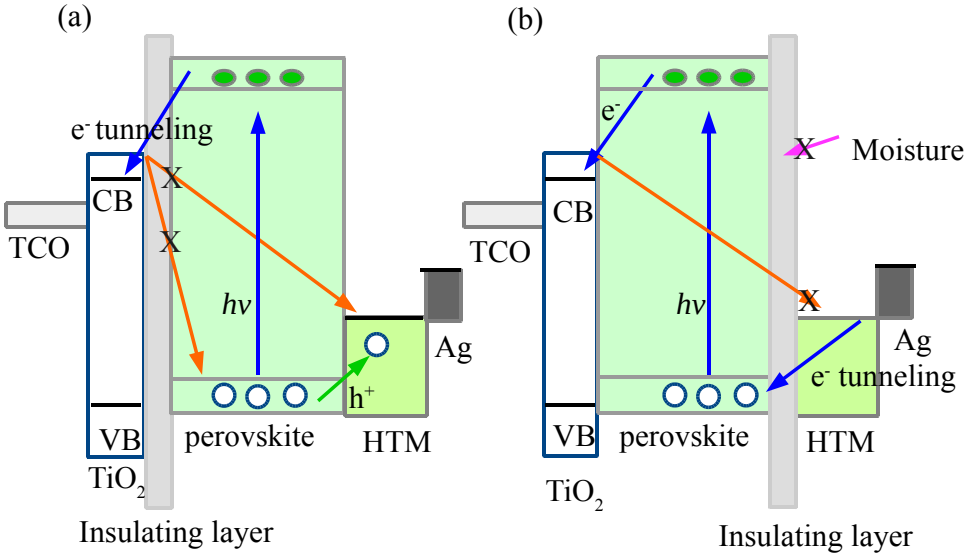


**Fig. 15** Schematic representation of a device with an ultra-thin layer of coating or insulating material before (a) or after (b) Omh-perovskite-sensitization on the mesoporous $TiO_2$ surface

Similarly, the interface between counter electrode and p or n-type layers ((Metal/HTM or p-type layer) and metal/ETL or n-type layers interface) could be sensitive to a chemical reaction which can deform



Energy & Environmental Science Accepted Manuscript

interface properties. Deposition processes, for instance, thermal evaporation technique can cause diffusion of hot reactive metals across interface and this normally changes the behavior of the interface.[221, 222] The formation of new aluminum-carbon bond is supposed to be main cause of interface instability for devices based on aluminum counter electrode.[223, 224] In order to overcome such problems, it is better to consider to: (1) use other techniques like spray-deposition technique,[225, 226] (2) replace the reactive metals such as silver by other alternatives such as carbon and (3) apply small work function metals like Ba, Ca and Mg, for applications in inverted architecture device. More interestingly, blade-coating technique has been demonstrated to improve ambient stability of Omh-perovskite, acting as air-protection patches to block oxygen/moisture infiltration by encouraging the development of self-assembled crystalline domains at the Omh-perovskite surface.[227] All these findings indicate the fundamental role of interfacial engineering in improving the interface stability of Omh-PSCs.

### 5.4 Device operation aspect

#### 5.4.1 UV filters

The exposure of Omh-PSCs to UV light can retard their performance during long-term operation. For instance, UV light can result in $TiO_2$ direct band excitation which may lead to oxidation of the perovskite and HTMs. In order to prevent direct band gap excitation of $TiO_2$, the easiest solution would be to apply a UV cut-off filter and in fact there are reports where UV cut-off filters have been used in stability testing.[76,228-233,241] UV cutoff filters are usually used during long-term stability measurements.[234-238] Interestingly, the use of a UV-filter has been stated as beneficial for the stability of Omh-PSCs based on $CH_3NH_3PbI_3$ and $TiO_2$ nanoparticles.[6] It is then clear that the perfect way to keep products from UV deprivation is to have some way of removing all the UV light before it strikes the material which it will degrade. Unfortunately, it is not always feasible to attain this in practice.

#### 5.4.2 Device encapsulation

Encapsulation enables scientists to eliminate the most damaging components of an Omh-PSCs solar cell from UV radiation or environmental molecules as shown in Fig. 16, which is an important approach to protect the device, and increase its stability.[239] An encapsulation method which retains device flexibility is essential from the viewpoint of industrial engineering.[240] The most extreme illustration is perhaps a device sealed completely in glass.[241] These techniques result in inflexible solar cells free from oxygen and water diffusion. Other more advanced encapsulation approach is to



Energy & Environmental Science Accepted Manuscript

use thermosetting epoxy glue device sealing approach.[228] Moisture and oxygen can't penetrate this type of encapsulation and extend long term stability. Yang's group reported primary stability investigations on Omh-PSCs stored in different environments including nitrogen, dry air, and ambient atmosphere.[36] The Omh-PSCs devices showed a rigorous decay in ambient air compared with devices stored in dry air and nitrogen atmospheres, indicating that the decomposition/dissolving of the Omh-perovskite materials is induced by moisture or air. This indicates better stability can be achieved with more advanced encapsulation methods.[36]

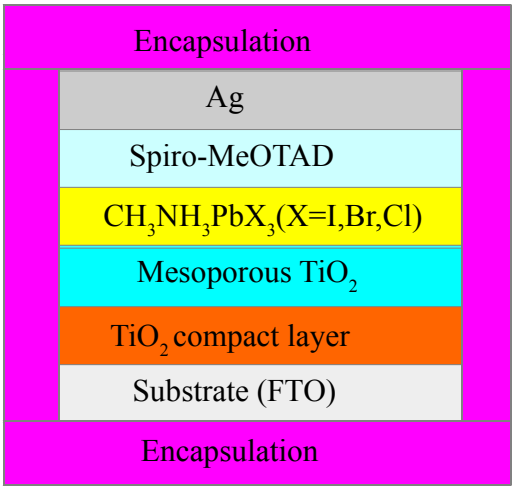


**Fig.16** Schematic representation of Omh-PSCs encapsulation

More interestingly (and as yet still unexplained), higher performance loss is observed for the sealed (encapsulated) device compared to the unsealed (unencapsulated) one as shown in Fig. 17. This could be due to: (1) progressive occurrence of shunting during operation and (2) formation of deep trap sites in the mesoporous electrode. However, there are alternative approaches to overcome such performance loss during operation. First approach, the combination of encapsulation with UV filter would be better for improved stability of the device compared to device without UV filter as indicated in Fig. 17. Second approach, to use both doping and encapsulation assisted reduction of trap states: Fig. 18 shows the parameter evolution for aged devices under inert atmosphere operation. The cell which is not doped decayed drastically in the first 30 min, but not the Al doped device. This indicates the decrease in sub-band gap density of states raise from Al doping assisting the reduction of short-term device deteriorations. Thus Aluminum enduringly appeases these defects through interstitial substitution of Ti adjacent to oxygen defect sites.



Energy & Environmental Science Accepted Manuscript

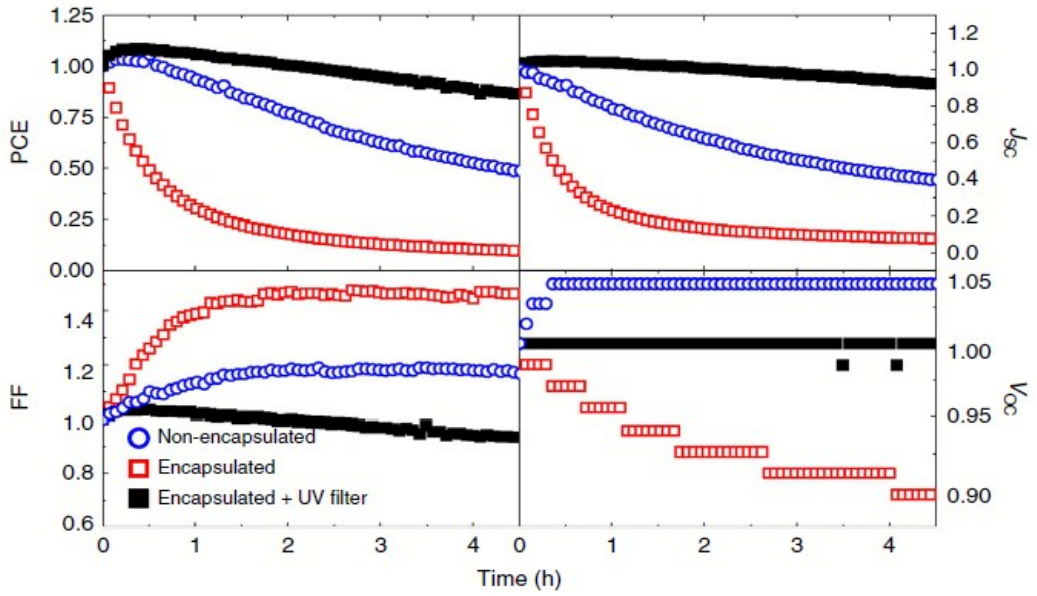


**Fig. 17** Non-encapsulated (blue open circles) and encapsulated (filled black squares) with and without a <435-nm cutoff filter (open red squares) aged Omh-perovskite solar cell device. Reprinted with permission.[6]

Moreover, three optional methods[6] are proposed to minimize $TiO_2$-based solar device power loss during operation: first, build up a means to efficiently and firmly appease the $TiO_2$ surface states, second, stop the UV light from getting the mesoporous $TiO_2$,[64] third, to use down-converting nanoparticles, efficiently absorb UV light and re-emit visible light.[242, 243] Establishing routes to harvest all the shorter wavelength light (<435 nm) before it contacts the mesoporous $TiO_2$ be supposed to let for improved stability with no cost of reduced photocurrents.[238,243]



Energy & Environmental Science Accepted Manuscript

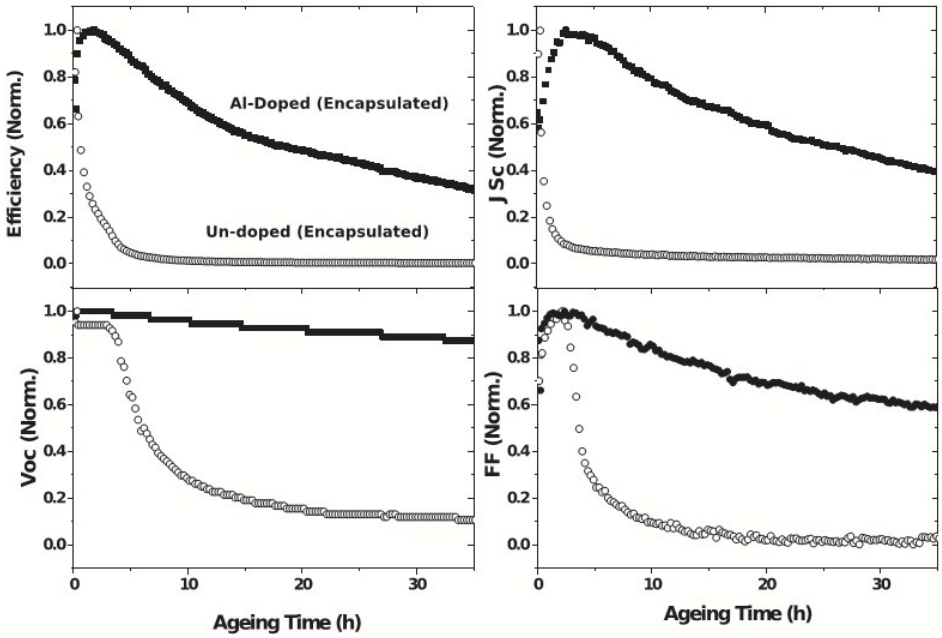


**Fig. 18** Plot of performance parameters versus ageing time for $TiO_2$ based ssDSSCs device doped with aluminum followed by encapsulation. Reproduced with permission from ref. 64.

## 6. Protocols and methods for studying degradation mechanisms

After establishing all the causes and degradation processes, as well as the origins of degradations and approaches to improve stability, it is a precondition to be able to understand the underlying degradation mechanisms and, causes and origins for these degradations using appropriate physical and chemical, and theoretical (computational) techniques. There are also various protocols to study fading mechanisms, such as lifetime and IV curve (most detailed source of information), isotopic labeling, and accelerated testing conditions. There are some procedures which are important for lifetime testing protocols, e.g. dark, laboratory weathering, thermal cycling tests, as well as low light testing, commonly carried out under accelerated conditions of temperature, humidity and illumination. This will help extract all the limitations and challenges for practical applications. Establishing methods and protocols would be critical and essential aspect to overcome the differences or gaps among various research reports released from different groups.

### 6.1 Possible methods for studying degradation of Omh-PSCs

Degradation process includes a multifaceted sort of process which is not easy to illustrate. Some of



Energy & Environmental Science Accepted Manuscript

them are: flow of $H_2O$ and $O_2$ induced device degradation, active material and interface degradation, electrode and interlayer migration, reaction of hot metal with the ETL and HTM, macroscopic and morphology related modifications. It is thus a challenging task for identifying degradation mechanisms and quantifying to the degree of contributions from every mechanism of the whole loss of device performance. Degradation processes can be studied in terms of different useful properties such as (1) bulk and surface behaviour, (2) interface properties and (3) array of device architecture. This can be achieved using both computational or theoretical and, physical and chemical characterization techniques. Information can be obtained from specific study methods and/or from entire devices, which is averaged information. These methods should be considered as key ways to obtain accurate information, while possibly also suggesting new routes of investigation.

### 6.1.1 Characterization of Omh-perovskite material bulk and surface properties

Studies of material behavior (crystal structures, phase changes, and surface traps) are ways to identify problems that may compromise material stability. Bulk and surface properties of Omh-perovskite materials can be studied to: characterize changes in the surface chemistry, structural and phase changes, carrier lifetime, mass loss, thermal behavior, and mechanical properties. All these properties provide chemical and/or physical information about the Omh-perovskite material stability and degradation. Furthermore, degradation information can be obtained from both theoretical and experimental investigations. Although most of the literature reports are from experimental analysis the contributions from theoretical or computational viewpoints using first principle, *ab-initio* and DFT methods are also essential to investigate the structure, orientations, vibrational frequencies, interaction energy, charge distributions and other properties.

#### 6.1.1.1 Chemistry of surface

The study of surface chemical processes plays a significant role in basic chemical research. At the molecular level, the surface atoms (compared to the bulk) experience a different chemical environment, due largely to the reduced number of neighbouring atoms. As a consequence, these surface atoms with changed atomic and electronic structures exhibit high chemical reactivity. This chemical reactivity can lead to corrosion or degradation when in contact with the environment; therefore, studying the surface changes in Omh-perovskite materials, when exposed to different conditions, such as, moisture, temperature, and air essential. At present, a vast number of



Energy & Environmental Science Accepted Manuscript

experimental and theoretical surface chemistry techniques have been developed. The *in-situ* techniques are specifically of great importance. X-ray photoelectron spectroscopy(XPS), [244, 245, 246] Scanning Kelvin probe microscopy (SKPM),[112, 185] Rutherford backscattering (RBS),[247] X-rays for the reflectometry, Surface Enhanced Raman spectroscopy (SERS), Ambient pressure X-Ray Photoelectron Spectroscopy (AP-XPS) are some of surface sensitive techniques.

#### 6.1.1.2 Structural/phase and optical properties

Omh-perovskites are intrinsically complex materials, where the presence of various types of interactions and structural disorder may play an important role in the material properties. *Ex-situ* and *in-situ* measurements, such as UV vis, X-ray diffraction, vibrational spectroscopy (Infrared[248, 249] and, DFT simulation assisted Raman[250] and Raman[251, 252]), spectroscopic ellipsometry[88] and X-ray absorption spectroscopy (XAS) are essential techniques for studying optical properties, structure and phase transformations in materials. Light soaking has been identified to split XRD peaks in $CH_3NH_3PbI_{3-x}Br_x$ film, indicating crystalline phases segregation into Br as main species and iodine as minor species with the latter could act as trap site.[253] While the *in-situ* absorbance measurements provide a convenient spectroscopic method to track film degradation kinetics, they provide no structural information on changes in crystallinity or phase that occurs during degradation. *Ex situ* powder X-ray diffraction (pXRD) experiments could be carried out in order to identify both the initial Omh-perovskite phase and any crystalline degradation products. While pXRD could be set to study the crystallographic structure, crystallite size (grain size), and preferred orientation in polycrystalline or powdered solid sample *in-situ* grazing incidence X-ray diffraction (GIXRD) measurements is more useful to elucidate the reaction mechanism for the decomposition process upon accelerating conditions such as moisture and light.[86] Moreover, the combination of a fast 2D area detector with a high brightness synchrotron X-ray source allows the acquisition of 2D diffraction data in real time, providing important insight into the film decomposition process.

#### 6.1.1.3 Carrier lifetime

The carrier lifetime of materials can be studied by monitoring Time-resolved photoluminescence (TRPL) measurements. Snaith and co-workers reported TRPL measurements for Omh-PSCs and TRPL curve decay ($\tau_e$ = 273 ± 7 ns, where $\tau_e$ is the time taken for the PL to fall to 1/e of its initial intensity) was observed.[26] A PL lifetime as high as 200.1 ns was also demonstrated, and the long



Energy & Environmental Science Accepted Manuscript

lifetime is tentatively ascribed to the Cl doping effect.[245] In order to investigate the feasibility and impact of these Lewis base treatments, Noel and coworkers performed a spectroscopic, theoretical, and device based investigation.[118] Nonradiative decay inhibited significantly within the treated perovskite films, especially under low levels of photoexcitation. More research needs to be done to understand how this novel family of solar absorber materials gives rise to long charge carrier lifetimes. Comparison of hysteretic effect and transient behavior on mesoporous titania based perovskite devices to regular thin film devices was done using IV curves and slow transient external quantum efficiency measurements.[94] Currently, more advanced techniques, correlated scanning electron microscopy and confocal photoluminescence measurements, have been applied to explore structure/function relationship in Omh-perovskite film. The results obtained indicated the presence of considerable local PL heterogeneity with average carrier lifetime of >1005 ns for $CH_3NH_3PbI_3$ (Cl) films,[120] implying that a substantial scope remains for minimizing nonradiative decay. Regardless of these wonderful advancements in studying and understanding from both the experimental and the theoretical observations, until now the cause for the prolonged carrier lifetime of Omh-perovskites remains unclear. Some theoretical observations imply that a dynamic position of the conduction band minimum could be the reason for this prolonged carrier lifetime in $MAPbI_3$ films.[134]

#### 6.1.1.4 Thermal property

Since the formation of $CH_3NH_3PbI_3$ is influenced by the release of MAX, it is important to characterize the thermal properties of $CH_3NH_3I$ and $CH_3NH_3Cl$. As shown in Fig. 19a, the thermal gravimetric analysis (TGA) curves show nearly 100% weight loss between 250 °C and 360 °C for $CH_3NH_3Cl$ and between 290 °C and 370 °C for $CH_3NH_3I$, respectively. The lower onset of the weight loss temperature of $CH_3NH_3Cl$ suggests that it is easier to turn into gaseous phase as compared to $CH_3NH_3I$. Moreover, it is important to understand in what manner $CH_3NH_3Cl$ and $CH_3NH_3I$ could possibly escape from the precursor films during the annealing process. As shown in Fig. 19b, the endothermic peaks in the differential scanning calorimetry curves indicates escape of $CH_3NH_3Cl$ and $CH_3NH_3I$ is related to a sublimation process.[49]



Energy & Environmental Science Accepted Manuscript

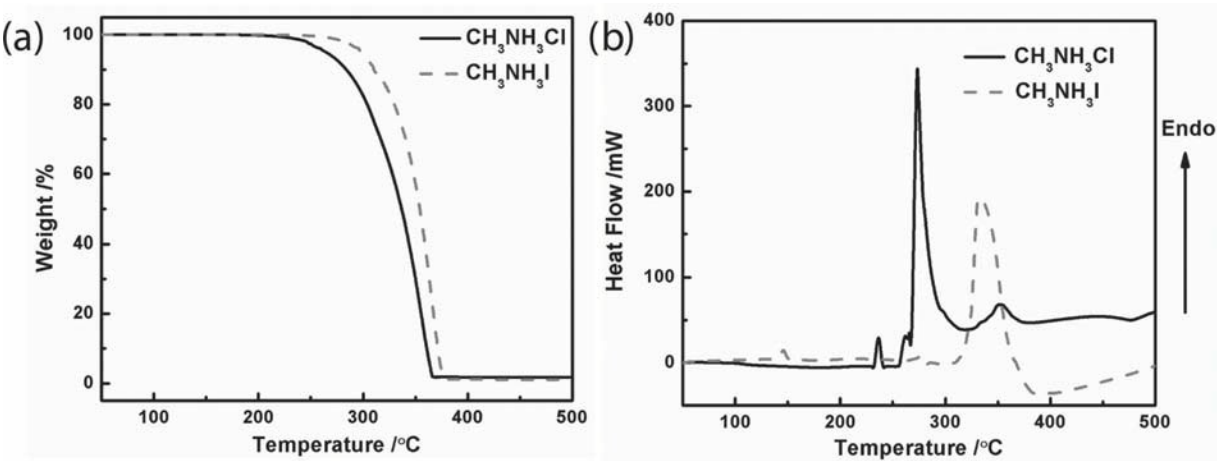


**Fig. 19.** a) TGA and b) DSC curves for $CH_3NH_3I$ and $CH_3NH_3Cl$ powders. Reproduced with permission from ref.49.

Both the TGA and DSC results confirm that the release of $CH_3NH_3I$ occurs at higher temperature as compared to $CH_3NH_3Cl$. This confirms that the higher annealing temperature is required for the $CH_3NH_3I/PbI_2$ precursor mixtures.

#### 6.1.1.5 Mechanical properties

The mechanical properties[254] of Omh-perovskite materials and the mechanical failure mechanisms of devices can play critical roles in the operational stability of Omh-PSCs for portable and outdoor applications. This section highlights mechanical properties-principally the stiffness and brittleness of pure films of these semiconductors and component layers e.g. fullerenes. The ubiquitous acceptor PCBM has many deleterious effects on the mechanical stability of OPV devices. Pure PCBM phases have low cohesive energy,[255] high tensile and low crack onset strains,[256] and weak interfaces with other device layers.[161] Several potential determinants of mechanical properties, including molecular structures, polymorphisms, microstructures and textures have not yet been critically reported.

### 6.1.2 Device architecture

The most in depth source of information is the measurement of IV-curves as a function of time. From the evolution of the IV-curves information on $J_{sc}$, $V_{oc}$, FF, PCE, $R_{sh}$ and $R_s$ can be extracted and the broad-spectrum of the curve can be applied to follow the decay of the device's performance. The principles of equivalent circuit play an important role to model characteristics of diode for extracting extra device parameters such as parallel and series resistances. The IV curve for Omh-PSCs can,



Energy & Environmental Science Accepted Manuscript

however, change dramatically as it decays. Recently, Grätzel and coworkers demonstrated that an IV-curve of the device measurements at different light intensities of the light source using an array of white LEDs could be ascribed to a decrease in the shunt resistance.[35] Measuring all diode parameters at a standard interval is therefore helpful rather than just measuring a single diode characteristic.

Different analytical technique can be used in addition to IV curve such as intensity-modulated photocurrent/ photovoltage spectroscopies (IMPS/IMVS),[257, 258] impedance,[259] time-of-flight,[260] and open-circuit voltage decay.[261] The different layers in both mesoporous $TiO_2$ and compact $TiO_2$ device structures affect the separation, transport, and recombination kinetics of the photoinduced charge carriers. According to Wang and co-workers, a mesoporous electron conductor is necessary to optimize $CH_3NH_3PbI_3$-based solar cell devices with high PCE.[178] This mesoporous $TiO_2$ is more likely to induce the formation of $PbI_2$ than compact $TiO_2$.[178] Fementosecond time-resolved transient absorption spectroscopy probed in the visible spectrum, when coupled with XRD, is a useful tool for this purpose.[178]

### 6.1.3 Interface characterization

Identifying issues related to interfaces are quite complex, including many concerns of transport barriers, charge separation, band bending, and charge transfer. Analytical techniques/methods such as IV characterizations, angle-resolved XPS (AR-XPS),[262] Fourier transform photocurrent spectroscopy (FTPS) and transient absorption spectroscopy (TAS) measurements, charge extractions by linearly increasing voltage (CELIV), first-principles DFT modeling,[262] Transient absorption spectroscopy (TAS), and energy dispersive X-ray spectroscopy (EDX) and electron energy loss spectroscopy (EELS) and surface-sensitive XPS measurements,[49, 112, 263] spectroscopic ellipsometry or X-ray reflectivity,[264] energy dispersive X-ray reflectometry,[159] are helpful to study interfacial issues. Miscellaneous processes can be integrated while interfaces/surfaces are exposing to water and oxygen, and finally, can cause segregation on the surface. The best option to investigate the interior of Omh-PSCs with respect to chemistry is to systematically get rid of each layer in the device and examine the exposed interfaces 2-6 as shown in Fig. 20.

For chemical degradation, oxygen or water-induced degradation, chemical characterization is preferred such as TOF-SIMS, together with isotopic labeling using $H_2{}^{18}O$ and $^{18}O_2$ to acquire in-depth



Energy & Environmental Science Accepted Manuscript

information on where, and to what degree of the capture takes place. $^{18}O$ has a natural abundance of

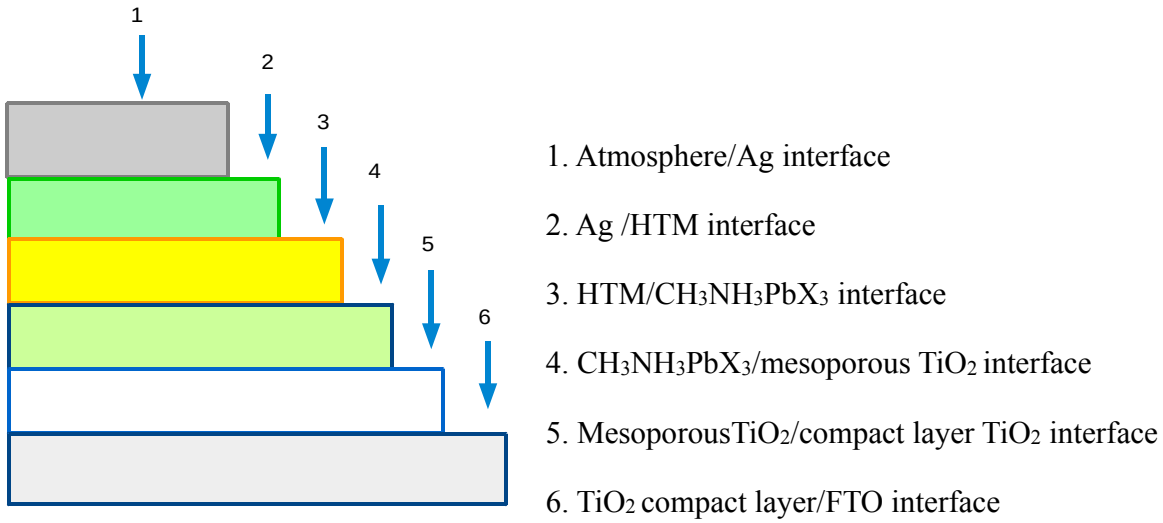


**Fig. 20** Schematic drawing of an Omh-PSC cross-section with the configuration Ag/HTM/$CH_3NH_3PbX_3$/mp-$TiO_2$/cl-$TiO_2$/FTO showing all the relevant interfaces, where X is I, Br, Cl or mixed halides.

0.2%, i.e. simply remunerated through the measurements of intensity of $^{16}O$ signal. In order to obtain a semi-quantitative measure of $^{18}O$ incorporation, and thereby of the process, Equation (22) is used:[240]

$$\frac{\left[\frac{I(^{18}O)}{I(^{16}O)}\right]_{hv} - \left[\frac{I(^{18}O)}{I(^{16}O)}\right]_{ref}}{\left[\frac{I(^{18}O)}{I(^{16}O)}\right]_{ref}} x100\% \qquad (22)$$

Where $I(^{18}O)$ is the intensity of the $^{18}O$ isotope of a given species and $I(^{16}O)$ is the corresponding intensity of the $^{16}O$ isotope.

### 6.2 Accelerated testing conditions and protocols

Accelerated testing protocols are useful to analyse the effects of artificially rapid chemical degradation or physical changes of a solar cell device, brought about by exaggerated storage conditions; these studies can be used to support long-term stability studies of solar devices. The practices for organic PV materials and devices could offer a reference point, where the most frequent



Energy & Environmental Science Accepted Manuscript

accelerated testing protocols include solar-thermal cycling, solar-thermal cycling, solar-thermal-humidity cycling and solar-thermal-humidity-freeze, laboratory weathering and thermal cycling.[265] Moreover, concentrated sunlight may be a novel approach to explore degradation of Omh-perovskite.[122] In addition to the accelerating protocols, accelerated test equipment facilitates a combination of tests. For example, a temperature/humidity test (typically 85 $^{0}$C/85% RH) by a pressure cooker test/highly-accelerated temperature and humidity stress test (PCT/HAST) chamber is frequently used for electronic components, semiconductors, and PV modules, while illumination/temperature is a popular test for materials. It is believed that similar environmental stress screening can be adopted to evaluate the reliability of Omh-PSC components accordingly.

### 6.3 $H_2{}^{18}O$ and $^{18}O_2$ isotopic labeling protocols

Characterizing the performance of the solar cell under various atmosphere conditions can verify the stability of the device in a particular atmosphere, but does not in any way measure the degree of atmospheric oxidation.[266] In addition, as each layer in the cell acts as a barrier, varying a layer may modify the overall need for encapsulation. This barrier effect could be verified by dealing with oxygen transmission inside the solar cell by an isotopically labelled dry oxygen ($^{18}O_2$) atmosphere or with an oxygen-free humid ($H_2{}^{18}O$) atmosphere.

## 7. Conclusion and prospects

The field of Omh-PSCs is undergoing rapid development, in which the majority of research attempts is to fabricate devices with better efficiencies. An evenly vital topic that has gained less concentration is to improve the quite deprived stability. Only promising steps have been achieved from a few minutes to thousands of hours (2000 hrs). Thus, there may be various causes of device failure, which need to be explored in-depth. The major causes responsible for this kind of degradation may be related to various possible external factors, such as moisture, oxygen, temperature, UV light, etc., as well as internal intrinsic factors such as ion migration, electro-migrations and interfacial reactions. Knowledge of degradation mechanisms, structures and phase transformations under different operating conditions play key roles to predict material and device behaviour. In this review, we have reviewed various causes and their associated mechanisms of degradation. These degradations could be originated mainly from different components of the device, the architecture of the device itself and/or



Energy & Environmental Science Accepted Manuscript

from various interfaces connecting different layers of the device.

Degradation of different device components such as Omh-perovskites itself, hole transporting materials and counter electrodes can take place for different reasons. These component degradations will collectively lead to the overall device degradation and may further restrict practical applications. Thus, identifying the contributions from each component to the device degradation would be more beneficial. For instance, Omh-perovskites are easy to degrade under different environmental conditions. Primary emphasis should be given to a comprehensive understanding of the crystal structure of these materials under varying conditions. Other families of these materials are also available and showed promising stability. In addition, The use of HTMs such as spiro-MeOTAD and PEDOT:PSS is found to be destructive to the device. It would be more useful avoiding these materials, due to their obvious drawbacks, as mentioned. Additionally, the HTM additives such as Li-TFSI and 4-*tert*-butylpyridine are hygroscopic, which will directly affect Omh-perovskite and leads to device deterioration. It is more important to avoid the use of such deliquescent additives. Similarly, the use of different metal counter electrodes such as silver and aluminum can also be detrimental to device stability. Replacing such electrodes made of these metals would be beneficial. The deposition techniques of these metal electrodes such as thermal deposition can also have a strong influence on the device stability. Carbon electrode printing is a promising deposition method compared to thermal deposition, in which hot metal diffusion into organic layers could attack the active Omh-perovskite.

The issues of device architecture remain impenetrable and this should also be considered when performing future long-term stability tests. Stability studies of such devices with various designs are insufficient; thus an in-depth comparative stability study for the three different device architectures (planar, inverted and mesoporous) is still highly required. Similarly, the effect interface appears to be another urgent concern and as such requires additional in-depth investigation. Destructive interfacial reactions may occur in the metal/organic interface due to the diffusion of hot metal during deposition, while ion migration can also encourage confounding hysteresis effects – all of which promote device deterioration. The other critical issue at the $TiO_2$/perovskite interface is the depletion of iodine, due to the strong n-type character of $TiO_2$ semiconductor. The surface of $TiO_2$ is thought to play a catalytic role in Omh-perovskite degradation. This depletion may be further exacerbated by high temperatures or by illumination during device operation. Omh-PSCs devices have complex multilayer



Energy & Environmental Science Accepted Manuscript

configurations in which each party may not succeed for various reasons and the layers can undergo an interaction chemically and physically in such a way that can raise instability.

In this regard, it is necessary to establish efficient solutions for improving stability to an extent that will make Omh-PSCs technology attractive and feasible from commercial perspectives. Based on the current information and future outlooks, we suggested possible stability improvement approaches mainly from three perspectives: Omh-perovskite materials, device architecture and interfacial aspects. Upon various structural modifications, different alternative mixed Omh-perovskites and new layered Omh-perovskite materials with promising stability under operating conditions have been explored. There is still 'a room to explore various families of Omh-perovskites,' which could be more stable and better candidates for future applications and fabrications of stable Omh-PSCs devices. To date, the best stability was achieved using HTM and metal electrode free mesoporous device architecture, which used a carbon as counter electrode. Interestingly, the commercial carbon paste is now a promising candidate for Omh-PSCs cathodes. In our opinion, the mesoporous device architecture with further improvement has great potential for practical applications not only from a stability point of view, but also for reasons of simplicity and ease of fabrication. For better improvement of this device architecture, all possible interfacial problems should be able to be solved by careful interface engineering. A good choice of anode and cathode interlayer materials may protect the active layer by means of blocking the diffusion of oxygen and water through the metal cathode/electron transport layer, or the ITO/hole-transporting layer. Above all, efficient perovskite structure engineering, suitable counter electrodes and its deposition, suitable device architecture and careful interface engineering, which consider all the mentioned environmental and intrinsic factors as well as all other existing challenges ought to be cautiously taken to establish an all-purpose method for the production of stable Omh-PSCs. It can be confidently warm up that there is much work to be done and the guarantee of Omh-PSCs for future choice of solution processed energy technology is everlasting.

The degradation of different Omh-perovskites, interfaces and devices remains largely unexplored. Fundamental studies on the photochemical, chemical, physical, and mechanical properties; interfacial processes and degradation mechanisms of various device components and its architecture are still needed to advance the field. Systematic studies of the relationships between Omh-perovskite materials' properties, including chemical composition, phase and crystal structure, morphology,



Energy & Environmental Science Accepted Manuscript

surface and bulk chemistry, material crystalline quality correlated to grain size are required. The degradation of Omh-perovskites caused by extrinsic and intrinsic factors should be explored to understand the origin of instability during long term use. Furthermore, the interface properties (interface defect structure relaxation, grain boundary phase transformations, grain boundary size) among different layers determine the final stability of the resulting device. In this regard, systematic cross-sectional cell configurations showing every interface profile can be very useful in investigating the interfacial stability problems. Taking the information presented as a whole, we conclude that the understanding the multifaceted chemistry of Omh-PSCs will be the key for developing new materials that will bring this nascent technology to fruition. It is also imperative to investigate all proposed degradations further and decide possible approaches for stability improvements. Accelerated testing protocols, such as temperature/RH combinations, illumination and moisture must be established and documented for stability studies under indoor and outdoor situations, so that the inconsistency in stability reports from various research groups can be gradually harmonized under standardized conditions.

**Acknowledgement**

The financial support from Ministry of Science and Technology (MoST) (104-3113-E-011-001-, 104-ET-E-001-ET, 103-2221-E-011-156-MY3, 102-2221-E-011-157- ) and the Top University Projects of Ministry of Education (MoE) (100H45140), as well as the facilities of supports from National Taiwan University of Science and Technology (NTUST) are acknowledged.

**References**

1. C. R. Osterwald and T. J. McMahon, *Prog. Photovolt: Res. Appl.*, 2009, **17**, 11-33.
2. *OXFORD PVs-Next generation solar power*, January 2015.
3. H.-S. Kim, C.-R. Lee, J.-H. Im, K.-B. Lee, T. Moehl, A. Marchioro, S.-J. Moon, R. Humphry-Baker, J.-H. Yum, J. E. Moser, M. Grätzel and N.-G. Park, *Sci. Rep.*, 2012, **2**.
4. A. Mei, X. Li, L. Liu, Z. Ku, T. Liu, Y. Rong, M. Xu, M. Hu, J. Chen, Y. Yang, M. Grätzel and H. Han, *Science*, 2014, **345**, 295-298.
5. J. Burschka, N. Pellet, S.-J. Moon, R. Humphry-Baker, P. Gao, M. K. Nazeeruddin and M. Gratzel, *Nature*, 2013, **499**, 316-319.
6. T. Leijtens, G. E. Eperon, S. Pathak, A. Abate, M. M. Lee and H. J. Snaith, *Nat Commun*, 2013, **4**.
7. H. Zhou, Y. Shi, Q. Dong, H. Zhang, Y. Xing, K. Wang, Y. Du and T. Ma, *J. Phys. Chem. Lett.*, 2014, **5**, 3241-3246.



Energy & Environmental Science Accepted Manuscript

8. G. Hodes, *Science*, 2013, **342**, 317-318.
9. M. Antonietta Loi and J. C. Hummelen, *Nature Mater.*, 2013, **12**, 1087-1089.
10. M. A. Green, K. Emery, Y. Hishikawa, W. Warta and E. D. Dunlop, *Progress in Photovoltaics: Research and Applications*, 2015, **23**, 1-9.
11. S. Kim, J.-W. Chung, H. Lee, J. Park, Y. Heo and H.-M. Lee, *Solar Energy Materials and Solar Cells*, 2013, **119**, 26-35.
12. S. Mathew, A. Yella, P. Gao, R. Humphry-Baker, F. E. CurchodBasile, N. Ashari-Astani, I. Tavernelli, U. Rothlisberger, K. NazeeruddinMd and M. Grätzel, *Nat Chem.*, 2014, **6**, 242-247.
13. *http://mms.businesswire.com/bwapps/mediaserver/ViewMedia?mgid=354751&vid=4Heliatek*, *Press release*, 2013.
14. J. C. B. A. Marchioro, J. Teuscher, M. Grätzel, and J.-E. Moser, , *Proc. of SPIE*, 2013, **8811**, 881108.
15. H.-S. Kim, C.-R. Lee, J.-H. Im, K.-B. Lee, T. Moehl, A. Marchioro, S.-J. Moon, R. Humphry-Baker, J.-H. Yum, J. E. Moser, M. Gratzel and N.-G. Park, *Sci. Rep.*, 2012, **2**.
16. D. B. Mitzi, *J. Mater. Chem.*, 2004, **14**, 2355-2365.
17. D. B. Mitzi, K. Chondroudis and C. R. Kagan, *IBM J. Res. Dev.*, 2001, **45**, 29-45.
18. D. B. Mitzi, C. A. Feild, W. T. A. Harrison and A. M. Guloy, *Nature*, 1994, **369**, 467-469.
19. D. B. Mitzi, S. Wang, C. A. Feild, C. A. Chess and A. M. Guloy, *Science*, 1995, **267**, 1473-1476.
20. K. Chondroudis and D. B. Mitzi, *Chem. Mater.*, 1999, **11**, 3028-3030.
21. A. Kojima, K. Teshima, Y. Shirai and T. Miyasaka, *J. Am. Chem. Soc.*, 2009, **131**, 6050-6051.
22. L. Etgar, P. Gao, Z. Xue, Q. Peng, A. K. Chandiran, B. Liu, M. K. Nazeeruddin and M. Grätzel, *J. Am. Chem. Soc.*, 2012, **134**, 17396-17399.
23. D. B. Mitzi, *Journal of Chemical Society, Dalton Transactions*, 2001, DOI: 10.1039/B007070J, 1-12.
24. C. C. Stoumpos, C. D. Malliakas and M. G. Kanatzidis, *Inorg. Chem.*, 2013, **52**, 9019-9038.
25. G. Xing, N. Mathews, S. Sun, S. S. Lim, Y. M. Lam, M. Grätzel, S. Mhaisalkar and T. C. Sum, *Science*, 2013, **342**, 344-347.
26. S. D. Stranks, G. E. Eperon, G. Grancini, C. Menelaou, M. J. P. Alcocer, T. Leijtens, L. M. Herz, A. Petrozza and H. J. Snaith, *Science*, 2013, **342**, 341-344.
27. J.-H. Im, C.-R. Lee, J.-W. Lee, S.-W. Park and N.-G. Park, *Nanoscale*, 2011, **3**, 4088-4093.
28. M. M. Lee, Teuscher, J., Miyasaka, T., Murakami, T. N. & Snaith, H. J. , *Science* 2012, **338**, 643-647
29. J. Salbeck, N. Yu, J. Bauer, F. Weissörtel and H. Bestgen, *Synth. Met.*, 1997, **91**, 209-215.
30. U. Bach, D. Lupo, P. Comte, J. E. Moser, F. Weissortel, J. Salbeck, H. Spreitzer and M. Gratzel, *Nature*, 1998, **395**, 583-585.
31. G. Giorgi, J.-I. Fujisawa, H. Segawa and K. Yamashita, *J. Phys. Chem. Lett.*, 2013, **4**, 4213-4216.
32. J. H. Heo, S. H. Im, J. H. Noh, T. N. Mandal, C.-S. Lim, J. A. Chang, Y. H. Lee, H.-j. Kim, A. Sarkar, K. NazeeruddinMd, M. Gratzel and S. I. Seok, *Nat. Photonics*, 2013, **7**, 486-491.
33. J. H. Noh, S. H. Im, J. H. Heo, T. N. Mandal and S. I. Seok, *Nano Lett.*, 2013, **13**, 1764-1769.
34. M. Liu, M. B. Johnston and H. J. Snaith, *Nature*, 2013, **501**, 395-398.
35. M. A. Green, A. Ho-Baillie and H. J. Snaith, *Nat Photon*, 2014, **8**, 506-514.
36. H. Zhou, Q. Chen, G. Li, S. Luo, T.-b. Song, H.-S. Duan, Z. Hong, J. You, Y. Liu and Y. Yang, *Science*, 2014, **345**, 542-546.
37. J. A. Christians, J. S. Manser and P. V. Kamat, *J. Phys. Chem. Lett.*, 2015, **6**, 852-857.
38. N. J. Jeon, J. H. Noh, W. S. Yang, Y. C. Kim, S. Ryu, J. Seo and S. I. Seok, *Nature*, 2015, **517**,




Energy & Environmental Science Accepted Manuscript

476-480.
39. G. Hodes and D. Cahen, *Nat Photon*, 2014, **8**, 87-88.
40. O. Malinkiewicz, A. Yella, Y. H. Lee, G. M. Espallargas, M. Graetzel, M. K. Nazeeruddin and H. J. Bolink, *Nat Photon*, 2014, **8**, 128-132.
41. N. K. Noel, S. D. Stranks, A. Abate, C. Wehrenfennig, S. Guarnera, A.-A. Haghighirad, A. Sadhanala, G. E. Eperon, S. K. Pathak, M. B. Johnston, A. Petrozza, L. M. Herz and H. J. Snaith, *Energy Environ. Sci.*, 2014, **7**, 3061-3068.
42. F. Hao, C. C. Stoumpos, D. H. Cao, R. P. H. Chang and M. G. Kanatzidis, *Nat Photon*, 2014, **8**, 489-494.
43. J. Burschka, A. Dualeh, F. Kessler, E. Baranoff, N.-L. Cevey-Ha, C. Yi, M. K. Nazeeruddin and M. Grätzel, *J. Am. Chem. Soc.*, 2011, **133**, 18042-18045.
44. Y. S. Kwon, J. Lim, H.-J. Yun, Y.-H. Kim and T. Park, *Energy Environ. Sci.*, 2014, **7**, 1454-1460.
45. B. Suarez, V. Gonzalez-Pedro, T. S. Ripolles, R. S. Sanchez, L. Otero and I. Mora-Sero, *J. Phys. Chem. Lett.*, 2014, **5**, 1628-1635.
46. J. J. Choi, X. Yang, Z. M. Norman, S. J. L. Billinge and J. S. Owen, *Nano Lett.*, 2013, **14**, 127-133.
47. V. Roiati, S. Colella, G. Lerario, L. De Marco, A. Rizzo, A. Listorti and G. Gigli, *Energy Environ. Sci.*, 2014, **7**, 1889-1894.
48. V. Roiati, E. Mosconi, A. Listorti, S. Colella, G. Gigli and F. De Angelis, *Nano Lett.*, 2014, **14**, 2168-2174.
49. H. Yu, F. Wang, F. Xie, W. Li, J. Chen and N. Zhao, *Adv. Funct. Mater.*, 2014, **24**, 7102-7108.
50. T. Supasai, N. Rujisamphan, K. Ullrich, A. Chemseddine and T. Dittrich, *Appl. Phys. Lett.*, 2013, **103**, 183906.
51. A. Dualeh, N. Tétreault, T. Moehl, P. Gao, M. K. Nazeeruddin and M. Grätzel, *Adv. Funct. Mater.*, 2014, **24**, 3250-3258.
52. A. Dualeh, P. Gao, S. I. Seok, M. K. Nazeeruddin and M. Grätzel, *Chem. Mater.*, 2014, **26**, 6160-6164.
53. A. Seemann, H. J. Egelhaaf, C. J. Brabec and J. A. Hauch, *Org. Electron.*, 2009, **10**, 1424-1428.
54. M. O. Reese, A. M. Nardes, B. L. Rupert, R. E. Larsen, D. C. Olson, M. T. Lloyd, S. E. Shaheen, D. S. Ginley, G. Rumbles and N. Kopidakis, *Adv. Funct. Mater.*, 2010, **20**, 3476-3483.
55. M. Manceau, S. Chambon, A. Rivaton, J.-L. Gardette, S. Guillerez and N. Lemaître, *Solar Energy Materials and Solar Cells*, 2010, **94**, 1572-1577.
56. F. C. Krebs and K. Norrman, *Prog. Photovolt: Res. Appl.*, 2007, **15**, 697-712.
57. E. Carter, A. F. Carley and D. M. Murphy, *J. Phys. Chem. C*, 2007, **111**, 10630-10638.
58. D. C. Hurum, A. G. Agrios, K. A. Gray, T. Rajh and M. C. Thurnauer, *J. Phys. Chem. B*, 2003, **107**, 4545-4549.
59. H. Al-Dmour and D. M. Taylor, *Appl. Phys. Lett.*, 2009, **94**, -.
60. M. Iwamoto, Y. Yoda, M. Egashira and T. Seiyama, *J. Phys. Chem.*, 1976, **80**, 1989-1994.
61. U. B. Cappel, T. Daeneke and U. Bach, *Nano Lett.*, 2012, **12**, 4925-4931.
62. A. Stevanovic, M. Büttner, Z. Zhang and J. T. Yates, *J. Am. Chem. Soc.*, 2011, **134**, 324-332.
63. Z. Zhang and J. T. Yates, *Chem. Rev.*, 2012, **112**, 5520-5551.
64. S. K. Pathak, A. Abate, P. Ruckdeschel, B. Roose, K. C. Gödel, Y. Vaynzof, A. Santhala, S.-I. Watanabe, D. J. Hollman, N. Noel, A. Sepe, U. Wiesner, R. Friend, H. J. Snaith and U. Steiner, *Adv. Funct. Mater.*, 2014, **24**, 6046-6055.
65. S. K. Pathak, A. Abate, T. Leijtens, D. J. Hollman, J. Teuscher, L. Pazos, P. Docampo, U.



Energy & Environmental Science Accepted Manuscript

Steiner and H. J. Snaith, *Adv. Energy Mater.*, 2014, **4**, n/a-n/a.
66. K. Schwanitz, U. Weiler, R. Hunger, T. Mayer and W. Jaegermann, *J. Phys. Chem. C*, 2006, **111**, 849-854.
67. K. Schwanitz, E. Mankel, R. Hunger, T. Mayer and W. Jaegermann, *CHIMIA International Journal for Chemistry*, 2007, **61**, 796-800.
68. I. Nakamura, N. Negishi, S. Kutsuna, T. Ihara, S. Sugihara and K. Takeuchi, *Journal of Molecular Catalysis A: Chemical*, 2000, **161**, 205-212.
69. D. C. Cronemeyer, *Physical Review*, 1959, **113**, 1222-1226.
70. J. Bisquert, F. Fabregat-Santiago, I. Mora-Seró, G. Garcia-Belmonte, E. M. Barea and E. Palomares, *Inorg. Chim. Acta*, 2008, **361**, 684-698.
71. M. A. Henderson, W. S. Epling, C. L. Perkins, C. H. F. Peden and U. Diebold, *J. Phys. Chem. B*, 1999, **103**, 5328-5337.
72. G. Lu, A. Linsebigler and J. T. Yates, *J. Chem. Phys.*, 1995, **102**, 4657-4662.
73. G. Munuera, V. Rives-Arnau and A. Saucedo, *J. Chem. Soc., Faraday Trans. 1*, 1979, **75**, 736-747.
74. A. Abate, T. Leijtens, S. Pathak, J. Teuscher, R. Avolio, M. E. Errico, J. Kirkpatrik, J. M. Ball, P. Docampo, I. McPherson and H. J. Snaith, *PCCP*, 2013, **15**, 2572-2579.
75. T. Leijtens, J. Lim, J. Teuscher, T. Park and H. J. Snaith, *Adv. Mater.*, 2013, **25**, 3227-3233.
76. J. Bisquert, A. Zaban and P. Salvador, *J. Phys. Chem. B*, 2002, **106**, 8774-8782.
77. Y. Yu, K. Wu and D. Wang, *Appl. Phys. Lett.*, 2011, **99**, -.
78. J. Weidmann, T. Dittrich, E. Konstantinova, I. Lauermann, I. Uhlendorf and F. Koch, *Solar Energy Materials and Solar Cells*, 1999, **56**, 153-165.
79. S. N. Habisreutinger, T. Leijtens, G. E. Eperon, S. D. Stranks, R. J. Nicholas and H. J. Snaith, *Nano Letters*, 2014, **14**, 5561-5568.
80. I. C. Smith, E. T. Hoke, D. Solis-Ibarra, M. D. McGehee and H. I. Karunadasa, *Angew. Chem. Int. Ed.*, 2014, **53**, 11232-11235.
81. J. You, Y. Yang, Z. Hong, T.-B. Song, L. Meng, Y. Liu, C. Jiang, H. Zhou, W.-H. Chang, G. Li and Y. Yang, *Appl. Phys. Lett.*, 2014, **105**, 183902.
82. G. E. Eperon, V. M. Burlakov, P. Docampo, A. Goriely and H. J. Snaith, *Adv. Funct. Mater.*, 2014, **24**, 151-157.
83. G. Niu, W. Li, F. Meng, L. Wang, H. Dong and Y. Qiu, *J. Mater. Chem. A*, 2014, **2**, 705-710.
84. J. A. Christians, P. A. Miranda Herrera and P. V. Kamat, *Journal of American Chemical Society*, 2015, **137**, 1530-1538.
85. B. R. Vincent, K. N. Robertson, T. S. Cameron and O. Knop, *Can. J. Chem.*, 1987, **65**, 1042-1046.
86. J. Yang, B. D. Siempelkamp, D. Liu and T. L. Kelly, *ACS Nano*, 2015, **9**, 1955-1963.
87. X. Dong, X. Fang, M. Lv, B. Lin, S. Zhang, J. Ding and N. Yuan, *J. Mater. Chem. A*, 2015, **3**, 5360-5367.
88. A. M. A. Leguy, Y. Hu, M. Campoy-Quiles, M. I. Alonso, O. J. Weber, P. Azarhoosh, M. van Schilfgaarde, M. T. Weller, T. Bein, J. Nelson, P. Docampo and P. R. F. Barnes, *Chem. Mater.*, 2015, **27**, 3397-3407.
89. B. Hailegnaw, S. Kirmayer, E. Edri, G. Hodes and D. Cahen, *J. Phys. Chem. Lett.*, 2015, **6**, 1543-1547.
90. M. Jørgensen, K. Norrman, S. A. Gevorgyan, T. Tromholt, B. Andreasen and F. C. Krebs, *Adv. Mater.*, 2012, **24**, 580-612.
91. T. Baikie, Y. Fang, J. M. Kadro, M. Schreyer, F. Wei, S. G. Mhaisalkar, M. Graetzel and T. J. White, *Journal of Materials Chemistry A*, 2013, **1**, 5628-5641.



Energy & Environmental Science Accepted Manuscript

92. S. Aharon, A. Dymshits, A. Rotem and L. Etgar, *J. Mater. Chem. A*, 2015, DOI: 10.1039/C4TA05149A.
93. C. Herring, *J. Appl. Phys.*, 1950, **21**, 437-445.
94. E. L. Unger, E. T. Hoke, C. D. Bailie, W. H. Nguyen, A. R. Bowring, T. Heumuller, M. G. Christoforo and M. D. McGehee, *Energy Environ. Sci.*, 2014, **7**, 3690-3698.
95. S. Ito, S. Tanaka, K. Manabe and H. Nishino, *J. Phys. Chem. C*, 2014, **118**, 16995-17000.
96. H.-S. Kim, S. H. Im and N.-G. Park, *J. Phys. Chem. C*, 2014, **118**, 5615-5625.
97. E. Mosconi, A. Amat, M. K. Nazeeruddin, M. Grätzel and F. De Angelis, *J. Phys. Chem. C*, 2013, **117**, 13902-13913.
98. R. E. Wasylishen, O. Knop and J. B. Macdonald, *Solid State Commun.*, 1985, **56**, 581-582.
99. A. Poglitsch and D. Weber, *J. Chem. Phys.*, 1987, **87**, 6373-6378.
100. M. L. Agiorgousis, Y.-Y. Sun, H. Zeng and S. Zhang, *J. Am. Chem. Soc.*, 2014, **136**, 14570-14575.
101. A. Buin, P. Pietsch, J. Xu, O. Voznyy, A. H. Ip, R. Comin and E. H. Sargent, *Nano Lett.*, 2014, **14**, 6281-6286.
102. W.-J. Yin, T. Shi and Y. Yan, *Appl. Phys. Lett.*, 2014, **104**, 063903.
103. A. Walsh, D. O. Scanlon, S. Chen, X. G. Gong and S.-H. Wei, *Angew. Chem. Int. Ed.*, 2015, **54**, 1791-1794.
104. M. H. Du, *J. Mater. Chem. A*, 2014, **2**, 9091-9098.
105. J. M. Azpiroz, E. Mosconi, J. Bisquert and F. De Angelis, *Energy Environ. Sci.*, 2015, **8**, 2118-2127.
106. M.-H. Du, *J. Phys. Chem. Lett.*, 2015, **6**, 1461-1466.
107. Y. Zhao and K. Zhu, *Chem. Commun.*, 2014, **50**, 1605-1607.
108. A. Pisoni, J. Jaćimović, O. S. Barišić, M. Spina, R. Gaál, L. Forró and E. Horváth, *J. Phys. Chem. Lett.*, 2014, **5**, 2488-2492.
109. R. Gottesman, E. Haltzi, L. Gouda, S. Tirosh, Y. Bouhadana, A. Zaban, E. Mosconi and F. De Angelis, *J. Phys. Chem. Lett.*, 2014, **5**, 2662-2669.
110. T. Oku, M. Zushi, Y. Imanishi, A. Suzuki and K. Suzuki, *Appl. Phys. Express*, 2014, **7**, 121601.
111. Z. Song, S. C. Watthage, A. B. Phillips, B. L. Tompkins, R. J. Ellingson and M. J. Heben, *Chemistry of Materials*, 2015, **27**, 4612-4619.
112. E. Edri, S. Kirmayer, A. Henning, S. Mukhopadhyay, K. Gartsman, Y. Rosenwaks, G. Hodes and D. Cahen, *Nano Lett.*, 2014, **14**, 1000-1004.
113. W.-J. Yin, T. Shi and Y. Yan, *Adv. Mater.*, 2014, **26**, 4653-4658.
114. J. S. Yun, A. Ho-Baillie, S. Huang, S. H. Woo, Y. Heo, J. Seidel, F. Huang, Y.-B. Cheng and M. A. Green, *J. Phys. Chem. Lett.*, 2015, **6**, 875-880.
115. Q. Dong, Y. Fang, Y. Shao, P. Mulligan, J. Qiu, L. Cao and J. Huang, *Science*, 2015, **347**, 967-970.
116. W. Nie, H. Tsai, R. Asadpour, J.-C. Blancon, A. J. Neukirch, G. Gupta, J. J. Crochet, M. Chhowalla, S. Tretiak, M. A. Alam, H.-L. Wang and A. D. Mohite, *Science*, 2015, **347**, 522-525.
117. D. Shi, V. Adinolfi, R. Comin, M. Yuan, E. Alarousu, A. Buin, Y. Chen, S. Hoogland, A. Rothenberger, K. Katsiev, Y. Losovyj, X. Zhang, P. A. Dowben, O. F. Mohammed, E. H. Sargent and O. M. Bakr, *Science*, 2015, **347**, 519-522.
118. N. K. Noel, A. Abate, S. D. Stranks, E. S. Parrott, V. M. Burlakov, A. Goriely and H. J. Snaith, *ACS Nano*, 2014, **8**, 9815-9821.
119. A. Abate, M. Saliba, D. J. Hollman, S. D. Stranks, K. Wojciechowski, R. Avolio, G. Grancini, A. Petrozza and H. J. Snaith, *Nano Lett.*, 2014, **14**, 3247-3254.




Energy & Environmental Science Accepted Manuscript

120. D. W. de Quilettes, S. M. Vorpahl, S. D. Stranks, H. Nagaoka, G. E. Eperon, M. E. Ziffer, H. J. Snaith and D. S. Ginger, *Science*, 2015, **348**, 683-686.
121. M. Zhang, H. Yu, M. Lyu, Q. Wang, J.-H. Yun and L. Wang, *Chem. Commun.*, 2014, **50**, 11727-11730.
122. R. K. Misra, S. Aharon, B. Li, D. Mogilyansky, I. Visoly-Fisher, L. Etgar and E. A. Katz, *J. Phys. Chem. Lett.*, 2015, **6**, 326-330.
123. I. P. Swainson, M. G. Tucker, D. J. Wilson, B. Winkler and V. Milman, *Chem. Mater.*, 2007, **19**, 2401-2405.
124. N. Onoda-Yamamuro, O. Yamamuro, T. Matsuo and H. Suga, *J. Phys. Chem. Solids*, 1992, **53**, 277-281.
125. J. Kim, S. Choi, A. Jun, H. Y. Jeong, J. Shin and G. Kim, *ChemSusChem*, 2014, **7**, 1669-1675.
126. G. Niu, X. Guo and L. Wang, *J. Mater. Chem. A*, 2015, DOI: 10.1039/C4TA04994B.
127. A. S. Bhalla, R. Guo and R. Roy, *Mat Res Innovat*, 2000, **4**, 3-26.
128. H. J. Snaith, A. Abate, J. M. Ball, G. E. Eperon, T. Leijtens, N. K. Noel, S. D. Stranks, J. T.-W. Wang, K. Wojciechowski and W. Zhang, *J. Phys. Chem. Lett.*, 2014, **5**, 1511-1515.
129. J. Even, L. Pedesseau, J.-M. Jancu and C. Katan, *J. Phys. Chem. Lett.*, 2013, **4**, 2999-3005.
130. P. E. Shaw, A. Ruseckas and I. D. W. Samuel, *Adv. Mater.*, 2008, **20**, 3516-3520.
131. C. Li, X. Lu, W. Ding, L. Feng, Y. Gao and Z. Guo, *Acta Crystallographica Section B*, 2008, **64**, 702-707.
132. C. A. Randall, A. S. Bhalla, T. R. Shrout and L. E. Cross, *J. Mater. Res.*, 1990, **5**, 829-834.
133. F. S. Galasso, *Structure, properties, and preparation of perovskite-type compounds*, Pergamon Press, Oxford, New York, 1969.
134. C. Motta, F. El-Mellouhi, S. Kais, N. Tabet, F. Alharbi and S. Sanvito, *Nat Commun*, 2015, **6**.
135. D. B. Mitzi, in *Prog. Inorg. Chem.*, John Wiley & Sons, Inc., 2007, DOI: 10.1002/9780470166499.ch1, pp. 1-121.
136. I. Borriello, G. Cantele and D. Ninno, *Phys. Rev. B*, 2008, **77**, 235214.
137. G. E. Eperon, S. D. Stranks, C. Menelaou, M. B. Johnston, L. M. Herz and H. J. Snaith, *Energy & Environmental Science*, 2014, **7**, 982-988.
138. N. Pellet, P. Gao, G. Gregori, T.-Y. Yang, M. K. Nazeeruddin, J. Maier and M. Grätzel, *Angew. Chem. Int. Ed.*, 2014, **53**, 3151-3157.
139. M. M. Lee, J. Teuscher, T. Miyasaka, T. N. Murakami and H. J. Snaith, *Science*, 2012, **338**, 643-647.
140. S. Aharon, S. Gamliel, B. E. Cohen and L. Etgar, *PCCP*, 2014, **16**, 10512-10518.
141. S. Aharon, B. E. Cohen and L. Etgar, *J. Phys. Chem. C*, 2014, **118**, 17160-17165.
142. J. M. Ball, M. M. Lee, A. Hey and H. J. Snaith, *Energy Environ. Sci.*, 2013, **6**, 1739-1743.
143. E. Edri, S. Kirmayer, D. Cahen and G. Hodes, *J. Phys. Chem. Lett.*, 2013, **4**, 897-902.
144. E. Edri, S. Kirmayer, M. Kulbak, G. Hodes and D. Cahen, *J. Phys. Chem. Lett.*, 2014, **5**, 429-433.
145. J. M. Frost, K. T. Butler, F. Brivio, C. H. Hendon, M. van Schilfgaarde and A. Walsh, *Nano Lett.*, 2014, **14**, 2584-2590.
146. Y. Tidhar, E. Edri, H. Weissman, D. Zohar, G. Hodes, D. Cahen, B. Rybtchinski and S. Kirmayer, *J. Am. Chem. Soc.*, 2014, **136**, 13249-13256.
147. O. Yamamuro, M. Oguni, T. Matsuo and H. Suga, *Thermochimica Acta*, 1986, **98**, 327-338.
148. S. T. Williams, F. Zuo, C.-C. Chueh, C.-Y. Liao, P.-W. Liang and A. K. Y. Jen, *ACS Nano*, 2014, **8**, 10640-10654.
149. M. Antoniadou, E. Siranidi, N. Vaenas, A. G. Kontos, E. Stathatos and P. Falaras, *Journal of Surfaces and Interfaces of Materials*, 2014, **2**, 323-327.




Energy & Environmental Science Accepted Manuscript

150. Q. Chen, H. Zhou, Y. Fang, A. Z. Stieg, T.-B. Song, H.-H. Wang, X. Xu, Y. Liu, S. Lu, J. You, P. Sun, J. McKay, M. S. Goorsky and Y. Yang, *Nat Commun*, 2015, **6**.
151. S. Colella, E. Mosconi, P. Fedeli, A. Listorti, F. Gazza, F. Orlandi, P. Ferro, T. Besagni, A. Rizzo, G. Calestani, G. Gigli, F. De Angelis and R. Mosca, *Chem. Mater.*, 2013, **25**, 4613-4618.
152. Z. Hawash, L. K. Ono, S. R. Raga, M. V. Lee and Y. Qi, *Chem. Mater.*, 2015, **27**, 562-569.
153. L. K. Ono, P. Schulz, J. J. Endres, G. O. Nikiforov, Y. Kato, A. Kahn and Y. Qi, *J. Phys. Chem. Lett.*, 2014, **5**, 1374-1379.
154. M.-C. Jung, S. R. Raga, L. K. Ono and Y. Qi, *Sci. Rep.*, 2015, **5**.
155. F. C. Krebs, S. A. Gevorgyan and J. Alstrup, *J. Mater. Chem.*, 2009, **19**, 5442-5451.
156. W. Chen, Y. Wu, J. Liu, C. Qin, X. Yang, A. Islam, Y.-B. Cheng and L. Han, *Energy Environ. Sci.*, 2015, **8**, 629-640.
157. C.-H. Chiang, Z.-L. Tseng and C.-G. Wu, *J. Mater. Chem. A*, 2014, **2**, 15897-15903.
158. Y.-J. Jeon, S. Lee, R. Kang, J.-E. Kim, J.-S. Yeo, S.-H. Lee, S.-S. Kim, J.-M. Yun and D.-Y. Kim, *Sci. Rep.*, 2014, **4**.
159. M. Jørgensen, K. Norrman and F. C. Krebs, *Solar Energy Materials and Solar Cells*, 2008, **92**, 686-714.
160. M. P. de Jong, L. J. van IJzendoorn and M. J. A. de Voigt, *Appl. Phys. Lett.*, 2000, **77**, 2255-2257.
161. S. R. Dupont, M. Oliver, F. C. Krebs, R. H. Dauskardt, S. R. Dupont, M. Oliver, F. C. Krebs and R. H. Dauskardt, 2012.
162. T. C. Sum and N. Mathews, *Energy Environ. Sci.*, 2014, **7**, 2518-2534.
163. S. P. Singh and P. Nagarjuna, *Dalton Trans.*, 2014, **43**, 5247-5251.
164. H. J. Snaith, *J. Phys. Chem. Lett.*, 2013, **4**, 3623-3630.
165. P. Gao, M. Gratzel and M. K. Nazeeruddin, *Energy Environ. Sci.*, 2014, **7**, 2448-2463.
166. Y. Shao, Z. Xiao, C. Bi, Y. Yuan and J. Huang, *Nat Commun*, 2014, **5**.
167. J.-Y. Jeng, Y.-F. Chiang, M.-H. Lee, S.-R. Peng, T.-F. Guo, P. Chen and T.-C. Wen, *Adv. Mater.*, 2013, **25**, 3727-3732.
168. G. Li, R. Zhu and Y. Yang, *Nat Photon*, 2012, **6**, 153-161.
169. Y. Zhou, C. Fuentes-Hernandez, J. Shim, J. Meyer, A. J. Giordano, H. Li, P. Winget, T. Papadopoulos, H. Cheun, J. Kim, M. Fenoll, A. Dindar, W. Haske, E. Najafabadi, T. M. Khan, H. Sojoudi, S. Barlow, S. Graham, J.-L. Brédas, S. R. Marder, A. Kahn and B. Kippelen, *Science*, 2012, **336**, 327-332.
170. W. Zhang, B. Zhao, Z. He, X. Zhao, H. Wang, S. Yang, H. Wu and Y. Cao, *Energy Environ. Sci.*, 2013, **6**, 1956-1964.
171. D. A. Mengistie, M. A. Ibrahem, P.-C. Wang and C.-W. Chu, *ACS Appl. Mater. Interfaces*, 2014, **6**, 2292-2299.
172. O. Malinkiewicz, C. Roldán-Carmona, A. Soriano, E. Bandiello, L. Camacho, M. K. Nazeeruddin and H. J. Bolink, *Adv. Energy Mater.*, 2014, **4**, n/a-n/a.
173. J. Seo, S. Park, Y. Chan Kim, N. J. Jeon, J. H. Noh, S. C. Yoon and S. I. Seok, *Energy Environ. Sci.*, 2014, **7**, 2642-2646.
174. P. Docampo, J. M. Ball, M. Darwich, G. E. Eperon and H. J. Snaith, *Nat Commun*, 2013, **4**.
175. J. Bisquert, *J. Phys. Chem. B*, 2004, **108**, 2323-2332.
176. H. J. Snaith and M. Grätzel, *Adv. Mater.*, 2007, **19**, 3643-3647.
177. K. Zhu, N. R. Neale, A. F. Halverson, J. Y. Kim and A. J. Frank, *J. Phys. Chem. C*, 2010, **114**, 13433-13441.
178. L. Wang, C. McCleese, A. Kovalsky, Y. Zhao and C. Burda, *J. Am. Chem. Soc.*, 2014, **136**, 12205-12208.




Energy & Environmental Science Accepted Manuscript

179. Y. Zhao, A. M. Nardes and K. Zhu, *Faraday Discuss.*, 2014, DOI: 10.1039/C4FD00128A.
180. T. Salim, S. Sun, Y. Abe, A. Krishna, A. C. Grimsdale and Y. M. Lam, *J. Mater. Chem. A*, 2015, DOI: 10.1039/C4TA05226A.
181. P. Qin, S. Tanaka, S. Ito, N. Tetreault, K. Manabe, H. Nishino, M. K. Nazeeruddin and M. Grätzel, *Nat Commun*, 2014, **5**.
182. K.-C. Wang, P.-S. Shen, M.-H. Li, S. Chen, M.-W. Lin, P. Chen and T.-F. Guo, *ACS Appl. Mater. Interfaces*, 2014, **6**, 11851-11858.
183. J. A. Christians, R. C. M. Fung and P. V. Kamat, *J. Am. Chem. Soc.*, 2014, **136**, 758-764.
184. W. Wang, J. Yuan, G. Shi, X. Zhu, S. Shi, Z. Liu, L. Han, H.-Q. Wang and W. Ma, *ACS Applied Materials & Interfaces*, 2015, **7**, 3994-3999.
185. J. Liu, Y. Wu, C. Qin, X. Yang, T. Yasuda, A. Islam, K. Zhang, W. Peng, W. Chen and L. Han, *Energy Environ. Sci.*, 2014, **7**, 2963-2967.
186. H. Greijer, J. Lindgren and A. Hagfeldt, *J. Phys. Chem. B*, 2001, **105**, 6314-6320.
187. J. Shi, J. Dong, S. Lv, Y. Xu, L. Zhu, J. Xiao, X. Xu, H. Wu, D. Li, Y. Luo and Q. Meng, *Appl. Phys. Lett.*, 2014, **104**, 063901.
188. R. Zuo, L. Li and Z. Gui, *Ceram. Int.*, 2000, **26**, 673-676.
189. R. Shannon, *Acta Crys.*, 1976, **32**, 751-767.
190. J. F. Verwey, *J. Phys. Chem. Solids*, 1970, **31**, 163-168.
191. P. Docampo and H. J. Snaith, *Nanotechnology*, 2011, **22**, 225403.
192. S. Guarnera, A. Abate, W. Zhang, J. M. Foster, G. Richardson, A. Petrozza and H. J. Snaith, *J. Phys. Chem. Lett.*, 2015, **6**, 432-437.
193. A. Dutta, C.-T. Huang, T.-C. Chen, C.-Y. Lin, C.-H. Chiu, Y.-C. Lin, C.-S. Chang and Y.-C. He, *Nat Commun*, 2015, **6**.
194. H. L. Clever and F. J. Johnston, *Journal of Physical and Chemical Reference Data*, 1980, **9**, 751-784.
195. L. Zheng, Y.-H. Chung, Y. Ma, L. Zhang, L. Xiao, Z. Chen, S. Wang, B. Qu and Q. Gong, *Chem. Commun.*, 2014, **50**, 11196-11199.
196. F. Zhang, X. Yang, H. Wang, M. Cheng, J. Zhao and L. Sun, *ACS Appl. Mater. Interfaces*, 2014, **6**, 16140-16146.
197. Z. Wei, H. Chen, K. Yan and S. Yang, *Angew. Chem.*, 2014, **126**, 13455-13459.
198. M.-C. Hsiao, S.-H. Liao, M.-Y. Yen, P.-I. Liu, N.-W. Pu, C.-A. Wang and C.-C. M. Ma, *ACS Appl. Mater. Interfaces*, 2010, **2**, 3092-3099.
199. D. Liu and T. L. Kelly, *Nat Photon*, 2014, **8**, 133-138.
200. Z. Ku, Y. Rong, M. Xu, T. Liu and H. Han, *Sci. Rep.*, 2013, **3**, 3132.
201. Z. Li, S. A. Kulkarni, P. P. Boix, E. Shi, A. Cao, K. Fu, S. K. Batabyal, J. Zhang, Q. Xiong, L. H. Wong, N. Mathews and S. G. Mhaisalkar, *ACS Nano*, 2014, **8**, 6797-6804.
202. E. Edri, S. Kirmayer, S. Mukhopadhyay, K. Gartsman, G. Hodes and D. Cahen, *Nat Commun*, 2014, **5**.
203. M. K. I. Senevirathna, P. K. D. D. P. Pitigala, E. V. A. Premalal, K. Tennakone, G. R. A. Kumara and A. Konno, *Solar Energy Materials and Solar Cells*, 2007, **91**, 544-547.
204. D. Kuang, P. Wang, S. Ito, S. M. Zakeeruddin and M. Grätzel, *J. Am. Chem. Soc.*, 2006, **128**, 7732-7733.
205. M. Lira-Cantu, K. Norrman, J. W. Andreasen, N. Casan-Pastor and F. C. Krebs, *J. Electrochem. Soc.*, 2007, **154**, B508-B513.
206. A. Kay and M. Grätzel, *Chem. Mater.*, 2002, **14**, 2930-2935.
207. E. Palomares, J. N. Clifford, S. A. Haque, T. Lutz and J. R. Durrant, *J. Am. Chem. Soc.*, 2002, **125**, 475-482.




Energy & Environmental Science Accepted Manuscript

208. Z. Liu, K. Pan, M. Liu, M. Wang, Q. Lü, J. Li, Y. Bai and T. Li, *Electrochimica Acta*, 2005, **50**, 2583-2589.
209. X.-t. Zhang, I. Sutanto, T. Taguchi, K. Tokuhiro, Q.-b. Meng, T. N. Rao, A. Fujishima, H. Watanabe, T. Nakamori and M. Uragami, *Solar Energy Materials and Solar Cells*, 2003, **80**, 315-326.
210. E. Palomares, J. N. Clifford, S. A. Haque, T. Lutz and J. R. Durrant, *J. Am. Chem. Soc.*, 2003, **125**, 475-482.
211. H.-S. Kim, J.-W. Lee, N. Yantara, P. P. Boix, S. A. Kulkarni, S. Mhaisalkar, M. Grätzel and N.-G. Park, *Nano Lett.*, 2013, **13**, 2412-2417.
212. M. K. Nazeeruddin, A. Kay, I. Rodicio, R. Humphry-Baker, E. Mueller, P. Liska, N. Vlachopoulos and M. Graetzel, *J. Am. Chem. Soc.*, 1993, **115**, 6382-6390.
213. L. W. R. Gao, B. Ma, C. Zhan, and Y. Qiu, *Langmuir*, 2010, **26**, 2460-2465.
214. R. Gao, L. Wang, Y. Geng, B. Ma, Y. Zhu, H. Dong and Y. Qiu, *J. Phys. Chem. C*, 2011, **115**, 17986-17992.
215. E. Palomares, J. N. Clifford, S. A. Haque, T. Lutz and J. R. Durrant, *Chem. Commun.*, 2002, DOI: 10.1039/B202515A, 1464-1465.
216. F. Luo, L. Wang, B. Ma and Y. Qiu, *Journal of Photochemistry and Photobiology A: Chemistry*, 2008, **197**, 375-381.
217. T. Zewdu, J. N. Clifford and E. Palomares, *PCCP*, 2012, **14**, 13076-13080.
218. J. Tian, R. Gao, Q. Zhang, S. Zhang, Y. Li, J. Lan, X. Qu and G. Cao, *J. Phys. Chem. C*, 2012, **116**, 18655-18662.
219. G. Niu, L. Wang, R. Gao, B. Ma, H. Dong and Y. Qiu, *J. Mater. Chem.*, 2012, **22**, 16914-16919.
220. Y. Ogomi, K. Kukihara, S. Qing, T. Toyoda, K. Yoshino, S. Pandey, H. Momose and S. Hayase, *ChemPhysChem*, 2014, **15**, 1062-1069.
221. B. G. Frost, N. F. van Hulst, E. Lunedei, G. Matteucci and E. Rikkers, *Appl. Phys. Lett.*, 1996, **68**, 1865-1867.
222. H. Oji, E. Ito, M. Furuta, K. Kajikawa, H. Ishii, Y. Ouchi and K. Seki, *Journal of Electron Spectroscopy and Related Phenomena*, 1999, **101–103**, 517-521.
223. M. Lögdlund and J. L. Brédas, *J. Chem. Phys.*, 1994, **101**, 4357-4364.
224. H. Antoniadis, B. R. Hsieh, M. A. Abkowitz, S. A. Jenekhe and M. Stolka, *Synth. Met.*, 1994, **62**, 265-271.
225. V. I. Annenkov, S. G. Garanin, V. A. Eroshenko, N. V. Zhidkov, A. V. Zubkov, S. V. Kalipanov, N. A. Kalmykov, V. P. Kovalenko, V. A. Krotov, S. G. Lapin, S. P. Martynenko, V. I. Pankratov, V. S. Faizullin, V. A. Khrustalev, N. M. Khudikov and V. S. Chebotar, *Quantum Electron.*, 2009, **39**, 719.
226. J.-Y. Lee, S. T. Connor, Y. Cui and P. Peumans, *Nano Lett.*, 2008, **8**, 689-692.
227. J. H. Kim, S. T. Williams, N. Cho, C.-C. Chueh and A. K. Y. Jen, *Adv. Energy Mater.*, 2015, **5**, n/a-n/a.
228. F. C. Krebs, *Solar Energy Materials and Solar Cells*, 2006, **90**, 3633-3643.
229. C. J. Brabec, N. S. Sariciftci and J. C. Hummelen, *Adv. Funct. Mater.*, 2001, **11**, 15-26.
230. K. Tennakone, G. R. R. A. Kumara, I. R. M. Kottegoda, K. G. U. Wijayantha and V. P. S. Perera, *J. Phys. D: Appl. Phys.*, 1998, **31**, 1492.
231. P. Wang, S. M. Zakeeruddin, P. Comte, R. Charvet, R. Humphry-Baker and M. Grätzel, *J. Phys. Chem. B*, 2003, **107**, 14336-14341.
232. P. Wang, S. M. Zakeeruddin, R. Humphry-Baker and M. Grätzel, *Chem. Mater.*, 2004, **16**, 2694-2696.
233. T. W. Matthew Carnie, and David Worsley, *International Journal of Photoenergy*, 2012, **2012**,




Energy & Environmental Science Accepted Manuscript

9.
234. A. Abate, J. Martí-Rujas, P. Metrangolo, T. Pilati, G. Resnati and G. Terraneo, *Cryst. Growth Des.*, 2011, **11**, 4220-4226.
235. A. Hinsch, J. M. Kroon, R. Kern, I. Uhlendorf, J. Holzbock, A. Meyer and J. Ferber, *Prog. Photovolt: Res. Appl.*, 2001, **9**, 425-438.
236. H. Pettersson and T. Gruszecki, *Solar Energy Materials and Solar Cells*, 2001, **70**, 203-212.
237. P. M. Sommeling, M. Späth, H. J. P. Smit, N. J. Bakker and J. M. Kroon, *Journal of Photochemistry and Photobiology A: Chemistry*, 2004, **164**, 137-144.
238. M. Grätzel, *Journal of Photochemistry and Photobiology C: Photochemistry Reviews*, 2003, **4**, 145-153.
239. S. Gevorgyan, M. V. Madsen, H. F. Dam, M. Jørgensen, C. J. Fell, K. F. Anderson, B. C. Duck, A. Mescheloff, E. A. Katz, A. Elschner, R. Roesch, H. Hoppe, M. Hermenau, M. Riede, F. C. Krebs, S. Gevorgyan, M. V. Madsen, H. F. Dam, M. Jørgensen, C. J. Fell, K. F. Anderson, B. C. Duck, A. Mescheloff, E. A. Katz, A. Elschner, R. Roesch, H. Hoppe, M. Hermenau, M. Riede and F. C. Krebs, *Solar Energy Materials & Solar Cells*, 2013, **116**, 187-196.
240. K. Norrman and F. C. Krebs, *Surface and Interface Analysis*, 2004, **36**, 1542-1549.
241. J. A. Hauch, P. Schilinsky, S. A. Choulis, R. Childers, M. Biele and C. J. Brabec, *Solar Energy Materials and Solar Cells*, 2008, **92**, 727-731.
242. J. Wu, J. Wang, J. Lin, Y. Xiao, G. Yue, M. Huang, Z. Lan, Y. Huang, L. Fan, S. Yin and T. Sato, *Sci. Rep.*, 2013, **3**.
243. J. Wu, J. Wang, J. Lin, Z. Lan, Q. Tang, M. Huang, Y. Huang, L. Fan, Q. Li and Z. Tang, *Adv. Energy Mater.*, 2012, **2**, 78-81.
244. Y. Chen, T. Chen and L. Dai, *Adv. Mater.*, 2015, **27**, 1053-1059.
245. J. You, Z. Hong, Y. Yang, Q. Chen, M. Cai, T.-B. Song, C.-C. Chen, S. Lu, Y. Liu, H. Zhou and Y. Yang, *ACS Nano*, 2014, **8**, 1674-1680.
246. B. Conings, L. Baeten, C. De Dobbelaere, J. D'Haen, J. Manca and H.-G. Boyen, *Adv. Mater.*, 2014, **26**, 2041-2046.
247. F. Lang, A. Juma, V. Somsongkul, T. Dittrich and M. Arunchaiya, *Hybrid Materials*, 2014, **1**.
248. N. Onoda-Yamamuro, T. Matsuo and H. Suga, *J. Phys. Chem. Solids*, 1990, **51**, 1383-1395.
249. E. Mosconi, C. Quarti, T. Ivanovska, G. Ruani and F. De Angelis, *PCCP*, 2014, **16**, 16137-16144.
250. C. Quarti, G. Grancini, E. Mosconi, P. Bruno, J. M. Ball, M. M. Lee, H. J. Snaith, A. Petrozza and F. D. Angelis, *J. Phys. Chem. Lett.*, 2014, **5**, 279-284.
251. A. Maalej, Y. Abid, A. Kallel, A. Daoud, A. Lautié and F. Romain, *Solid State Commun.*, 1997, **103**, 279-284.
252. M. Ledinský, P. Löper, B. Niesen, J. Holovský, S.-J. Moon, J.-H. Yum, S. De Wolf, A. Fejfar and C. Ballif, *J. Phys. Chem. Lett.*, 2015, **6**, 401-406.
253. E. T. Hoke, D. J. Slotcavage, E. R. Dohner, A. R. Bowring, H. I. Karunadasa and M. D. McGehee, *Chem. Sci.*, 2015, **6**, 613-617.
254. J. Feng, *APL Materials*, 2014, **2**, 081801.
255. V. Brand, C. Bruner and R. H. Dauskardt, *Solar Energy Materials and Solar Cells*, 2012, **99**, 182-189.
256. S. Savagatrup, A. D. Printz, T. F. O'Connor, A. V. Zaretski and D. J. Lipomi, *Chem. Mater.*, 2014, **26**, 3028-3041.
257. Y. Zhao, A. M. Nardes and K. Zhu, *Faraday Discuss.*, 2014, **176**, 301-312.
258. A. J. Frank, N. Kopidakis and J. v. d. Lagemaat, *Coordination Chemistry Reviews*, 2004, **248**, 1165-1179.



Energy & Environmental Science Accepted Manuscript

259. Q. Wang, S. Ito, M. Grätzel, F. Fabregat-Santiago, I. Mora-Seró, J. Bisquert, T. Bessho and H. Imai, *J. Phys. Chem. B*, 2006, **110**, 25210-25221.
260. N. Kopidakis, E. A. Schiff, N. G. Park, J. van de Lagemaat and A. J. Frank, *J. Phys. Chem. B*, 2000, **104**, 3930-3936.
261. A. Zaban, M. Greenshtein and J. Bisquert, *ChemPhysChem*, 2003, **4**, 859-864.
262. G. Pellegrino, A. Alberti, G. G. Condorelli, F. Giannazzo, A. La Magna, A. M. Paoletti, G. Pennesi, G. Rossi and G. Zanotti, *J. Phys. Chem. C*, 2013, **117**, 11176-11185.
263. P. Docampo, F. C. Hanusch, S. D. Stranks, M. Döblinger, J. M. Feckl, M. Ehrensperger, N. K. Minar, M. B. Johnston, H. J. Snaith and T. Bein, *Adv. Energy Mater.*, 2014, **4**, n/a-n/a.
264. S. A. Gevorgyan, M. Jørgensen and F. C. Krebs, *Solar Energy Materials and Solar Cells*, 2008, **92**, 736-745.
265. M. O. Reese, S. A. Gevorgyan, M. Jørgensen, E. Bundgaard, S. R. Kurtz, D. S. Ginley, D. C. Olson, M. T. Lloyd, P. Morvillo, E. A. Katz, A. Elschner, O. Haillant, T. R. Currier, V. Shrotriya, M. Hermenau, M. Riede, K. R. Kirov, G. Trimmel, T. Rath, O. Inganäs, F. Zhang, M. Andersson, K. Tvingstedt, M. Lira-Cantu, D. Laird, C. McGuiness, S. Gowrisanker, M. Pannone, M. Xiao, J. Hauch, R. Steim, D. M. DeLongchamp, R. Rösch, H. Hoppe, N. Espinosa, A. Urbina, G. Yaman-Uzunoglu, J.-B. Bonekamp, A. J. J. M. van Breemen, C. Girotto, E. Voroshazi and F. C. Krebs, *Solar Energy Materials and Solar Cells*, 2011, **95**, 1253-1267.
266. H. Neugebauer, C. Brabec, J. C. Hummelen and N. S. Sariciftci, *Solar Energy Materials and Solar Cells*, 2000, **61**, 35-42.




Energy & Environmental Science Accepted Manuscript

**TOC entry**

What are the bottlenecks for organometal halide perovskite solar cells to achieve the stability required for commercialization?

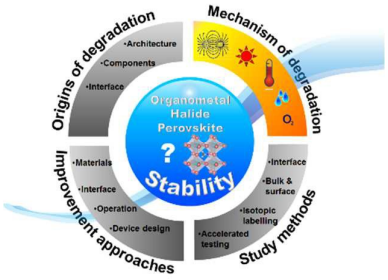


Energy & Environmental Science Accepted Manuscript

## Broader context

Low cost, stable and efficient light harvesting crystalline materials have a great promise for future cost-effective clean energy and the environment. Solar cell devices made of organometal halide perovskite materials are now revolutionizing the area of photovoltaics with energy conversion efficiency of 20.1%, which is a fivefold jump in cell efficiency within three years. The major obstacle of bringing organometal halide perovskite solar cells to the commercial market is device poor long term stability, which has not been able to exceed a few thousands of hours until now. This review article presents an in-depth and updated discussion on the progress in stability, addressing mechanisms and origins behind degradation, approaches to improve stability, protocols and related analytical methods to study the existing and other unknown limitations on the stability of organometal halide perovskite solar cells. Furthermore, it is also meant to give an overview to readers who are new to this topic.

Energy & Environmental Science Accepted Manuscript